

University of New Hampshire

## University of New Hampshire Scholars' Repository

---

Doctoral Dissertations

Student Scholarship

---

Spring 1986

### THE EFFECT OF RAIN ON INTERTIDAL ESTUARINE SEDIMENT TRANSPORT (VORTEX RINGS, OXYGENATION, DROP/SPLASH FEATURES, FECAL PELLETS)

THOMAS CORTLAND SHEVENELL  
*University of New Hampshire, Durham*

Follow this and additional works at: <https://scholars.unh.edu/dissertation>

---

#### Recommended Citation

SHEVENELL, THOMAS CORTLAND, "THE EFFECT OF RAIN ON INTERTIDAL ESTUARINE SEDIMENT TRANSPORT (VORTEX RINGS, OXYGENATION, DROP/SPLASH FEATURES, FECAL PELLETS)" (1986). *Doctoral Dissertations*. 1485.  
<https://scholars.unh.edu/dissertation/1485>

This Dissertation is brought to you for free and open access by the Student Scholarship at University of New Hampshire Scholars' Repository. It has been accepted for inclusion in Doctoral Dissertations by an authorized administrator of University of New Hampshire Scholars' Repository. For more information, please contact [Scholarly.Communication@unh.edu](mailto:Scholarly.Communication@unh.edu).

## INFORMATION TO USERS

This reproduction was made from a copy of a manuscript sent to us for publication and microfilming. While the most advanced technology has been used to photograph and reproduce this manuscript, the quality of the reproduction is heavily dependent upon the quality of the material submitted. Pages in any manuscript may have indistinct print. In all cases the best available copy has been filmed.

The following explanation of techniques is provided to help clarify notations which may appear on this reproduction.

1. Manuscripts may not always be complete. When it is not possible to obtain missing pages, a note appears to indicate this.
2. When copyrighted materials are removed from the manuscript, a note appears to indicate this.
3. Oversize materials (maps, drawings, and charts) are photographed by sectioning the original, beginning at the upper left hand corner and continuing from left to right in equal sections with small overlaps. Each oversize page is also filmed as one exposure and is available, for an additional charge, as a standard 35mm slide or in black and white paper format.\*
4. Most photographs reproduce acceptably on positive microfilm or microfiche but lack clarity on xerographic copies made from the microfilm. For an additional charge, all photographs are available in black and white standard 35mm slide format.\*

**\*For more information about black and white slides or enlarged paper reproductions, please contact the Dissertations Customer Services Department.**

**U·M·I** Dissertation  
Information Service

University Microfilms International  
A Bell & Howell Information Company  
300 N. Zeeb Road, Ann Arbor, Michigan 48106



8621609

**Shevenell, Thomas Cortland**

THE EFFECT OF RAIN ON INTERTIDAL ESTUARINE SEDIMENT TRANSPORT

*University of New Hampshire*

PH.D. 1986

University

Microfilms

International 300 N. Zeeb Road, Ann Arbor, MI 48106

11

11

**PLEASE NOTE:**

In all cases this material has been filmed in the best possible way from the available copy. Problems encountered with this document have been identified here with a check mark .

1. Glossy photographs or pages
2. Colored illustrations, paper or print \_\_\_\_\_
3. Photographs with dark background
4. Illustrations are poor copy \_\_\_\_\_
5. Pages with black marks, not original copy \_\_\_\_\_
6. Print shows through as there is text on both sides of page \_\_\_\_\_
7. Indistinct, broken or small print on several pages
8. Print exceeds margin requirements \_\_\_\_\_
9. Tightly bound copy with print lost in spine \_\_\_\_\_
10. Computer printout pages with indistinct print \_\_\_\_\_
11. Page(s) \_\_\_\_\_ lacking when material received, and not available from school or author.
12. Page(s) \_\_\_\_\_ seem to be missing in numbering only as text follows.
13. Two pages numbered \_\_\_\_\_. Text follows.
14. Curling and wrinkled pages \_\_\_\_\_
15. Dissertation contains pages with print at a slant, filmed as received \_\_\_\_\_
16. Other \_\_\_\_\_  
\_\_\_\_\_  
\_\_\_\_\_

University  
Microfilms  
International



**THE EFFECT OF RAIN ON INTERTIDAL  
ESTUARINE SEDIMENT TRANSPORT**

By

**THOMAS C. SHEVENELL**  
B.A. University of New Hampshire, 1970  
M. Phil. Columbia University, 1974

**A DISSERTATION**

**Submitted to the University of New Hampshire  
in Partial Fulfillment of  
the Requirements for the Degree of**

**Doctor of Philosophy**

**in**

**Earth Sciences**

**May 1986**

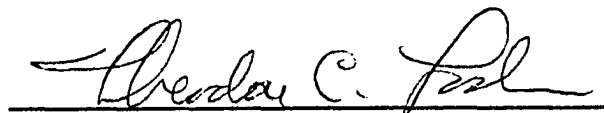
This dissertation has been examined and approved



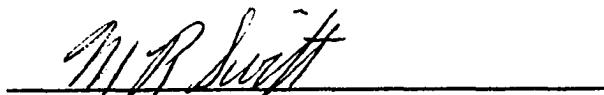
Dissertation Director  
Franz E. Anderson  
Professor of Oceanography



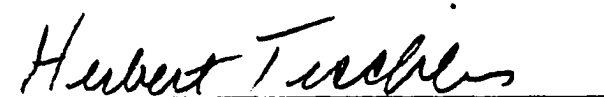
Thomas Ballestero  
Asstant Professor of Civil Engineering



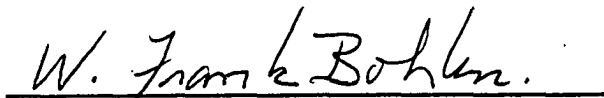
Theodore C. Loder  
Associate Professor of Earth Sciences



M. Robinson Swift  
Associate Professor of Mech. Engineering



Herbert Tischler  
Professor of Geology



W. Frank Bohlen,  
Associate Professor of Oceanography  
University of Connecticut

Date : April 15, 1986

## DEDICATION

**This dissertation is dedicated to Susie. Her love, encouragement and belief in my capabilities have provided me with the drive and sense of purpose to reach this goal. This is just a small thank you to my best friend and companion.**

## ACKNOWLEDGEMENTS

I wish to express my gratitude to Dr. Franz E. Anderson for his guidance and encouragement during these graduate student years, and throughout the many years of our scientific collaboration. I would also like to express thanks to my guidance committee, who were able to test my technical limits and keep me focused on the problem: Dr. Thomas Ballestero, Dr. W. Frank Bohlen (University of Connecticut), Dr. Theodore C. Loder, Dr. M. Robinson Swift, and Dr. Herbert Tischler. I would also like to acknowledge Dr. Wallace A. Bothner for his encouragement and support during my graduate student years, and the many years since leaving UNH in 1970.

I would like to make a special acknowledgement to Dr. Bruce Heezen, Dr. John E. Sanders, Dr. Maurice Ewing, Dr. Marshall Kay and Dr. Rhodes Fairbridge at Columbia University, who kindled my interest in geology and oceanography. A special warm thanks to Mrs. Janet Sussman, who had faith that I would reach my goal.

The undergraduate students who have worked with me on various aspects of my research deserve acknowledgement for their enthusiasm and competency: Andrew Bennett, Paul Butler, Dan Howard, and Kelley Leavett-Pond. I would like to thank Carl Mulgram-Royce and Dr. Win Watson for the use of their video equipment. EnviroSystems, Inc. and Dr. Richard Sugatt were kind enough to allow me the use of their space and equipment for the oxygenation experiment. I would like to thank Eduardo Jaramillo for his understanding that sedimentologists can be quite ignorant of the biological

community, and his continued friendship, help and advice throughout our graduate student days.

I would like to thank Dr. Galen Jones, Director of the Jackson Estuarine Laboratory, for the use of facilities and supplies to conduct my thesis research. Financial support for my research was provided by the University of New Hampshire-Maine Sea Grant Program, with partial funding by a CURF Grant.

## TABLE OF CONTENTS

DEDICATION.....	iii
ACKNOWLEDGEMENTS.....	iv
LIST OF TABLES.....	x
LIST OF FIGURES.....	xi
LIST OF SYMBOLS.....	xv
ABSTRACT.....	xix

### CHAPTER

#### 1. INTRODUCTION

<b>General Statement</b> .....	1
<b>Literature Review</b> .....	4
<b>Single-Drop Mechanics</b> .....	6
<b>Rainfall</b> .....	8
<b>Rain and Sedimentation</b> .....	10
<b>Sediment Response</b> .....	11
<b>Significance of Rainfall</b> .....	13
<b>Objectives</b> .....	19

#### 2. MECHANICS OF DROP-FORMED VORTEX RINGS

<b>Introduction</b> .....	22
<b>Methodology</b> .....	23
<b>Experimental Procedures</b> .....	23
<b>Drop Formation</b> .....	23
<b>Receiving Water</b> .....	27

<b>Analytical Procedures</b> .....	28
<b>Experiment 1</b> .....	28
<b>Experiment 2</b> .....	28
<b>Experiment 3</b> .....	28
<b>Experiment 4</b> .....	29
<b>Experimental Error Analysis</b> .....	30
<b>Drop Size Variability</b> .....	30
<b>Sample Size Analysis</b> .....	30
<b>Results</b> .....	31
<b>Controls on Vortex Ring Formation</b> .....	31
<b>Central Jet Formation</b> .....	32
<b>Drop Shape Oscillation</b> .....	35
<b>Vortex Ring Generation</b> .....	41
<b>Central Jet Characteristics</b> .....	41
<b>Effect of Drop Impact Energy</b> .....	43
<b>Effects of Receiving Water Temperature</b> .....	45
<b>Vortex Ring Characteristics</b> .....	47
<b>Vortex Ring Size</b> .....	47
<b>Vortex Ring Velocity</b> .....	48
<b>Vortex Ring Penetration</b> .....	55
<b>Discussion</b> .....	57

### **3. RAIN-INDUCED INCIPIENT MOTION OF NONCOHESIVE SEDIMENT**

<b>Introduction</b> .....	64
<b>Methodology</b> .....	64
<b>Results</b> .....	67
<b>Discussion</b> .....	72

### **4. MULTIDROP EXPERIMENTS ON RESUSPENSION OF MUDDY INTERTIDAL SEDIMENTS**

<b>Introduction</b> .....	74
<b>Methodology</b> .....	76
<b>Field Methods</b> .....	76
<b>Tower</b> .....	76
<b>Rain Module</b> .....	78
<b>Multidrop Experiment: Receiving Water</b> .....	81
<b>Multidrop Experiment: Substrate</b> .....	84
<b>Insitu Experiment</b> .....	84
<b>Storm Observations</b> .....	87
<b>Laboratory Methods</b> .....	87

<b>Artificial Rainfall Characteristics</b> .....	87
<b>Physical Characteristics of Receiving Water</b> .....	88
<b>Suspended Sediment</b> .....	88
<b>Results</b> .....	89
<b>Multidrop Experiment</b> .....	89
<b>Insitu Experiment</b> .....	104
<b>Storm Observations</b> .....	110
<b>Discussion</b> .....	113
<b>5. MULTIDROP EXPERIMENT ON BEDLOAD TRANSPORT OF MUDDY INTERTIDAL SEDIMENTS</b>	
<b>Introduction</b> .....	116
<b>Methodology</b> .....	117
<b>Results</b> .....	119
<b>Discussion</b> .....	122
<b>6. CHARACTERISTICS OF THE MUDDY INTERTIDAL SEDIMENTS USED IN EXPERIMENTS</b>	
<b>Introduction</b> .....	125
<b>Methodology</b> .....	125
<b>Results and Discussion</b> .....	126
<b>Description of Sediment Texture</b> .....	126
<b>Rain Effect on Sediment Texture</b> .....	126
<b>7. A TECHNIQUE TO OXYGENATE AQUACULTURE TANKS</b>	
<b>Introduction</b> .....	132
<b>Methodology</b> .....	133
<b>Results</b> .....	137
<b>Discussion</b> .....	141
<b>8. RAINFALL AND ESTUARINE SEDIMENTATION A DISCUSSION</b>	
<b>Introduction</b> .....	143
<b>Discussion</b> .....	143
<b>Erosion by Rain</b> .....	143
<b>Erosion Potential of Rainfall</b> .....	145
<b>Physical Properties of Tidalflats</b> .....	147
<b>Erodibility of the Sediment Surface</b> .....	150

<b>Modification of Surface Erodibility</b> .....	153
<b>Importance of Rainfall</b> .....	155
<b>Areas for Future Research</b> .....	158
<b>SUMMARY AND CONCLUSIONS</b> .....	160
<b>REFERENCES</b> .....	163
<b>APPENDICES</b> .....	174
1. Calculation of wave Reynolds numbers and energy dissipation rates.....	174
2. Summary of analytical data for the single drop studies.....	178
3. Summary of vortex ring observations in which sediment moved when rings touched bottom, and shear stress calculation of very-coarse quartz grains.....	186
4. Listing of data reports covering multidrop experiments.....	188
5. Sedimentological characteristics of fecal pellets from <i>M. balthica</i> and <i>H. filiformis</i> and critical shear stress calculation for <i>H. filiformis</i> pellets.....	189
6. Summary listing of the data collected during the oxygenation experiment.....	210

## LIST OF TABLES

TABLE 1-1. Physical and biological parameters, which control sedimentation on the muddy intertidal.....	14
TABLE 2-1. Summary of experimental operations.....	25
TABLE 2-2. Drop formers used in each single-drop experiment.....	26
TABLE 4-1. Summary of multidrop runs identified as conservative mixing or nonconservative cases.....	92
TABLE 4-2. Independent variables divided into rain, bottom sediment and water column characteristics.....	97
TABLE 4-3. Resuspension mechanisms observed in the suspended sediment concentration.....	109
TABLE 4-4. Summary of data from insitu experiments where rain showed an effect on the excess mass concentration (as determined between the impact area and control area).....	115
TABLE 5-1. Summary of the flume study results, including the amount of bedload sediment (mg) caught in the trap, the rainfall intensity and power, the flow velocity through the flume, and the erosion rate.....	121
TABLE 6-1. Results of analysis of variance testing on the paired samples from the insitu experiment and the flume study.....	128
TABLE 7-1. The water characteristics and sampling depths for each tank used in the oxygenation experiment.....	136

## LIST OF FIGURES

FIGURE 1-1. Conceptual model of how a raindrop may affect sedimentation in a shallow water column.....	5
FIGURE 1-2. Diagrammatic distributions of important rainstorm parameters.....	9
FIGURE 1-3. The effects of physical processes on sedimentation varies spatially in the estuary.....	15
FIGURE 1-4. Distribution of wave Reynolds Numbers for short period (0.5 to 1.5 sec) waves in water depths from 5 to 40 cm using solitary wave theory.....	18
FIGURE 1-5. The effect of rain on an idealized estuary with broad tidal flats.....	20
FIGURE 2-1. Schematic diagram of the experimental set up used to investigate the single drop-formed splashes and vortex rings.....	24
FIGURE 2-2. Scatter plots of percent bubbles (A) and percent jets (B) versus impact kinetic energy divided by the spherical drop area.....	33
FIGURE 2-3. The number of vortex ring produced by 25 drops, as a function of drop height from 1 to 184 cm in 1 cm increments.....	36
FIGURE 2-4. Diagram showing how an idealized drop oscillates in shape.....	38
FIGURE 2-5. The probability of vortex ring production, as a function of the normalized drop-shape oscillation number.....	40
FIGURE 2-6. Shadow diagrams of central jets produced by 0.545 cm drops falling from heights, ranging from 50 (top) to 600 cm (bottom) in 50 cm intervals.....	42

FIGURE 2-7. Scatter plots of cross-sectional area (A), jet height (B) and average jet diameter (C) as a function of impact kinetic energy per spherical drop area.....	44
FIGURE 2-8. Jet dimensions from Experiment 3 as a function of fall height..	46
FIGURE 2-9. Photograph of the inner core of a vortex ring impacting a clay covered tank bottom after passing through 40 cm of water.....	49
FIGURE 2-10. A diagram of the dimensions of the inner core of the vortex ring.....	50
FIGURE 2-11. Plots of vortex ring translational velocities with depth for the 24 runs in Experiment 4.....	52
FIGURE 2-12. The average translational velocities of vortex ring produced by both both small and large drops as measured from selected rings from Experiment 4.....	54
FIGURE 2-13. The penetration of vortex rings is shown as a probability function of depth.....	56
FIGURE 2-14. Profiles of vortex ring momentum as a function of depth for rings formed by the large and small drops used in Experiment 4.....	59
FIGURE 2-15. Diagram illustrating effects of salinity stratification on vortex ring penetration.....	61
FIGURE 2-16. Profiles of available momentum from drop-formed vortex rings at water depths from 1 to 19 cm.....	62
FIGURE 3-1. Schematic diagram of the experimental set-up.....	65
FIGURE 3-2. Photograph showing a vortex ring impacting estuarine mud.....	68
FIGURE 3-3. Percentage of vortex rings that initiated sediment motion for each water depth including all substrate textures.....	69

FIGURE 3-4. The difference in the percent of vortex rings.....	71
FIGURE 4-1. Schematic diagram of the experimental set up for the multi-drop experiment.....	77
FIGURE 4-2. Photograph of the insitu experimental set up.....	79
FIGURE 4-3. Schematic of the rain module and the rainwater reservoir system.....	80
FIGURE 4-4. Schematic of the receiving water tanks and water samplers..	82
FIGURE 4-5. Diagram showing the methodology used to measure the sediment microtopography in the receiving water tanks.....	83
FIGURE 4-6. Diagram showing the sediment collection technique. which minimized the disturbance of the sediment surface.....	85
FIGURE 4-7. Schematic diagram showing the sample collection set up for the insitu experiment.....	86
FIGURE 4-8. Examples from the multidrop experiments which illustrate the four basic cases in which the excess mass suspended in the receiving water column varies with time.....	94
FIGURE 4-9. Vertical distribution of R-squared for linear regression between excess mass at 11.5 minutes into the run and rain power..	101
FIGURE 4-10. The vertical distribution of the slope from the linear regression between excess mass at 11.5 minutes into the run and power.....	103
FIGURE 4-11. Insitu suspended sediment concentrations within the rain impact area and in the control site.....	106
FIGURE 4-12. Histograms of the measured drop size distribution during the two storm observations.....	111
FIGURE 4-13. The observed suspended sediment distribution with time during the storm period when the water level at the sampling site ebbed from about 30 cm to about 1 cm water depth.....	112

FIGURE 5-1. Experimental set up for the flume study.....	118
FIGURE 5-2. Conceptual diagram of how an impacting vortex ring initiates motion of coarse material on the sediment surface, and resuspends the fines into the water column.....	123
FIGURE 6-1. Histogram showing the percent composition of the sediments used in the multidrop and insitu experiments and the flume study.....	127
FIGURE 7-1. Experimental set up for the vortex ring oxygenation experiments.....	134
FIGURE 7-2. Relative changes in the dissolved oxygen content of the four tanks during the study period.....	138
FIGURE 7-3. Oxygen percent saturation with time into the experiment is plotted for each tank.....	140
FIGURE 8-1. Diagrammatic representation of the sediment surface showing the interrelationships between the organisms in the sediment and the microtopography of the sediment surface as interpreted by Jaramillo (personal communication).....	148
FIGURE 8-2. Photograph showing the microtopography of the sediment surface.....	149
FIGURE 8-3. Photograph showing the sediment surface under the microscope.....	152
FIGURE 8-4. Cartoon on how waves and rain interact in the shallow intertidal wedge.....	154
FIGURE 8-5. Diagram illustrating the three cases in the simple model which describes the distribution of the rain-induced suspended sediment concentration in the Great Bay estuary at low tide.....	156

## LIST OF SYMBOLS

SYMBOL	DEFINITION	EQUATION	PAGE
A	Pycnometer weight (DW only)	A5-7	194
$A_s$	Spherical area	2-1	34
B	Pycnometer weight (pellets)	A5-7	194
C	Cropping factor	8-1	144
$C_b$	Baselevel concentration	4-2	90
$C_d$	Drag coefficient	A5-1	191
$C_e$	Excess sediment concentration	4-2	90
$C_o$	Observed sediment conc.	4-2	90
$C_r$	Conc. of Sediment in rain	4-2	90
$C_d$	Drag coefficient	A5-1	191
D	Diameter	1-1	16
D	Drop diameter	A2-4	185
$D_n$	Nominal diameter	A5-8	200
E	Soil erosion	8-1	144
$E_d, E_d'$	Rainstorm energy dissipation	A1-6	175
$E_i$	Drop impact energy	2-1	34
$F_i$	Theoretical frequency	A2-1	181
H	Wave height	A1-4	175
I	Rainfall intensity	5-1	99
K	Soil erodibility factor	8-1	144

K	Correction factor	A5-9	205
K'	Correction factor	A5-10	205
L	Length of flow in supply area	8-1	144
L	Wave length	A1-4	175
L	Length of fecal pellet	---	204
M	Mass of sediment eroded	4-1	74
M <sub>e</sub>	Excess mass of sediment	4-2	90
P	Probability of ring penetration	2-4	55
P <sub>c</sub>	Type of concervation practice	8-1	144
P <sub>m</sub>	Mean percentage	A2-2	181
R	Erosion rate constant	4-1	74
R	Erosion potential of rainfall	8-1	144
Re	Reynolds number	1-1	16
Re <sub>w</sub>	Wave Reynolds number	A1-1	175
S	Land slope	8-1	144
S <sub>o</sub>	Observed salinity	4-2	90
S <sub>s</sub>	Base salinity of receiving water	4-2	90
S*	Modified Shields Diagram	3-1	70
T <sub>w</sub>	Wave period	A1-4	175
U	Velocity	1-1	16
V	Drop volume	2-2	35
V <sub>r</sub>	Vortex ring inner core volume	---	50
V <sub>r</sub>	Receiving water volume	4-2	90
W	Settling velocity of sphere	A5-1	191
W	Width of fecal pellet	---	204
W <sub>o</sub>	Observed pellet settling	A5-8	200
W <sub>p</sub>	Predicted settling velocity	A5-9	205

$\bar{W}_p$	Predicted settling velocity	A5-10	205
$\bar{W}_s$	Stokes settling velocity	A5-5	192
X	Wet weight of fecal pellet	A5-7	194
a	Vertical toroid radius	---	50
b	Horizontal toroid radius	---	50
$d_d$	Drop diameter	A2-4	185
$d_0$	displacement due to wave	A1-4	175
$d_s$	Diameter of sediment	3-1	70
f	Fraction of freshwater	4-2	90
$f_d$	Drop size efficiency factor	4-3	99
$f_i$	Observed $i^{\text{th}}$ frequency	A2-1	181
g	acceleration due to gravity	A1-4	175
h	Drop fall distance	2-3	37
k	Number of catagories	A2-1	181
n	sample size	A2-3	183
p	Power	4-3	99
s	Specific gravity of sediment	3-1	70
$s_p$	Standard error of sample	A2-3	183
t	Drop fall time	2-3	37
$t_r$	Receiving water temperature	2-6	57
$u_m$	Wave orbital velocity	A1-1	175
v	Velocity	A5-1	191
$v_i, U_i$	Impact velocity	2-3	37
w	radian frequency	A1-1	175
z	Water depth	2-4	55
$z_\alpha$	Stand. normal deviation	A2-2	181
$\psi$	Shield Parameter	3-2	70

$\chi^2$	Chi square	A2-1	181
$\nu$	Kinematic viscosity	1-1	16
$\mu$	Absolute viscosity	A5-3	192
$\rho$	Water density	2-2	35
$\rho_s$	Bulk density of sediment	A5-1	191
$\sigma$	Surface tension	2-2	35
$\tau$	Drop oscillation time	2-2	35
$\tau_a$	Applied shear stress	4-1	74
$\tau_b$	Wave shear stress on bottom	A1-5	175
$\tau_{ce}$	Critical stress for erosion	4-1	74
$\tau_o$	Bottom shear stress	3-2	70

## ABSTRACT

### THE EFFECT OF RAIN ON INTERTIDAL ESTUARINE SEDIMENT TRANSPORT

by

Thomas C. Shevenell

University of New Hampshire, May, 1986

Storms are important aperiodic events, which intensify erosional processes over short time periods. The effect of rain on the shallow intertidal water column was the focus of this study. The literature was extensively reviewed to identify parallel research in other scientific disciplines, which could be used to understand how raindrops may be acting as a sediment resuspension mechanism. Single-drop and multi-drop laboratory studies were conducted on the initiation of motion of sediment. Results indicate single vortex rings in a quiescent environment can initiate motion of sand-sized noncohesive sediment in all water depths tested, up to and including 22.5 cm. Multidrop experiments (with estuarine muds) indicated that rain can resuspend cohesive sediment at an average rate of  $2.8 \text{ gm/m}^2/\text{hr}$  in water depths to 8 cm. Insitu experiments were conducted to compare the magnitude of rain resuspension with wind wave and boat wake effects. Rain effects were observed in water depths less than 7 cm. In these water depths wind effects were decreasing, because the shallow water

dampened out the larger waves. Observations during two storms illustrated the problem of isolating rain resuspension from wind wave resuspension.

The ability of drops to form vortex rings was utilized in a mixing test of aquaculture tanks used in toxicity testing. Drop-formed vortex rings were more effective in oxygenating the tanks than air bubbling at the strengths typically used for the tests.

# CHAPTER 1

## INTRODUCTION

### General Statement

Erosion and deposition of muddy intertidal sediments are controlled by many physical factors, ( *e.g.* waves, currents, and ice formation ), which temporally and spatially vary in importance (Anderson, 1983). Storms, which may intensify these factors over a short period, are important aperiodic events, that have a pronounced effect in estuarine sedimentation patterns (Laird, 1976). Attention has been focused on the response to storms with respect to fluvial contributions (Schubel, 1971), changes in net-estuarine circulation patterns (Nichols, 1977), and wind-wave resuspension (Anderson, 1972; Gabrielson and Lukatelich, 1985). Another storm related factor is the importance of rain, acting either directly on exposed tidal flats or indirectly through shallow (<50 cm) water. This effect on estuarine sedimentation has only been inferred (Settlemyer and Gardner, 1975; Anderson, 1983 and 1984). Green and Houk (1980) hypothesized that drop-formed vortex rings may be a mechanism to transfer kinetic energy through the water column to the sediments. Laboratory studies of vortex ring dynamics indicate high translational and rotational velocities of the inner ring core may create sufficient shear stresses to initiate sediment movement (Maxworthy, 1977; Sutherland, 1967).

The primary purpose of this study was to investigate rain effects on sedimentation in the shallow intertidal water column. Anderson (1973 and 1980) recognized the importance of sediment resuspension processes at the leading (and trailing) edge of the flooding (ebbing) water. This shallow wedge of water can cover a significant area, because of the low gradient ( $<1$  degree), which typifies a mud flat environment (Anderson, 1980). The scope of this investigation was limited to the mechanics of rain-induced resuspension and the investigation into the ability of rain to resuspend muddy intertidal sediments. The approach to the problem was by a combination of laboratory and controlled field studies. The "microprocess" was studied by using single-drop laboratory experiments. The "net-results" were studied by using rain simulation in both laboratory and controlled field experiments. Field observations during natural events were made to estimate the relative importance of rain as a sedimentation process.

A secondary purpose of this research was to determine if knowledge of drop mechanics could be utilized in solving a practical problem. Aquaculture tanks, used in toxicity testing, require water replenishment and oxygenation, typically accomplished by inflow of new high-oxygen water at a single point and discharge of excess low-oxygen tank water via a drain. Oxygen is also added by bubbling air into the bottom of the tank. A simple experiment was conducted to determine if drop-formed vortex rings could efficiently mix oxygen throughout the tank, eliminating the need for and cost of a separate air supply.

The dissertation is organized with an introductory chapter which first reviews pertinent literature to develop a conceptual picture of rain-induced sediment resuspension, then presents why this process is significant, and finally summarizes the objectives of this study. Chapter 2 presents the

results of single drop studies, which define the important physical characteristics of the splash central jets and the resulting vortex rings. These studies can then be used to develop a conceptual model for the erosion potential of rain on a shallow water column. Chapter 3 presents the results of an experiment in which single drops were used to initiate motion of non-cohesive sediment, after passing through a range of water depths. This study was to confirm that drop-formed vortex rings are a potential mechanism for sediment transport. Chapter 4 expands the investigation of rain as an erosional process by studying the response of the muddy intertidal sediment to rain action, and to determine the importance of rain, relative to other processes such as wind and boat waves, as a physical mechanism in resuspending sediment. Chapter 5 investigates the ability of drop-formed vortex rings to cause bedload movement of the larger aggregates, such as fecal pellets, which are commonly found on the cohesive sediment surface. Chapter 6 investigates the sedimentological characteristics of the muddy intertidal sediment used in the various experiments to see if the rain process significantly modifies the surface texture. Chapter 7 presents a tank oxygenation technique using drop-formed vortex rings. The investigation of the effects of rain on sedimentation in the shallow intertidal water column is concluded in Chapter 8 with a discussion and an identification of areas for future research.

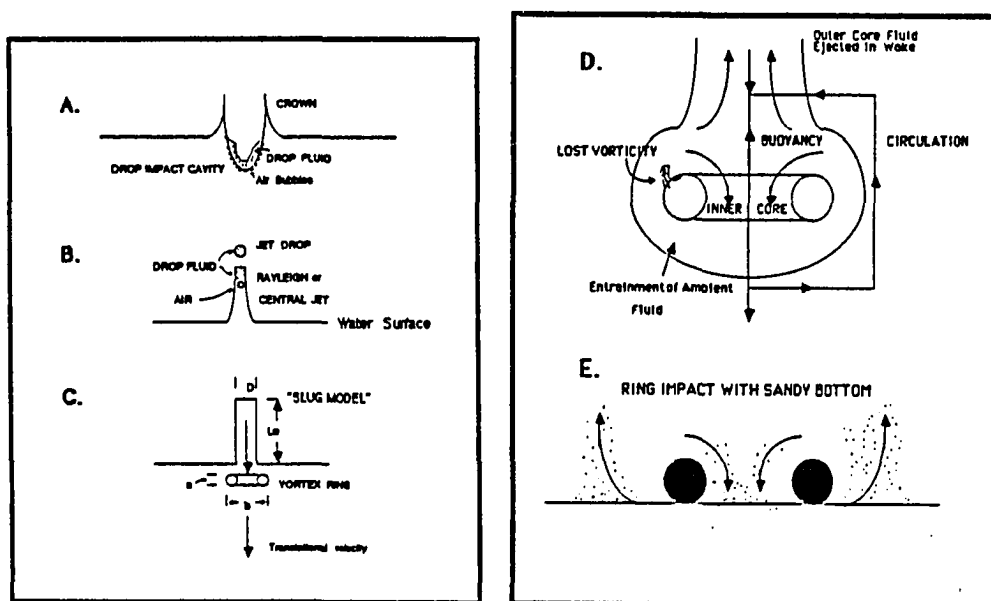
## Literature Review

The ability of rain to affect sedimentation in a shallow water column can be visualized with a conceptual model (Figure 1-1). Consider a single rain drop falling through the atmosphere attaining a terminal velocity and impacting a still water surface. The drop impact initiates a splash sequence, beginning with development of a drop-formed cavity, splash crown and bubble, if the crown closes over the cavity (Engel, 1964). With the loss of momentum, the crown and cavity collapse, a convergent flow develops, and a Rayleigh or central jet forms. Surface tension may segregate the central jet into one or more jet drops (Hobbs and Kezweeny, 1967). Collapse of the central jet (and/or fall of the jet drops) will form surface gravity-capillary waves, and subsurface turbulence or vortex rings (Green and Houk, 1980). If turbulence occurs, energy dissipation is restricted to the near-surface; whereas if a vortex ring forms then mass and energy is transported beyond the turbulence limits. As the vortex ring moves downward in the fluid, ring momentum dissipates and the ring mass disperses into the ambient fluid.

Vortex rings can effect the distribution of suspended sediment. When a rain induced vortex ring forms, it may entrain near-surface suspended matter and transport the material to depth, where it is "deposited" as the ring energy decays. If the rain would strike more dense water (colder or saltier) the ring momentum will eventually be exceeded by fluid buoyancy, causing entrainment and upward transport of suspended matter.

If the waters are shallow enough the vortex ring strikes the bottom and the ring energy is transferred to the sediment via dissipation of impact and shear velocity. The detaching shear stress on the bottom sediment near ring impact are caused by the rotational velocity within the ring's inner core.

FIGURE 1-1. Conceptual model of how a raindrop may affect sedimentation in a shallow water column. (A) The impact of the drop forms an impact cavity and a splash crown. (B) The collapse of the drop cavity causes the formation of the central jet and possibly jet drops. It is the collapsing of this central jet, which forms the vortex ring. (C) The central jet can be compared to a "slug model," which has been used to define and describe the formation of vortex rings. The dimensions of the slug control the dimension of the vortex ring and its transitional velocity. (D) The vortex ring is comprised of two components, an inner core and an outer core. The inner core consists of rapidly rotating fluid which has very little exchange with the outer core. The outer core moves very slowly, but readily exchanges with the receiving water by injecting fluid into the wake of the downward moving ring. (E) If the ring impacts the bottom the rotational velocities are strong enough to initiate motion of sediment.



Sediment may also be detached by direct impact of the ring mass with the bottom. Once motion is initiated, other physical mechanisms, such as weak tidal currents may transport the sediment.

Rain action may also cause secondary effects on other physical processes. for example: (1) dampening wave action (Houk, 1975; Reynolds, 1875); (2) decreasing currents by creating surface shear (Glass and Smerdon, 1967); (3) increasing density stratification (Katsaros, 1969); and (4) transferring momentum to settling particles (Bhuiyan *et al.* 1971).

### **Single-Drop Mechanics**

A drop falling at terminal velocity has an oblate shape in response to a balance between surface tension and the hydrodynamic and aerodynamic forces (Pruppacher and Pitter, 1971). However, natural rain drops vary greatly from this static shape because of modification by non-equilibrium forces (Jones, 1959; Jamison and Beard, 1982). Beard and Johnson (1984) suggest that the mechanism for forcing drop oscillation include: (1) turbulence of shear; (2) drop collision; and (3) resonance with the wake shedding frequency. Exactly how the shape changes near impact is not clear. This is because of the changes in the air turbulence near the ground. Drop shape and fall velocities have been investigated in detail in still air (Laws, 1941; Gunn and Kinzer, 1949; Spilhaus, 1948; Dingle and Lee, 1972; Berry and Pranger, 1974; Banks, 1978; and Beard and Johnson, 1984).

The splash sequence, when a drop hits a water surface, has been studied using high speed photography (Worthington and Cole, 1897; Engel, 1964 and 1967; Harlow and Shannon, 1967; Mutchler, 1967; Hobbs and Kezweeny, 1967; Macklin and Hobbs, 1969; Siscoe and Levin, 1971; and Macklin and Metaxas, 1976). Several studies have recognized that drops hitting a liquid

surface can form vortex rings (Rodgers, 1858; Thompson and Newell, 1885; Worthington, 1894; Blanchard and Woodcock, 1957; Chapman and Critchlow, 1967; and Carroll and Mesler, 1981).

How the drops form the rings has not been investigated quantitatively. Blanchard and Woodcock (1957) observed vortex rings forming when the central jet collapsed. Carroll and Mesler (1981) believe that the pinch-off jet drop, commonly observed above the central jet, forms the vortex ring. Chapman and Critchlow (1967) observed vortex rings forming without first creating the Rayleigh jet, when drops fell less than their splashing height. Not all drops will form vortex rings. Drops may form bubbles and/or disorganized turbulence. Chapman and Critchlow (1967) believed that this was related to the drop-shape oscillation. They observed that the most energetic vortex rings were produced when the drop impacted the surface as a sphere, going in shape from an oblate to a prolate spheroid.

The hydrodynamics of vortex rings has been studied theoretically (Batchelor, 1967; Whitehead, 1968; Maxworthy, 1972; Esudier and Maxworthy, 1973; Norbury, 1973; Widnall and Sullivan, 1973; and Linden, 1973), as well as in laboratory studies (Banerji and Barave, 1931; Krutzsch, 1939; Turner, 1957; Magarvey and MacLatchy, 1964a; Chapman and Critchlow, 1967; Oshima, 1972; Chen and Chang, 1972; Maxworthy, 1974 and 1977; Baird *et al.*, 1977; Rohatgi *et al.*, 1979; and Carroll and Mesler, 1981). All of the above laboratory studies used an orifice technique to form the vortex ring; whereby, a slug of dyed fluid is forced through a circular orifice by a plunger to produce the ring. The resulting ring dynamic history is then a function of the injection impulse. Magarvey and MacLatchy (1964b) investigated the disintegration of vortex rings upon collision with the boundary. Sutherland (1967) and Falco (1977) used vortex rings to

approximate turbulent phenomena in the boundary layer. Sutherland's work was used to investigate sediment transport by turbulent flow.

## **Rainfall**

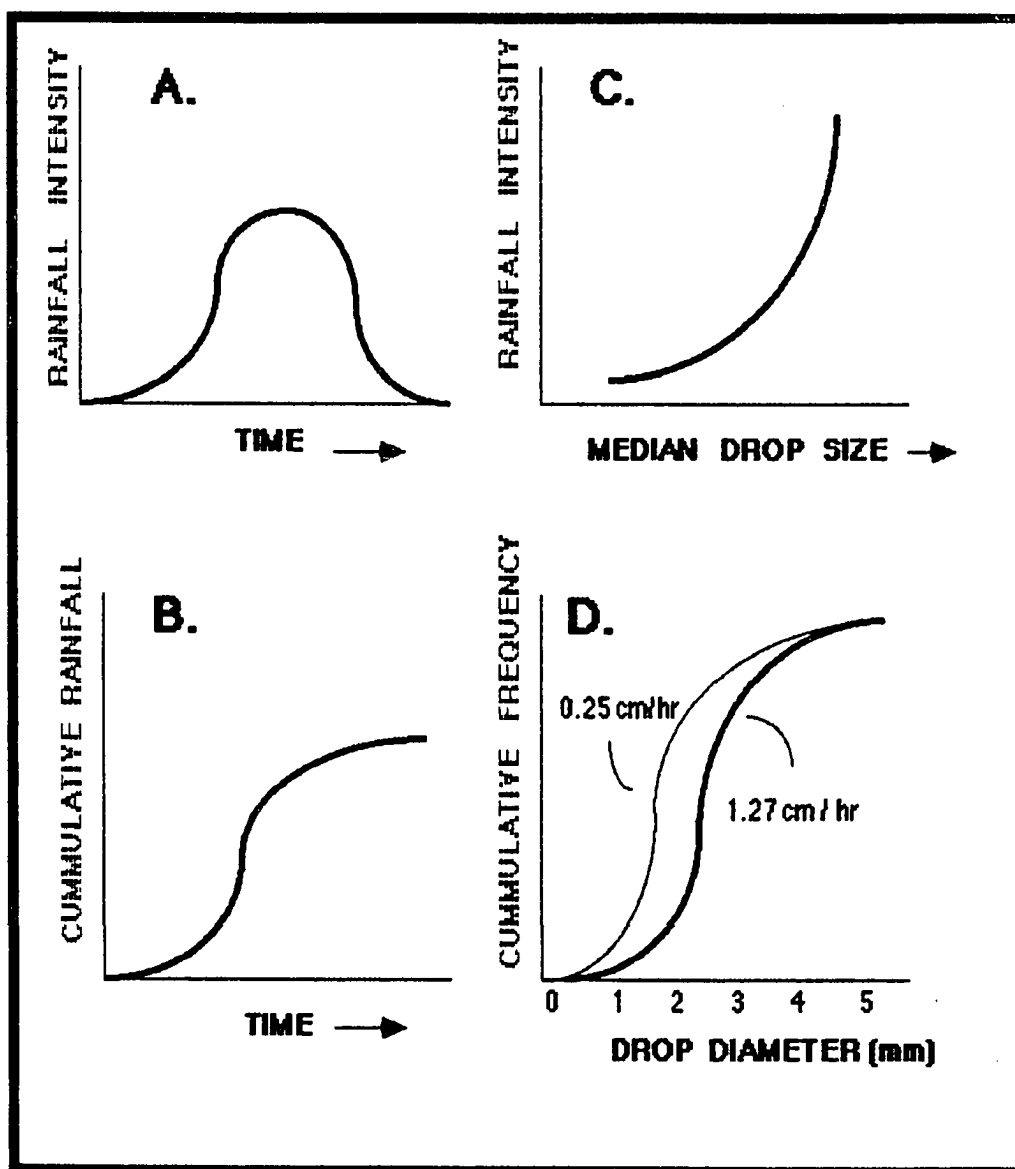
Rainfall characteristics vary considerably depending upon location and type of rainfall event. The important characteristics in defining a rainstorm for erosion problems are (1) intensity, (2) drop-size distribution, and (3) duration (McCool, 1979). Storm impact on a particular intertidal area will depend upon how fast the storm moves through the area, the lateral extent of the storm, and the duration of the peak intensity of rainfall.

Cyclonic precipitation is typical of the rainfall events in the field study area. This type of precipitation event, which includes warm, cold and occluded fronts, is caused by the lifting of air masses, due to pressure differences (Luthin, 1966). The steady rains and thunderstorms, common in cyclonic precipitation, provide for the maximum erosion potential.

Rainfall intensity varies with time into a storm, as illustrated in Figure 1-2. The one-hour rainfall expected once in ten years in the Northeast is 43 mm/hr (Luthin, 1966). The 2-yr., six-hour rainfall for the Northeast is 9.3 mm/hr (Hershfield, 1961). Thunderstorms are important storm events, which exhibit very high rainfall intensities over short duration. McCool (1979) observed that in one hour 16 to 65% of all rainfall occurs for a given storm (Figure 1-2B).

The drop size distribution varies as a function of rainfall intensity (Mutchler and MacGregor, 1979). Laws and Parsons (1943) related the median drop size, as determined by the volumetric distribution, to intensity. This relationship gives a median diameter of 1.86 and 2.45 mm for the 9.3

FIGURE 1-2. Diagrammatic distributions of important rainstorm parameters. (A) Rainfall intensity varies with time into storm. (B) Cumulative amount of rainfall with time into storm, with most rain occurring in less than the first hour. (C) The median drop size increases rainfall intensity. (D) Cumulative drop-size distribution for two rainfall intensities indicates that the entire drop-size spectra increases with intensity.



and 43 mm/hr intensity storms (Figure 1-2). The maximum size of raindrops has been reported by Laws (1941) to be 6.1 mm.

The impact velocity is related to drop size. Terminal velocity is reached by most drops from a fall distance of 20m, and ranges from 485 cm/sec for 1.25 mm drops to 930 cm/sec for 6.0 mm drops (Laws and Parsons, 1943). It is believed that impact velocities may be different than terminal in the natural environment because of superimposed wind velocity (Van Dorn, 1953; and Caldwell and Elliot, 1971) and turbulence (Bubenzer, 1979) in the boundary layer near the water surface.

### **Rain and Sedimentation**

Rain on shallow water will act to change the level of turbulent motion. Although most rain induced energy is dissipated near the surface, drop-formed vortex rings can penetrate to depths exceeding 0.4 m (Houk, 1975). This increased motion will have an effect on the capacity of the water to transport sediment. However, the effect of turbulence on particle settling is still debated. Fine-particle settling tends to be decreased by turbulence (Torobin and Gauvin, 1960; Businger, 1965; and Murray, 1970). This decrease has been explained theoretically, as a non-linear drag response due to changes in fluid speed relative to the particle (Murray, 1970). However, this observation assumes isotropic turbulence, which is very rare in the natural environment, and is probably not the case in rain-induced water motion. Bhuiyan *et al* (1971) observed the opposite effect in an experiment in quiescent water, where rainfall increased the settling rate of clay-sized particles.

Rain effects in flowing water is more difficult to interpret. Glass and Smerdon (1967) observed that rain reduced the mean flow by making the

vertical distribution of velocity more uniform. Barfield (1968) observed that rainfall tends to decrease the turbulent time scales of flowing water.

Smerdon (1964), in channel flow 2.3 to 14 cm deep, observed that rainfall not only decreased the ability of flow to erode the sediment surface, but also reduced the suspended sediment capacity of the flow. In contrast, Walker *et al* (1978) conclude that rain increases the transport capacity of sheet flow, less than 7 mm deep. They stressed the importance of impact frequency, rather than energy, in the sediment erosion process. This is analogous to the high energy "bursting" mechanism used by Sutherland (1966 and 1967) to describe entrainment of fine sediments by turbulent flow.

### **Sediment Response**

The response of sediment to bursts of high flow, such as vortex rings or strong turbulent eddies of flowing water, is dependent upon the force transferred to the particles on the sediment surface. The classical concept is that for erosion to occur, the hydraulic shear stress must exceed the critical shear stress of the sediment (Ariathurai and Krone, 1976). Sutherland (1966) expanded this concept to include lift forces, due to the presence of high velocity gradients in the flow. The response of cohesive muds to excess shear is different than non-cohesive sediments, because erosion is not only particle by particle, but also by mass erosion.

The approach to understanding sediment transport has been primarily by laboratory studies (*e.g.* Einstein, 1950; and Bagnold, 1966); however, significant deviation between theory and field observation typically occurs (White *et al.* 1975). This difference is probably due to scaling effects, such as the way the sediment beds were prepared for the laboratory study. Typically laboratory erosion experiments use either placed or flow deposited

beds, both usually quite different than one would expect in the natural environment.

The ability of cohesive sediment to resist erosion is controlled by properties that radically change if the bed is disturbed. These properties include compaction, desiccation, mucus binding by epifauna and infauna, and mat formation by flora. In addition, the antecedent stress history is quite important in governing the behavior of cohesive sediment (Mehta *et al.*, 1982; Amos and Mosher, 1985)

The muddy intertidal sediment presents a complicated (if not impossible) modelling problem, because of the extremely complex nature of the sediment fabric. This surface consists of cohesive flocculates and aggregates of clay and organic particles. Fecal pellets dominate the surface. Some of the feces (*e.g.* *Streblospio* *Benedicti* Webster, 1879) and pseudofeces are loosely bound together and easily disintegrate at very low shear stress. Other fecal pellets, such as those from *Heteromastus filiformis* (Claparède, 1864; Polychaeta, Capitellae) and *Macoma balthica* (Linnaeus, 1758; Bivalvico, Tellinidae), are quite rugged and act as low-density, sand-sized non-cohesive particles. Associated with the fecal pellets is mucus material, which tends to bind the surfaces of the individual pellets and groups of pellets together. Included in the sediment surface is gravel- and sand-sized organic debris. This material is light and irregularly shaped.

The muddy intertidal surface is not flat on the microscale ( $< 1 \text{ m}^2$ ). It typically consists of hummocks and depressions created by epifaunal activity (*e.g.* horseshoe crabs). This surface expression changes seasonally, as does the concentration of fecal material (Rust, 1980; Anderson, 1983).

### **Significance of Rainfall**

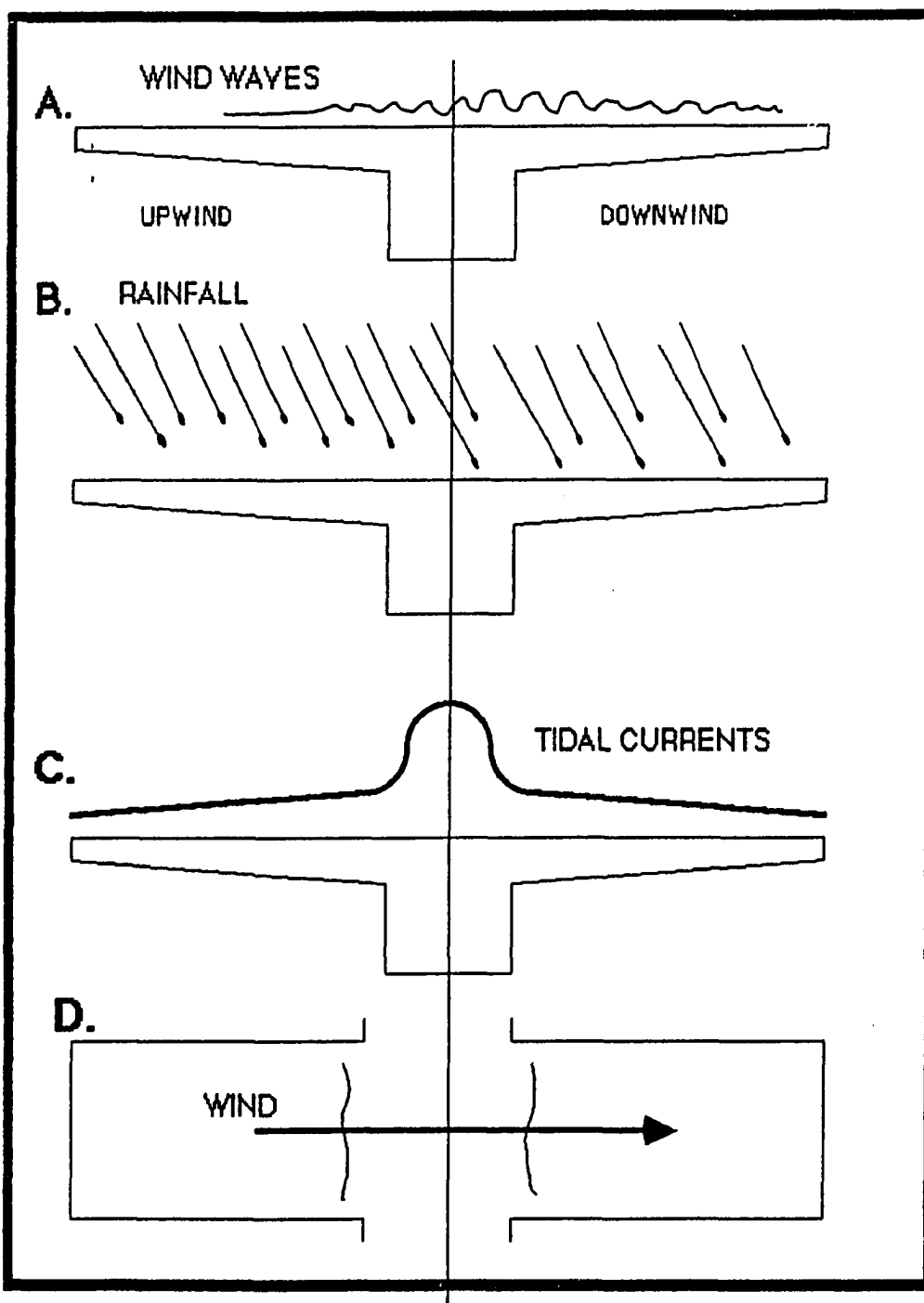
The complexity of sedimentary processes in the muddy intertidal environment can be appreciated by reviewing Table 1-1, which lists the important physical and biological factors, causing erosion or deposition, and how these factors vary seasonally (Anderson, 1983). This study focused on one of the physical factors in detail -- rain. Unfortunately, it is difficult to isolate the effects of rain from the two most common processes affecting tidal flat sedimentation, wind waves and tidal currents. Therefore, to estimate the significance of rain, as a sedimentation process, it is necessary to design appropriate laboratory and field studies.

Intuitively, wind-wave action appears to be the most important physical factor in erosion of muddy intertidal sediments. Tidal currents, although strong in confined channels, tend to be relatively weak in the shallow water overlying broad intertidal areas (Anderson, 1973). A simple picture of how the wind, weak tidal currents and rain may be interrelated, during a storm event, is illustrated in Figure 1-3. Consider a hypothetical estuary, which has two broad intertidal areas separated by a deep channel, and a wind perpendicular to the axis of the estuary (Figure 1-3). The wave heights and periods will vary as a function of fetch, duration and water depth. Consequently, the upwind tidal flat will have much smaller wind waves than the downward tidal flat. Maximum wave activity will occur at the channel edge of the downward flat. Wave heights will decrease across this flat as the larger waves are attenuated in the shallow water (Anderson, 1972; Figure 1-3B). This spatial variability is in contrast to rainfall, which

TABLE 1-1. Physical and biological parameters, which control sedimentation on the muddy intertidal. How each parameter contributes to erosion (E) or deposition (D) is suggested by season (Anderson,1983).

FACTORS	Spring	Summer	Fall	Winter
<b>PHYSICAL FACTORS</b>				
Waves	E	D	E	E
Ice	E			E/D
Rain	E	E	E	E
Groundwater Discharge	E	D	D	E
Mud/Water Temperature	D	E	D	E/D
<b>BIOLOGICAL FACTORS</b>				
Microbiology			D	D
Flora				
Unicellular, motile algae		D		
Algal Mats		D		
Other plants		D		
Fauna				
Bioturbation		E	E	
Pelletization		E	E	
Biodeposition by suspension feeders		D	D	
Epifaunal tracks and depressions		E/D	E/D	

FIGURE 1-3. The effects of physical processes on sedimentation varies spatially in the estuary. (A) Windwaves will be more important on the downwind tidal flat. (B) Rainfall will be randomly distributed over the estuary. (C) Tidal currents are quite strong in the channel but weak over the tidal flats. These conditions would be typical in an idealized estuary with broad tidal flats (D).



will tend to be random over the entire estuary (Figure 1-3C), and to tidal currents, which will be important only in the channels (Figure 1-3D).

Houk (1975) observed that almost all (97.7%) of the rain's kinetic energy flux goes into turbulent dissipation. The depth of mixing in his studies varied from 8 to 42 cm. Although Houk hypothesized that organized vortex ring structures are a mixing mechanism, his studies did not differentiate the turbulence and vortex ring components (Green and Houk, 1979). This differentiation is important from a sedimentological point of view, because the rings have the ability, if formed, to transport mass and energy to depths much deeper than disorganized turbulent eddies. In addition, the circulation of the inner core of a vortex ring is sufficiently intense to cause a significant shear stress at impact with the bottom.

If drop-formed vortex rings are important in resuspending bottom sediments, then it must be demonstrated that they can survive in a turbulent natural environment. For an initial approach to this problem, a dimensionless parameter can be calculated, which match the forces trying to maintain the structure of the ring, with the turbulent forces in the surrounding water, which are trying to break up the ring. The Reynolds number (Re) would be the most appropriate parameter, since it is a ratio of inertial to viscous forces. The general form is

$$Re = \frac{UD}{\nu} \quad (1-1)$$

where U = velocity  
 D = diameter  
 $\nu$  = kinematic viscosity.

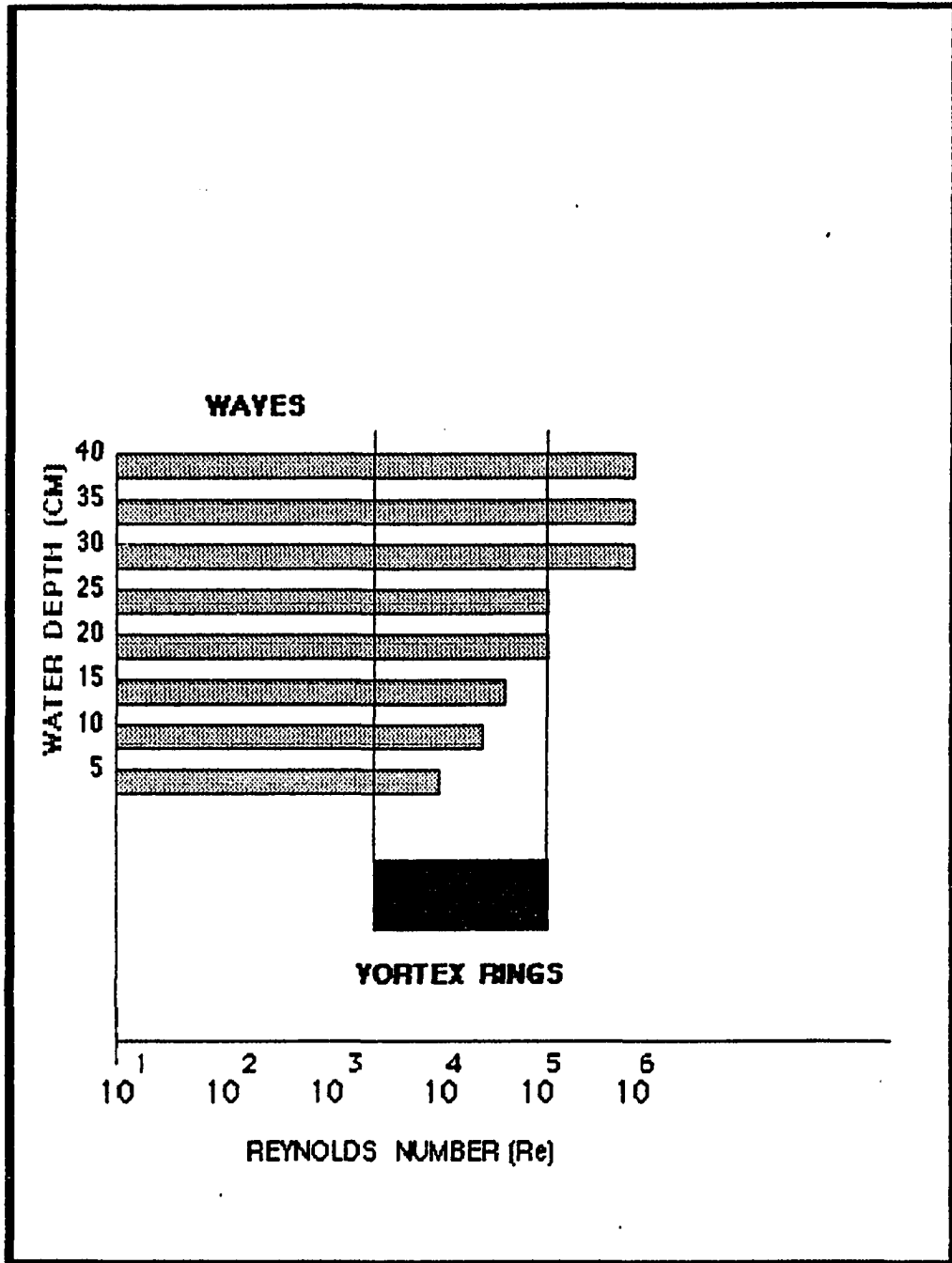
Maxworthy (1977) in his study of vortex rings calculated a ring Reynolds number by using the ring translational velocity, and the radius of the orifice through which the ring was generated (Figure 1-1). The Reynolds number for the rings studied by Maxworthy (1977) ranged from 2000 to 70,000 (Figure 1-4). By using Solitary Wave Theory to estimate the velocity and radius of the wave orbital at the water surface (U.S. Army Corps of Engineers, a similar Reynolds number for wind wave turbulence can be derived. The distribution of  $Re$  for waves, which can exist in water depths of 2.5 to 40 cm, range from 100 to 200,000 (Figure 1-4). The distribution of Reynolds numbers for the vortex rings and wind waves coincide, suggesting that a quiescent environment may not be needed for vortex rings to persist.

A second approach to assessing the significance of rain, relative to tidal currents and wind waves, is to compare gross energy dissipation rates for each process. Tidal energy dissipation has been estimated for the Great Bay Estuary, site of our field experiment, by Trask (1979). The average tidal energy dissipation ranged from 5.4 to 390 ergs/cm<sup>2</sup>/sec. Although Trask did not differentiate between the channel and the tidal flat regimes, one would expect much lower rates on the tidal flat, because frictional energy dissipation is a function of the current speed squared (Filloux, 1973).

Wave energy dissipation will result when waves exert a shear on the bottom. The rate of dissipation is equal to the loss of wave motion energy (Madsen, 1979). For waves in 20 cm of water, with a 1.0 sec period (typical for the field study site; Anderson, 1972), the calculated rate of energy dissipation ranges from 1 erg/cm<sup>2</sup>/sec for a 1 cm wave height to 222 ergs/cm<sup>2</sup>/sec for a 15 cm wave height.

Rainfall energy dissipation has been related to rainfall intensity by Wischmeier and Smith (1978). For a rainfall intensity of 43 mm/hr, the

FIGURE 1-4. Distribution of wave Reynolds numbers for short period (0.5 to 1.5 sec) waves in water depths from 5 to 40 cm, using Solitary Wave Theory. The range of Reynolds numbers for vortex rings used by Maxworthy (1977) in laboratory studies is shown for comparison.



dissipation rate is  $7.2 \text{ ergs/cm}^2/\text{sec}$ . This implies that there is a reasonable amount of energy associated with a moderately intense storm which can affect sediment transport.

As discussed, the spatial distribution of energy dissipation will vary for each source (Figure 1-5). This may have implications in terms of sedimentation processes within the estuary during a storm event. The upwind intertidal areas of the estuary may be rain dominated to the point where the water depth and fetch are sufficient for wind waves to cause sediment transport. On the downwind intertidal, wave action will be the most important process, perhaps, overwhelming any effects of rain or tidal currents. Currents will be important, only in the channels and the outer margins of the tidal flats.

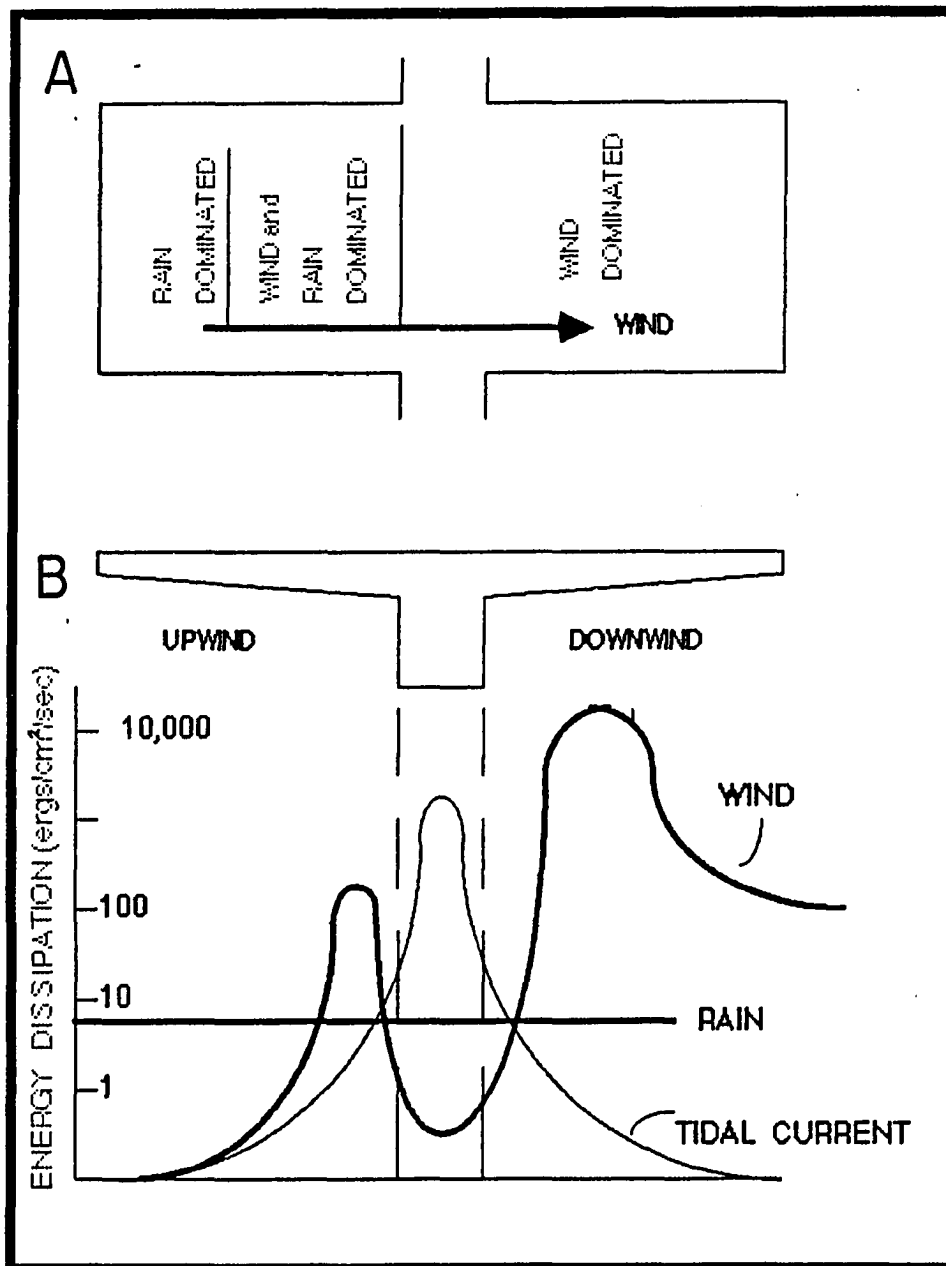
In summary, it appears that rainfall has the potential to be the most significant process on the upwind portions of the intertidal area, when the water is shallow ( $<50 \text{ cm}$ ), and wind waves are moderate ( $<5 \text{ cm}$  in height). It is with this justification that a better understanding of how rainfall acts as a sedimentation process is needed to fully understand the effects of a storm event in the estuarine environment.

### **Objectives**

The purpose of this investigation is to develop a better understanding of the role that rain plays in modifying estuarine sedimentation patterns during storm events. A secondary purpose was to identify a practical application for the use of drop-formed vortex rings. The objectives of this study are as follows:

1. Determine, in the laboratory, the percentage of drops which form

FIGURE 1-5. The effect of rain on an idealized estuary with broad tidal flats is shown in A. Rain should be a dominant process on the upwind tidal flat, where the fetch is too short for large wind waves to develop. The downwind tidal flat should be dominated by wind waves. An hypothesized spatial distribution of energy dissipation for rain, wind waves and tidal currents is shown in B. Tidal currents are strongest in the deeper channels. Wind energy will be greatest on the downwind tidal flat, except when the water depth is too shallow for the larger waves to penetrate. Rain energy will be uniform across the entire estuary if the rainfall intensity is uniform.



- vortex rings, rather than turbulence or bubbles.
2. Determine the physical properties of drop-formed vortex rings, including depth of penetration, dimensions and translational velocity profile.
  3. Determine the ability of vortex rings to initiate motion of sediment after passing through a range of water depths.
  4. Determine the resuspension ability of artificial rain with an estuarine mud substrate.
  5. Determine in the field, using artificial rain, the maximum depth of water in which rain can resuspend bottom sediment.
  6. Observe changes in suspended sediment concentrations, during storm events, to estimate the importance of rain.
  7. Develop a practical application for the use of drop-formed vortex rings.

## **CHAPTER 2**

### **MECHANICS OF DROP-FORMED VORTEX RINGS**

#### **Introduction**

The series of processes to transfer rain energy through a shallow water column to a sediment covered bottom are relatively complex. Therefore to better understand this mechanism, single-drop laboratory studies were conducted to describe these processes in a deterministic fashion. Although interaction effects are important, the single-drop studies can be used to conceptually model the effectiveness of rain as a sediment resuspension mechanism in a shallow water column. The model can then be tested using multidrop experiments and observations during natural rainfall events.

The single-drop studies were conducted in five separate experiments. These experiments are organized into four parts. Part 1 investigates how the drop impact controls the initial development of the vortex ring. Drops may cause either a splash central jet or bubbles; a central jet is needed for vortex ring formation. In addition, the nature of the drop-shape oscillation at impact may enhance vortex ring formation (Chapman and Critchlow, 1967). Part 2 investigates the central jet characteristics, how they are influenced by drop impact energy and water temperature, and how the drop energy relates to the vortex ring momentum. Salinity or density considerations were qualitatively observed, but were not tested in the single-drop studies, because accurate measurement of the surface water salinity was not possible. Part 3 develops the vortex ring characteristics, (*i.e.* inner core

dimensions, translational velocity and depth of penetration). Part 4 studies the ability of the vortex rings to initiate motion of non-cohesive sediment and is the topic of Chapter 3.

## **Methodology**

### **Experimental Procedure**

**Drop Formation.** Drop water was prepared from tapwater by the addition of water soluble red fluorescent dye. The density of each dye batch, although not significantly different than tapwater (greater by 0.000749 gm/cc), was determined by hydrometer. Dyed water was used for all experiments except Experiment 3 (Table 2-1). Drop temperature was maintained at approximately room temperature, and measured with a lab grade thermometer ( $\pm 0.2$  C) at the start and end of each run or set.

Drops were formed from either hypodermic needles or tubing (Figure 2-1), serving as capillary drip ends (Table 2-2). Silicone tubing with a 0.33 mm inside diameter (ID) was used as the flow restrictor between the drop fluid reservoir and the drip end. This technique produced relatively uniform drops. The size of the drop depended primarily on the tip diameter, and secondarily on surface tension and flow rate (Robinette and McCool, 1984). The flow rate was controlled by using either gravity feed (Experiment 3) or a Masterflex pump (Head No. 7013) with an electronic timer-dispenser (Figure 2-1). The rate of drop production was approximately 1 per 3 seconds. This time interval was sufficient to allow dissipation of the surface waves between drops (Siscoe and Levin, 1971).

Drop diameter was determined by collecting duplicate samples of 25 drops each in preweighed beakers. The drop volume was estimated using the fluid weight and density. Drop diameter was computed from drop

FIGURE 2-1. Schematic diagram of the experimental set up used to investigate the single drop-formed splashes and vortex rings. Two drops sizes depending upon the needle and/or adaptor size fell fixed distances to a receiving water tank. Scales were provided to measure fall distance, and dimensions of the splash and vortex ring. Drop rate was controlled by using a pumping system (S) with a timer (T) dispenser switch (S). The resultant splash and/or vortex ring was recorded on a video system. The water temperature was monitored with thermistors.

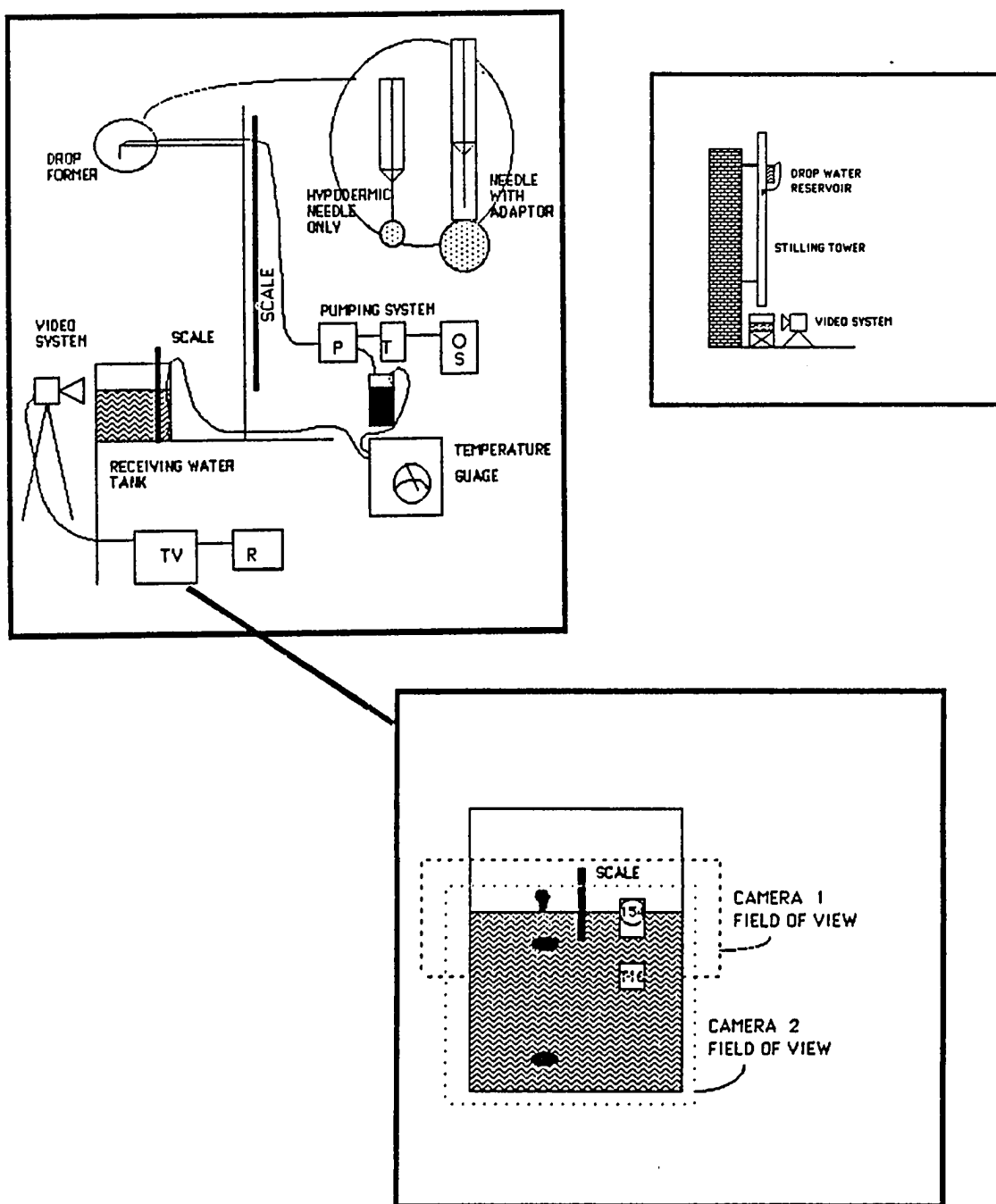


TABLE 2-1. Summary of experimental operations.

OPERATION	EXPERIMENT				
	1	2	3	4	5
Experiment Location	Lab	Lab	Stilling Tower	Lab	Lab
Drop Water	Dyed	Dyed	Undyed	Dyed	Dyed
Drop Generation	Masterflex Pump	Masterflex Pump	Gravity	Masterflex Pump	Masterflex Pump
No. Drops Per Set	Variable	25	100	50	100
Drop Heights	7-160cm	1-184cm	50-600cm	50-125cm	120cm
Receiving Tank Dimensions	14cm ID	14cm ID	30x240cm	15x14cm	14cm ID
Depth	18cm	18cm	40cm	16cm	Variable
Data Recording	Manual	Manual	Video	Video	Manual

Table 2-2. Drop formers used in each single-drop experiment.

TIP NO.	DROP SIZE	DESCRIPTION OF TIP USED	TIP ORIENTATION	EXPERIMENT				
				1	2	3	4	5
20V	0.242cm	26g SS Hypodermic	Vertical			X		
11V	0.304	21g SS Hypodermic	Vertical			X	X	
10V	0.330	18g SS Hypodermic	Vertical			X		
11	0.367	21g SS Hypodermic	Horizontal			X		
10	0.399	18g SS Hypodermic	Horizontal			X		
15	0.469	0.32cm ID Silicone Tubing	Vertical	X	X	X		
16	0.545	0.20cm ID Silicone Tubing	Vertical			X	X	X

volume by assuming a spherical shape. Drop diameter was varied depending upon the purpose of each experiment (Table 2-2).

Drop fall height was measured ( $\pm 0.5$  cm) from the needle end to the water surface. Drops were allowed to fall in calm air by conducting experiments either in the lab or outside in stilling towers (Figure 2-1; Table 2-1). Two stilling towers were used in Experiment 3, depending upon drop size. The larger drops fell through a 10 cm ID PVC pipe and the smaller drops through a plastic covered 30 cm square tower. The tower tops were closed and the tower extended to within 30 cm of the water surface to minimize any updrafting of air. The larger tower was needed for the smaller drops because of the observed side-wall effects in the smaller tower. Migration of drops toward the tower wall was probably due to the electrical charge differences between the wall and the drop (Engel, 1964), rather than boundary effects (Vanoni, 1977).

**Receiving Water.** The receiving water tanks varied in dimensions depending upon the purpose of the experiment (Table 2-1). Tapwater was used in all experiments. Except for Experiment 4, the water was allowed to equilibrate with atmospheric temperature. In Experiment 4 the tank water was cooled with ice to obtain 9-10° C water; heated tapwater was used in the 50° C receiving water tests. Temperature was monitored near surface for all experiments, and also near bottom for the vortex ring experiments. Either a laboratory grade thermometer or a YSI thermistor ( $\pm 0.2$  C) was used to make measurements. Special procedures unique to each experiment are summarized in Appendix 2A.

## **Analytical Procedure**

**Experiment 1.** This experiment consisted of several tests to determine the number of drops required to have statistically valid vortex ring data sets (Appendices 2A, 2B and 2C). The procedure was to first determine if a drop created a vortex ring, if not it was so noted. When a ring was produced it was categorized as either well-formed (a tight well-defined inner core with a high translational velocity) or marginal (a diffuse inner core moving slowly through the water column). The observations were then used in Chi Square analyses to determine significance in the observed ratio between ring formation and no ring.

**Experiment 2.** This experiment studied the effect of drop height on the formation of vortex rings. The rings were tallied as described above. The impact velocity from each drop height was calculated using the results of Laws (1941).

**Experiment 3.** This experiment studied the effect of drop energy on the splash central jet formation. Data collection was with a video system. Data on the splash characteristics were collected using a Panasonic color video camera (WV-3150) with recorder (NV-8420) and color display (CT-160). The recorded field of view was scaled to maximize the dimensions of the splash features. A metric scale was included in the video record at approximately the same depth of field as the splash. A status card, which included tip number, drop height and run data, was also included to document the splash sequence (Figure 2-1).

One hundred splashes from each of four heights (50 to 125 cm in 25 cm increments) were enumerated into three categories: (1) jet; (2)

jet/bubble complex (this was where the bubble did not completely close, but there was distortion of the central jet); and (3) bubble. Detailed measurements of jet height, cross-sectional area and impulse time were made on five jets, or those jets available. The measurement procedure is provided in Appendix 2D.

**Experiment 4.** This experiment investigated the relationship between the splash characteristics and the resultant vortex ring. The splash data were collected and reduced as described above. A second video camera and recorder system (Canon) was used to collect the vortex ring dynamics data. A digital stopwatch was positioned in the field of view of both cameras, allowing cross-referencing between splash and resultant vortex ring features.

Data reduction varied depending upon the parameter of interest. The time of impact, if a vortex ring formed and the depth of ring penetration were noted for all drops. Ten central jets (five jets that formed vortex rings and five which did not) were selected from each 50 drop set and analyzed in detail (Appendix 2D).

The vortex ring translational velocity distribution was computed for three well-defined rings for each temperature, drop size and height combination. The velocity was determined by noting the time of maximum cavity formation, after the collapse of the central jet. This was considered the ring start time. The video record was advanced frame-by-frame, and the time and depth of the rings was recorded. Velocity between the observations was computed from the change in depth versus the change in time. The accuracy of the velocity determination was limited by the speed of the video recorder, clarity of the ring and the readability of the digital

watch. Where visibility allowed, the horizontal and the vertical dimensions of the vortex ring inner core were measured.

### **Experimental Error Analysis**

**Drop Size Variability.** Eleven tests were conducted to determine temperature and dye concentration effects on drop size variability (Appendix 2A). Three drop temperatures were tested, 9-10°C, 20-25°C and 41-42°C. Dye concentration was varied from 290 to 1820 ppm. An analysis of variance indicated significant variability between runs at the 95% confidence interval (CI). Grouping the tests by temperature and dye concentration to eliminate variability within a group resulted in no significant relationship between drop size and either temperature or dye concentration. The drop size range when all data (3225 drops) are pooled was 0.449 to 0.479 cm with a mean of 0.464 cm and a standard deviation of 0.01cm. Based upon this error analysis, effects of dye and temperature on drop size were considered minimal. The reason for different drop sizes from the same tip may have been due to aging of the tips with time (McCool and Robinette, 1984). Therefore, drop size was measured for each experiment and each tip used (Appendix 2A), but was considered constant during each experiment.

**Sample Size Analysis.** The sample size for the number of raindrops needed to reach a desired level of precision required a previous knowledge of the population percentage (*e.g.* the ratio between the number of raindrops to the number of vortex rings), which one would expect to observe. Knowing this percentage, setting an acceptable level of significance, and defining a

range within which the data should fall, a better estimate of the requisite number of observations was made (Richmond, 1964).

A pilot study was conducted using six sample sizes (25, 50, 75, 100, 150 and 200 drops) for seven drop heights to estimate the optimum sample size. This was required because we lacked prior knowledge on the expected percentage of vortex rings produced by the drops. This study provided a set of observed frequencies which could be tested against theoretical distribution models, using a single classification technique for Chi Square. The results of this study are presented in Appendix 2B.

Three hypothetical Groups were tested against the observations. Group A where one out of three drops produced a ring, Group B where one out of two drops formed a ring, and Group C was where four out of five drops formed rings. The analytical results suggest that a sample size of 25 drops can distinguish between the two extremes, *e.g.* Group A and Group C (see Appendix 2B for details). A sample size of 150 drops or more was needed to distinguish between the three observed populations at the 95% CI. Based upon this analysis and the experimental limitation that about 50 drops obscured the visibility of the dyed ring in the receiving water, a sample size of 25 drops was used for subsequent experiments.

## **Results**

### **Controls on Vortex Ring Formation**

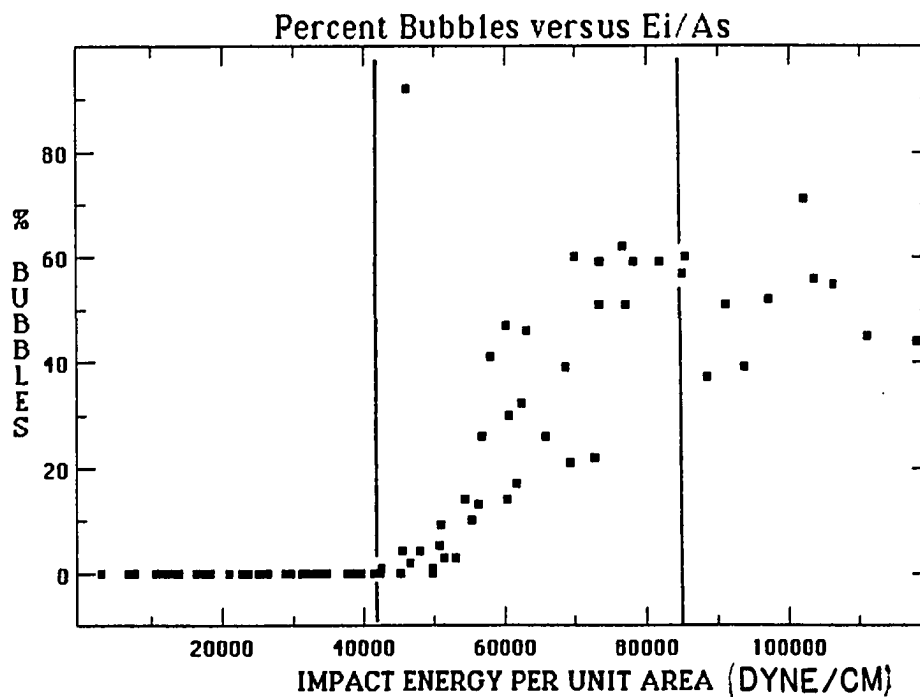
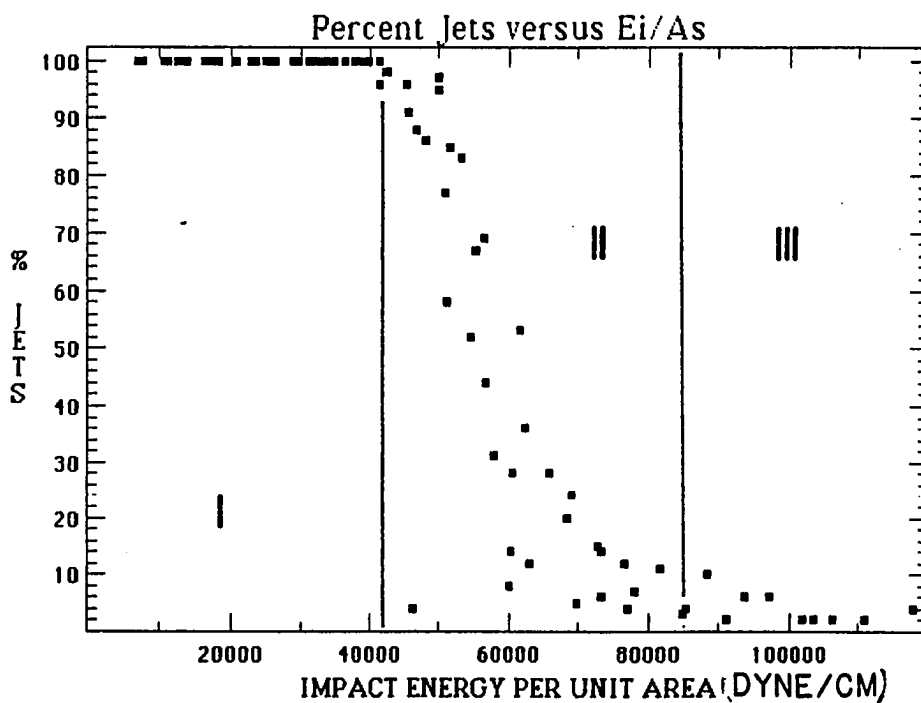
The formation of the drop-formed vortex ring is due to an impulse created by the collapse of the splash central jet (Blanchard and Woodcock, 1957). There are two effects that impacting drops may have on controlling the nature and frequency of the vortex rings. The work of Engel (1967), and

Macklin and Metaxas (1976) show that the formation of the central jet is directly related to the impact energy. Macklin and Metaxas (1976) observed from Engel's work that the splash crown edge collapses to form a spherical bubble over the cavity, when the drop impact energy exceeds a critical threshold. If drop impact energy is greater than this threshold, no vortex rings will form because no central jets form. Chapman and Critchlow (1967) observed that drop-shape oscillation was important in creating energetic vortex rings. They observed that the best rings were formed when the drop shape at impact was spherical changing in shape from an oblate to prolate spheroid.

Two experiments were conducted to evaluate these two effects on the vortex ring formation. The first experiment was to identify the impact energy threshold at which no central jets were formed. The second experiment was to determine if the change in drop shape could influence the probability of vortex ring formation.

**Central Jet Formation.** The physical properties of the splash central jet were evaluated over a range of impact energies. A range of drop sizes (0.255 to 0.545 cm) and drop heights (50 to 600 cm) were used to develop the impact energy range of 35.8 to 31,200 dyne/cm. When considering just impact energy of the drop, as proposed by Macklin and Metaxas (1976), a step function in the percent jets versus impact energy distribution was observed. The energy level at which splash bubbles began forming was different for the smaller drops than the larger drops. Considerable improvement in defining the step function for both drop sizes was obtained by normalizing the impact energy ( $E_i$ ) by the cross-sectional area ( $A_g$ ) of the drops (Figure 2-2). The percent jet distribution was also tested against drop

FIGURE 2-2. Scatter plots of percent bubbles (A) and percent jets (B) versus impact kinetic energy divided by the spherical drop area. The energy distribution is divided into three zones based upon the distribution of bubbles and jets. Zone I represents all jet formation, Zone II represents a transition zone to very low percentages of jets, and Zone III represents primarily bubble formation with few jets.



momentum and an elliptical drop impact area (Spilhaus, 1948), but neither improved the resolution in the percent jet distribution.

Three impact energy zones were identified by the distribution of percent jets and bubbles (Figure 2- 2). The limit of no jet formation was not reached in this experiment. However, the experiments extended through a transition from all drops forming jets to very few drops forming jets. Below an energy level of 42,500 dynes/cm, all drops formed central jets (Zone I). A transition zone (Zone II) was observed between 42,500 and 75,000 dynes/cm, where the percent jets linearly decreased as impact energy per unit area ( $E_i/A_s$ ) increased. This transition can be described by the linear regression (R-squared = 0.841):

$$\% \text{ Jets} = 231 - 0.00154(E_i/A_s) \quad (2-1)$$

At energy levels above 75,000 dynes/cm, less than 15% jets were formed. The asymptotic nature of the percent jet scatter, and the highly variable scatter in the percent bubble versus impact energy per unit area (Figure 2-2B), make it impossible to estimate from these data an upper limit of impact energy for jet formation.

The energy range of this experiment covered 65% of the expected energy range of drops 0.125 to 0.6 cm diameter falling at terminal velocity (Laws, 1941). Zone II or the transition zone would correspond to 0.25 to 0.325 cm drops falling at terminal velocity. Thus for a 1.27 cm/hr storm, which could occur for a three-hour period and have a return period of two years in the New England area (Bubenzer, 1979), 72.8% of the drops by volume would have an impact energy per unit area in Zone I; 20.4% in Zone II; and 6.8% in Zone III.

**Drop Shape Oscillation.** A detailed study of vortex ring production as a function of drop height from 1 to 184 cm was conducted using a 0.464 cm diameter drop. There was not a simple relationship between drop height and resulting vortex ring production (Figure 2-3). Using the same statistical approach as in the sample size analysis, drop height zones were identified, where there were statistically significant (95% CI) differences in vortex ring production. Three out of four drops (Group C) formed vortex rings at heights of 1-2 cm, 15-23 cm and 100-134 cm. At heights of 5-9 cm, 38-61 cm and 165-184 cm only one out of three drops (Group A) formed vortex rings (Figure 2-3).

Changes in drop shape at impact may influence the ability of the drops to produce vortex rings. The drop oscillation time ( $\tau$ ) is defined by Chapman and Critchlow (1967) as

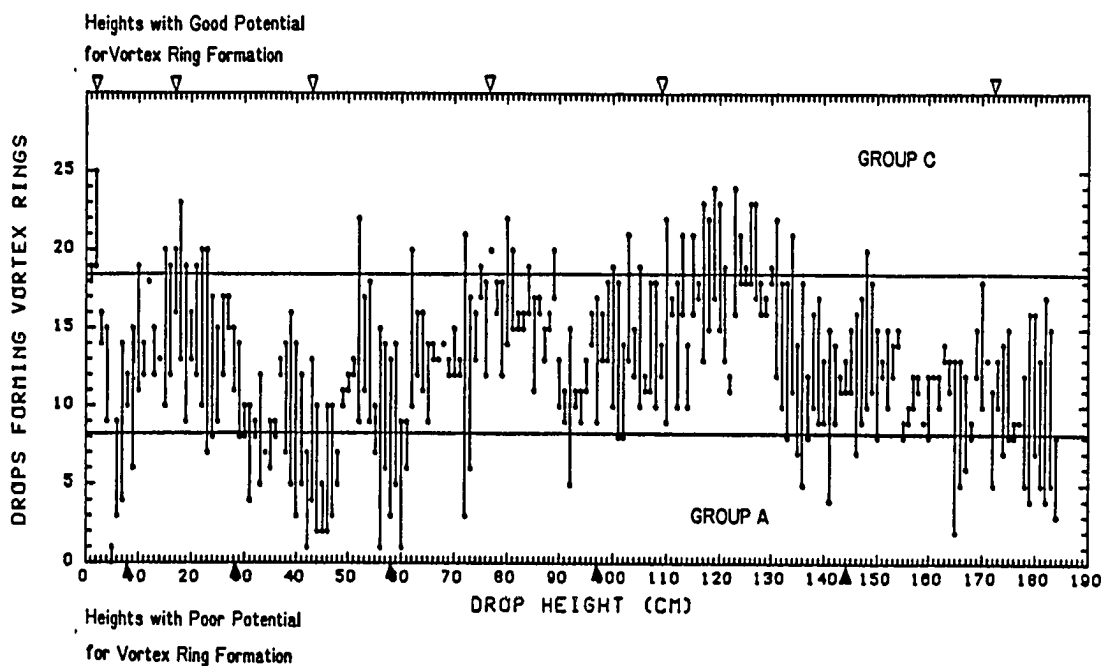
$$\tau = \frac{3\pi\rho V}{8\sigma} \quad (2-2)$$

where  $\rho$  = drop water density  
 $V$  = drop volume  
 $\sigma$  = surface tension.

The oscillation time was 0.029 sec. for the drop used in the fall height experiment. That is the time for the drop to change shape from a sphere to an oblate spheroid back to a sphere then to a prolate spheroid and finally back to a sphere.

An estimate can be made for the drop shape at impact by knowing the impact velocity and the fall distance. Assuming that at  $v=0$  the drop shape is spherical, and the fall time, is defined as

FIGURE 2-3. The number of vortex rings produced by 25 drops, as a function of drop height from 1 to 184 cm in 1 cm increments. The horizontal lines differentiate Group A ring probabilities from Group C probabilities. The triangles indicate the heights with good potential for vortex ring formation (open triangles at top of figure), and those heights with a poor potential for vortex ring formation (dark triangles at bottom of figure).



$$t = 2h/v_i \quad (2-3)$$

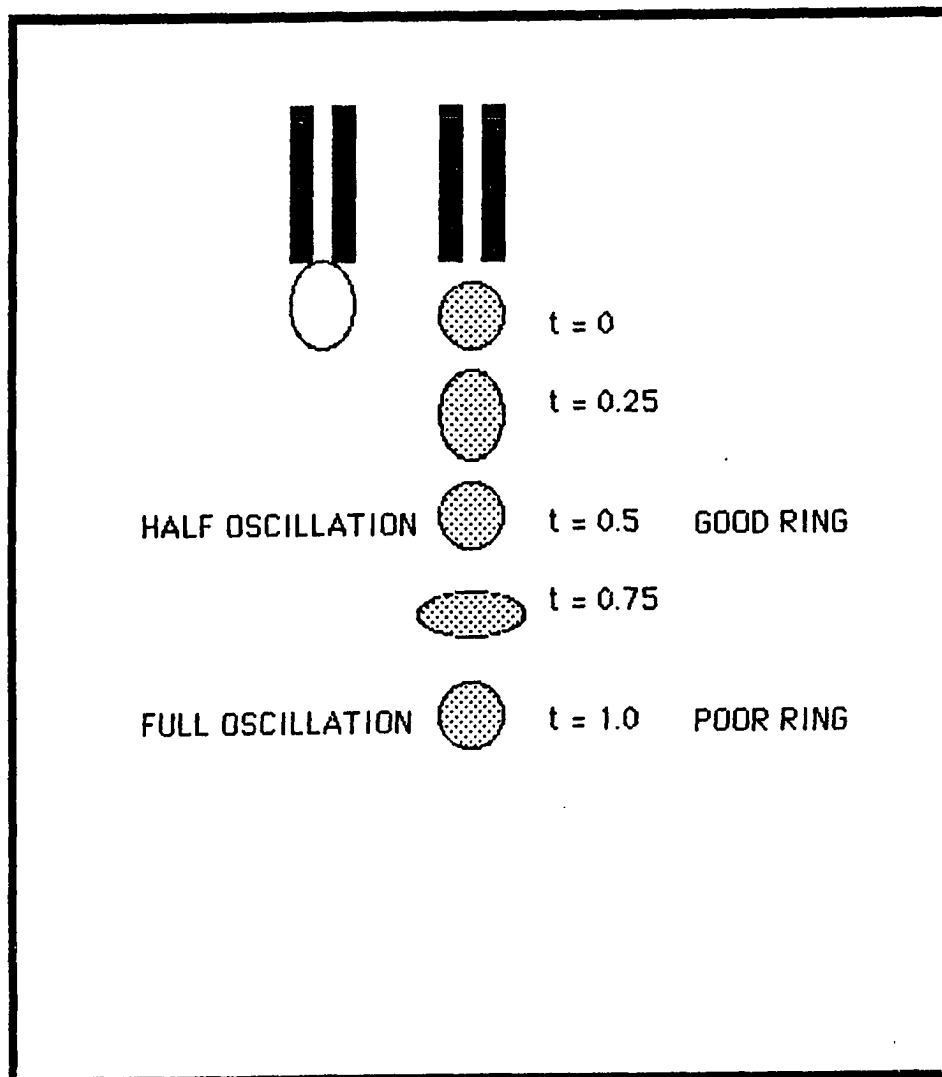
where  $h$  = fall distance  
 $v_i$  = impact velocity,

then the number of drop oscillations is determined by dividing the fall time by the drop oscillation time. Assuming that at a half and full oscillation the drop is spherical and the half oscillation represents the drop shape changing from an oblate to prolate spheroid, then the oscillation number can give an indication of drop shape at impact. According to Chapman and Critchlow (1967) the drop shape at the half oscillation number is best for producing vortex rings (Figure 2-3).

Two tests were made on the vortex ring production data. The drop heights, which correspond to the full and half-oscillation number, are shown on Figure 2-4. The hypothesis that the half-oscillation numbers correspond with relatively high probabilities of ring formation, and the full oscillation numbers coincide with low probabilities of ring formation was accepted at the 95% CI using a Chi Square test. The theoretical frequency predictions used to test against the observed frequency were that drops impacting at full oscillation produced a ring 1 in 3 times, and that drops impacting at half oscillation produced a ring 3 in 4 times.

The importance of drop shape oscillation on vortex ring production was also tested by comparing the oscillation number with the heights where more than 28 of 50 drops formed vortex rings (Group C). The oscillation number was normalized by rounding to the nearest whole number and subtracting this integer from the oscillation number. Values falling near zero represent full oscillations and values falling near +0.5 and -0.5 represent half

FIGURE 2-4. Diagram showing how an idealized drop oscillates in shape from a sphere ( $t=0$ ) to an oblate spheroid ( $t=0.25$ ) back to a sphere ( $t=0.5$ ), then to an oblate spheroid ( $t=0.75$ ) and finally back to a sphere ( $t=1.0$ ). Chapman and Critchlow (1967) hypothesize that if a drop hit the fluid surface at  $t=0.5$  it will form an energetic ring, and if it hits at  $t=1.0$ , then a poor or no ring will form.

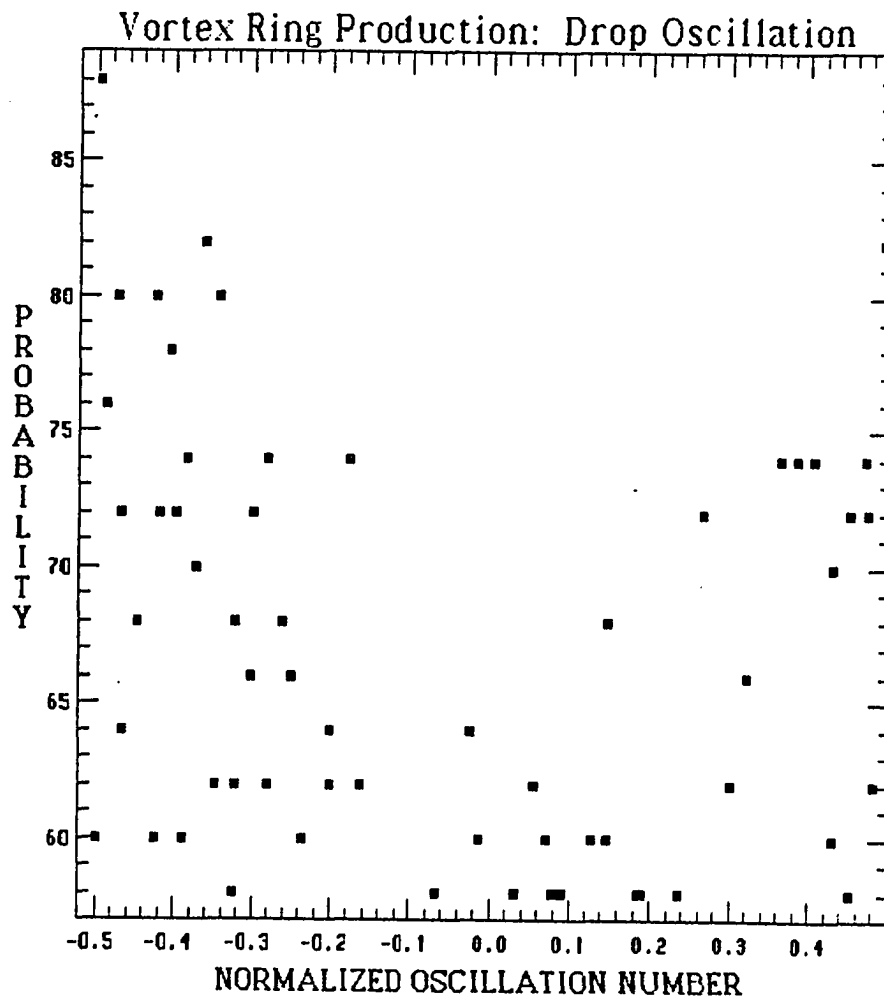


oscillations. Again it is at the half oscillations where maximum vortex ring production should occur. The scatter diagram, shown in Figure 2-5, supports this conclusion. However, the scatter also suggests that there are other factors resulting in less than the optimum number of vortex rings being produced. One factor may be that drop oscillation is due not only to the release of the drop from the needle, but also due to wake shedding as the drop falls.

These experiments demonstrate that vortex ring formation is controlled by both impact energy and drop shape oscillation. Above a specific impact energy per unit area threshold, bubble formation limits the production of vortex rings. Below this threshold all drops form a central jet which is a prerequisite to form vortex rings. Because of the drop shape oscillation, not all drops in this energy range will form energetic vortex rings.

These results can be applied to the other experiments and to natural rainfall. In the multidrop experiments all drops are falling the same distance (if the receiving water is held relatively constant) and are the same size. Therefore, efficiency of vortex ring production will depend upon the oscillation frequency and the drop height. The drop shape at impact in these experiments may not be randomly distributed, as they would be in a natural rainfall. Conversely, the time and fall distance history is not known in natural rainfall events; consequently, the changes in drop shape at impact are unknown. One would suspect a random distribution of drop shape oscillations. This would lead to the conclusion that the probability to form vortex rings by natural rain drops would be much less than experimental drops falling from drop heights designed to maximize vortex ring formation.

FIGURE 2-5. The probability of vortex ring production, as a function of the normalized drop-shape oscillation number. Only the drop heights which formed vortex rings in Group C (Figure 2-3) were plotted. A full oscillation (poor ring formation potential) at impact corresponds to 0.0, and a half oscillation (energetic ring formation potential) corresponds to  $\pm 0.5$ .



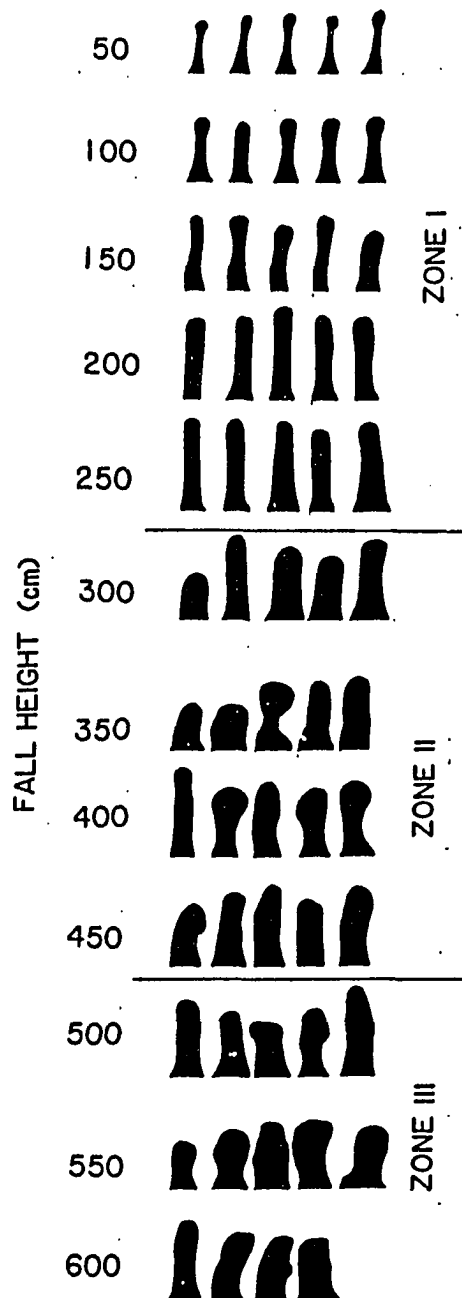
### **Vortex Ring Generation**

Hydrodynamic studies of vortex rings commonly use an initial impulse slug of fluid to create the vortex ring. In these studies a known volume of fluid is passed through a fixed diameter orifice, over a known impulse time (Baird *et al.* 1977; Maxworthy, 1977). The dynamic characteristics of the resulting rings are then related to the properties of this initial slug. The important ring parameters used in this comparison are the ring dimensions, the translational velocity of the ring and the circulation within the ring. These properties are not constant, but vary as the ring proceeds away from the generating source (Maxworthy, 1977). The size and the translational and rotational velocities of the ring at impact with the bottom are important in defining the energy available for initiation of sediment movement.

**Central Jet Characteristics.** Drop-formed vortex rings may differ from the theoretical and laboratory studies in that the splash central jet is an "imperfect" slug generator. The slug volume varies with drop impact energy and water temperature. In energy Zone I the jets are uniform and cylindrically shaped. In energy Zones II and III the jets become irregular and deformed (Figure 2-6). This deformation may influence vortex ring formation. The orifice for the drop-formed impulse is not fixed, but depends upon how the central jet collapses through the water surface. How the drop energy is transferred through the central jet to the vortex ring may be controlled by the flow-field on the small-scale turbulent levels and the ambient water temperature.

The important factors describing the impulse jet are (1) the jet cross-sectional area and diameter (*i.e.* volume); (2) the jet height at maximum extent (*i.e.* the potential energy contained in the jet); and (3) the time for

FIGURE 2-6. Shadow diagrams of central jets produced by 0.545 cm drops falling from heights, ranging from 50 (top) to 600 cm (bottom) in 50 cm intervals. The energy Zones I, II, and III, as defined by the percent central jets, are noted. The dimensions of the jets are correct relative to each other.



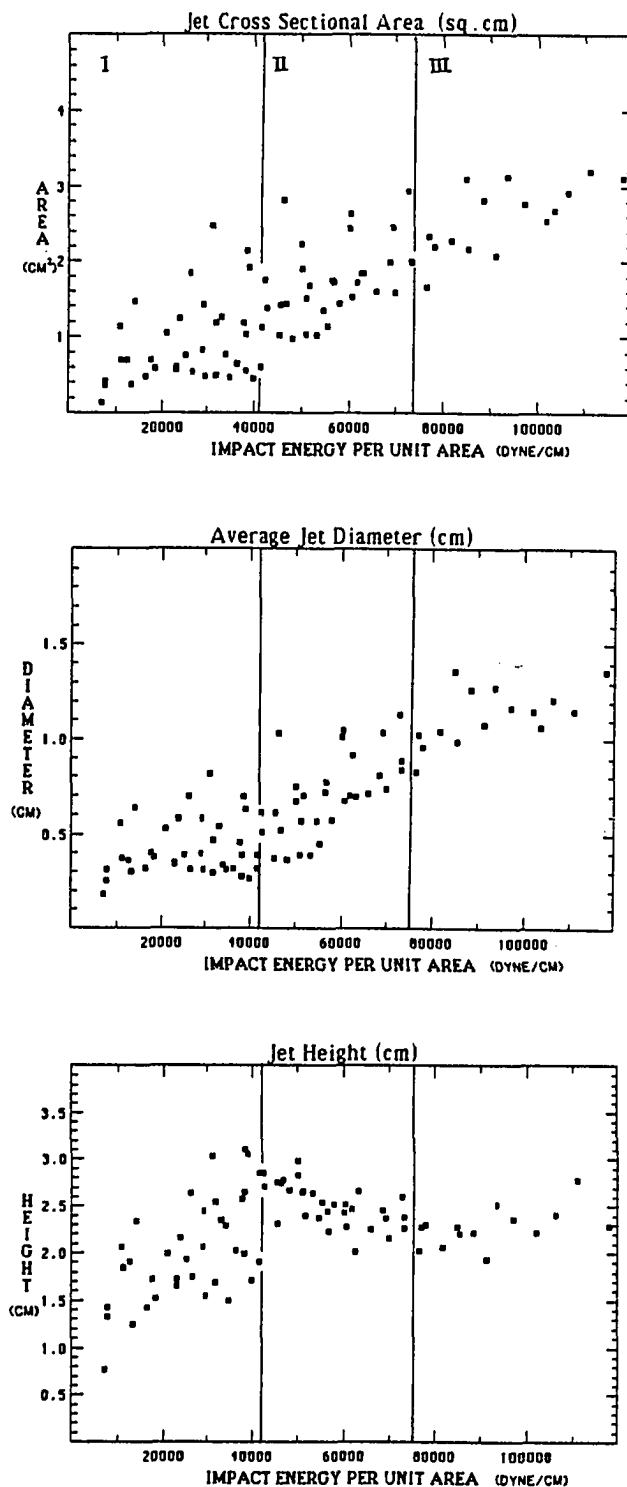
the jet to collapse. These parameters define the impulse generating slug and the initial energy, but do not describe the orifice through which the impulse jet passes. This is important because it is the size of the orifice relative to the volume of the impulse slug which determines whether or not a vortex ring will form (Chen and Chang, 1972). The maximum orifice diameter would possibly be the jet diameter, but the actual orifice may be much smaller. It was not possible in this study to establish a better estimate for the orifice diameter. Variations in the jet shape and how the jet collapses through the water surface are factors, which may control the development and the characteristics of the vortex rings.

**Effect of Drop Impact Energy.** The jet dimensions from Experiment 3, are best described as a function of impact energy per unit area at a single receiving water temperature.

Jet cross-sectional area increased linearly with impact energy per unit area (Figure 2-7A). The increase in area was due primarily to the increase in jet diameter rather than jet height. Jet height, as measured at maximum extent, increased in energy Zone I, decreased in energy Zone II, and finally increased in Zone III (Figure 2-7B). Like cross-sectional area, jet diameter increased linearly with impact energy (Figure 2-7C).

The impulse time was measured from the point of maximum jet extension to the point where the jet had completely passed through the water surface. The average measured impulse time was 0.07 sec (std. dev. = 0.015; n = 220). However, this time was difficult to measure accurately since the video equipment recorded at 25 frames per second.

FIGURE 2-7. Scatter plots of cross-sectional area (A), jet height (B) and average jet diameter (C) as a function of impact kinetic energy per spherical drop area. The energy Zones I, II, and III as determined from the percent jet distribution are shown for reference.

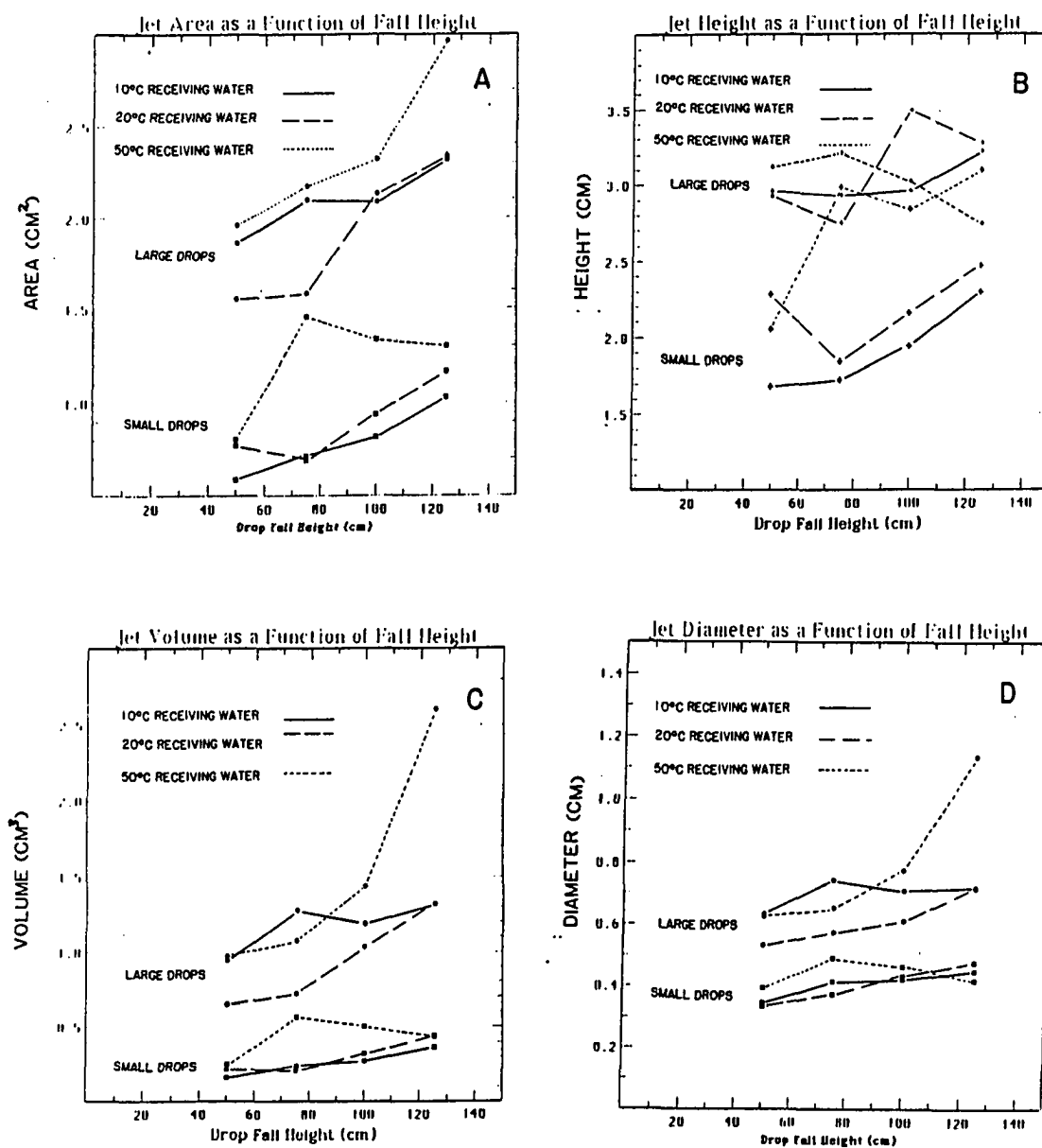


**Effects of Receiving Water Temperature.** The temperature effects on the central jet dimensions is expected, because of its influence on the physical nature of water. As temperature increases water becomes less viscous, has a lower surface tension and becomes less dense. All these factors would promote changes in the dimensions of the jet. The central jet formed by the same drop impact energy would increase in volume with an increase in water temperature, because the fluid would be less dense and less viscous. This effect will be enhanced because the surface tensional forces, which are opposing the upward growth of the central jet, will decrease with increased temperature.

Central jets produced in Experiment 4 were created by either small drops (0.351cm) or large drops (0.523 to 0.53 cm) falling 50 to 125 cm. The impact energy per unit area ranged from 10,770 to 39,250 dyne/cm, which corresponds to energy Zone I, where all drops formed central jets (Figure 2-7). The drop water was maintained at about 20° C, while the receiving water was varied from 9-10°C to 20-22°C and 45-55°C. By varying the receiving water it was possible to assess the temperature effects on the jet dimensions.

A two-way analysis of variance was conducted to determine if the change in receiving water temperature affected the central jet dimensions, and to determine if the thermal effects were comparable to changes in drop height (*e.g.* impact energy). The jets formed by the small drops showed an increase in jet cross-sectional area, height, diameter and volume with increased drop height (Figure 2-8). All the jet characteristics increased significantly (at 95% CI) between 9-10°C and 45-55°C receiving water temperatures. The jet diameter and volume for jets produced in 9-10°C to 20-22°C water were not significantly different.

FIGURE 2-8. Jet dimensions from Experiment 3 as a function of fall height. All impact energy per unit areas were confined to energy Zone I. The data are divided by receiving water temperature (10°C, 20°C and 50°C), and by drop size. The "large" drops were about 0.53 cm and the "small" drops were 0.35 cm in diameter. Panel A is jet area as a function of fall height; Panel B is jet height versus fall height; Panel C is jet volume; and Panel D is jet diameter as a function of drop height.



The jets formed by the large drops increased their cross-sectional area, diameter and volume with increased drop height (Figure 2-8). There was no significant difference in jet heights. Changes in receiving water temperature from 20-22 to 45-55° C resulted in significantly increased jet characteristics (except jet height).

The results for the 9-10°C water appear to be anomalous in that the dimensions are intermediate between those for 20-22°C and 45-55°C water (Figure 2-8). A possible rationale for this observation was inadequate temperature measurements. The near-surface water may have actually been warmer than that measured, due to exposure to the warmer air and to lighting for the video recording. It is possible that this surface warming, thermally stratified the water column, resulting in temperatures intermediate between 20 and 45° C. This surface warming may also have been enhanced by the relatively large volume of 20° C water added by each drop. The results of the smaller drops are probably also influenced by this experimental artifact, but is not as noticeable.

### **Vortex Ring Characteristics**

Measurements of the ring properties were made from the video recording, and include: (1) ring dimensions; (2) translational velocity; and (3) an estimate of rotational velocities in the inner core of the ring. The depth of ring penetration was also measured to estimate the depth of ring influence.

**Vortex Ring Size.** The size of the vortex ring is dependent upon the size of the impulse slug creating the ring. When dyed water drops are used to generate vortex rings, only a portion of the ring is visible. An example of

this torroidally-shaped inner core as it impacts the tank bottom is shown in Figure 2-9. Fluid in the inner core is rotating very rapidly within the core, with little exchange between this fluid and the surrounding water. The vortex ring also has an outer core which circulates very slowly and readily exchanges fluid with the ambient water Figure 1-1. This portion of the ring cannot be seen using just dyed drops. Consequently the descriptive properties of the vortex ring will be those of the inner core. Fortunately it is this inner core which contains the bulk of the ring energy.

Horizontal and vertical dimensions of the inner core of nine vortex rings from the Experiment 4 data set were measured from the video record. The drop diameter which generated these rings was 0.523 to 0.53 cm. The average horizontal length was 1.36 cm (+/- 0.157 cm std. deviation), and the average vertical length was 0.398 cm (+/- 0.93 cm). The volume of the inner core of these vortex rings was  $0.384 \text{ cm}^3$  (+/-  $0.152 \text{ cm}^3$ ), assuming a torroidal shape (Figure 2-10).

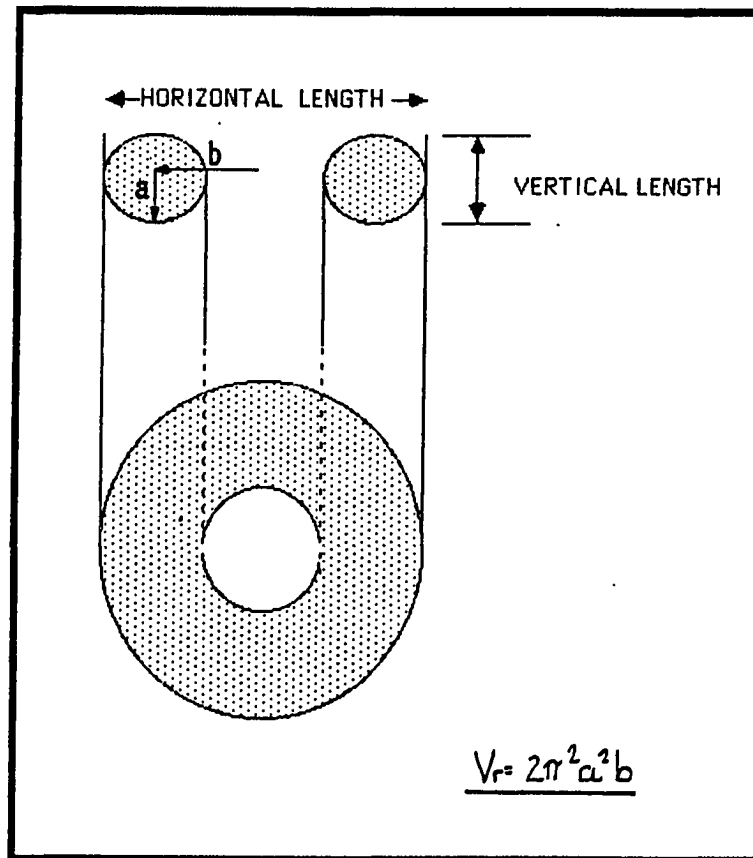
The small drops generated vortex rings with much smaller ring dimensions. The average horizontal length was 0.905 cm (n=8; Std. Dev. = 0.15). The vertical length was 0.244 cm (Std. Dev. = 0.04). The average volume of the inner core of the ring was  $0.0971 \text{ cm}^3$ , or about 4 X smaller than the inner core produced by the larger drops. The length to width ratio of the measured rings was about 3.5, this is smaller than the ring dimension ratio (approximately 10) observed by Johnson (1970).

**Vortex Ring Velocity.** There are two velocities to be considered when describing the ring energy. The translational velocity of the ring is the speed at which the ring moves downward through the water column. The



**FIGURE 2-9.** Photograph of the inner core of a vortex ring impacting a clay covered tank bottom after passing through 40 cm of water. The inner has been dyed, therefore it is visible. The outer core associated with this ring is not observed because there is very little exchange of dyed fluid between the inner core and the outer core.

FIGURE 2-10. A diagram of the dimensions of the inner core of the vortex ring. Notice the difference between the horizontal and vertical lengths, and the horizontal and vertical radii of the core.



rotational velocity is the speed the fluid in the inner core circulates about the torroidal axis of the ring (Figure 1-1).

The rotational velocity of the core fluid is important in sedimentological processes because this velocity will result in shear stress at the sediment surface if a ring impacts the bottom. Unfortunately this parameter is very difficult to measure, and requires instrumentation not available for this project. An estimate of rotational speed was made using photography and measuring the streak lengths of entrained estuarine mud particles. Approximate speeds of 50 to 75 cm/sec were computed by dividing the streak lengths by the camera shutter speed.

The translational velocity is at a maximum just after ring formation (near the water surface). Ring speed decreases as the ring moves down the water column. Maxworthy (1977) observed that ring velocity decreased with distance along the ring path in a relationship, where time was proportional to the depth squared. Deviations from this relationship occurred when the impulse energy was lost from the ring through the wake that trails off from the ring (Maxworthy, 1977).

The translational velocities of vortex rings produced in Experiment 4 were reduced from the video tape records. Maximum velocities were observed just after ring roll-up and formation. The velocities at 3 cm for the large rings ranged up to 98 cm/sec (Figure 2-11), averaging 31.5 cm/sec (Figure 2-12). Translational velocity decreased rapidly after formation. At 5cm depths the velocities averaged 19.4 cm/sec. Below a depth of 13 cm the translational velocity was relatively constant, averaging less than 7.8 cm/sec.

The translational velocities of the rings produced by the small drops were substantially less than the large rings (Figure 2-11). The maximum measured velocity averaged 11.1 cm/sec at 1 cm below the surface (Figure

FIGURE 2-11. Plots of vortex ring translational velocities with depth for the 24 runs in Experiment 4. Panels A, B and C show the translational velocities of the large rings in 10°C, 20°C and 50°C receiving water. Panels D, E and F show the translational velocities of the small ring in 10°C, 20°C and 50°C receiving water.

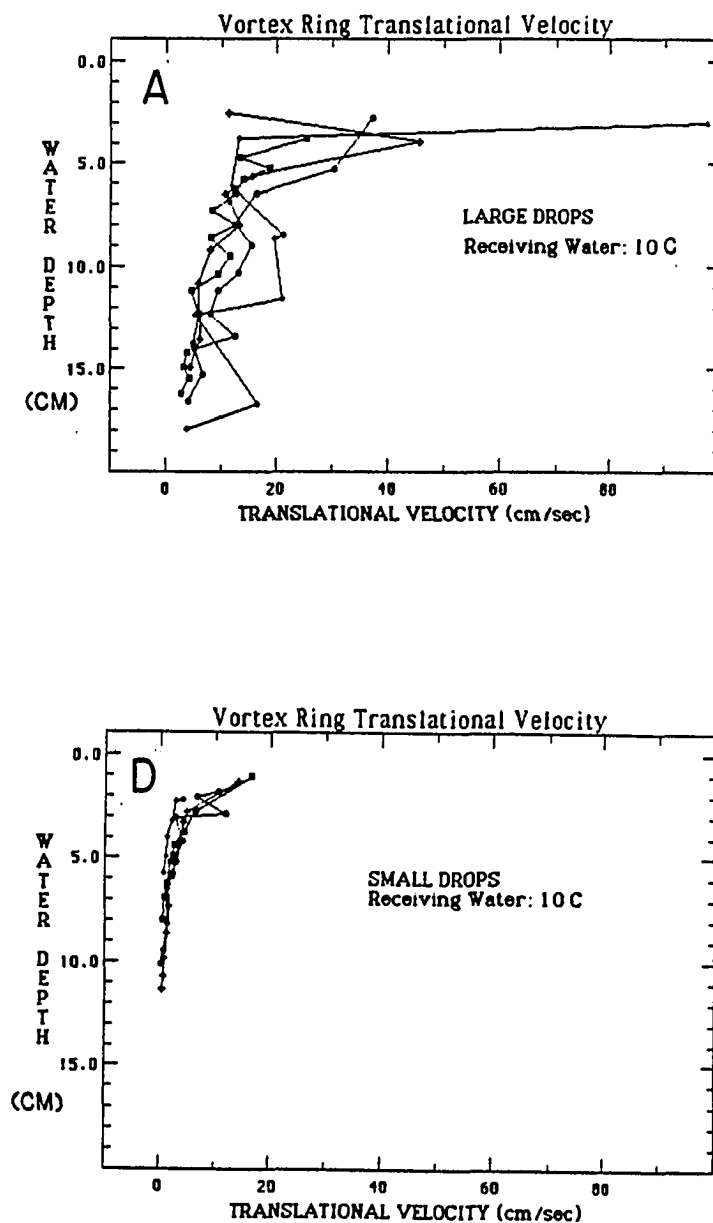


FIGURE 2-11. Continued.

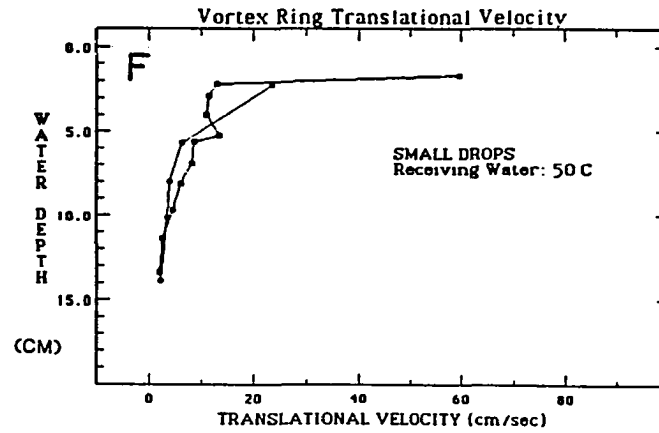
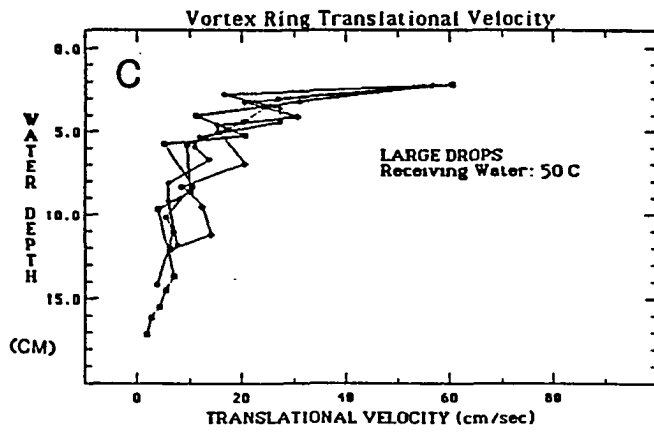
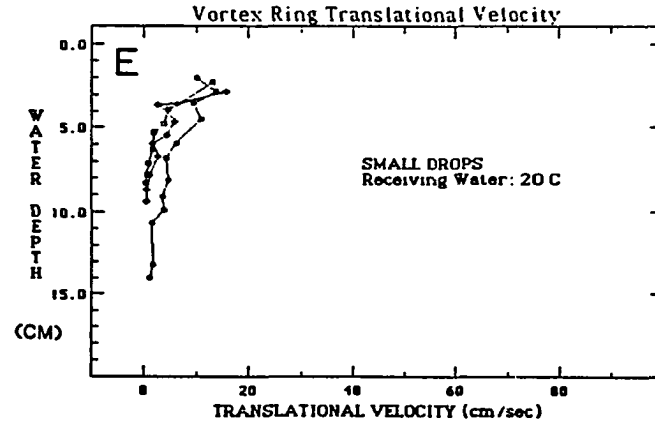
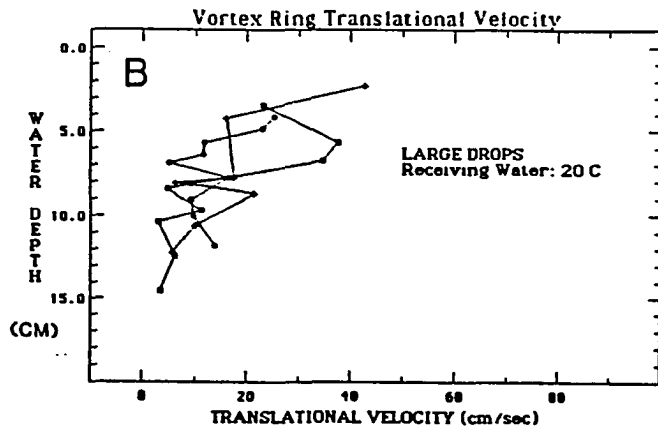
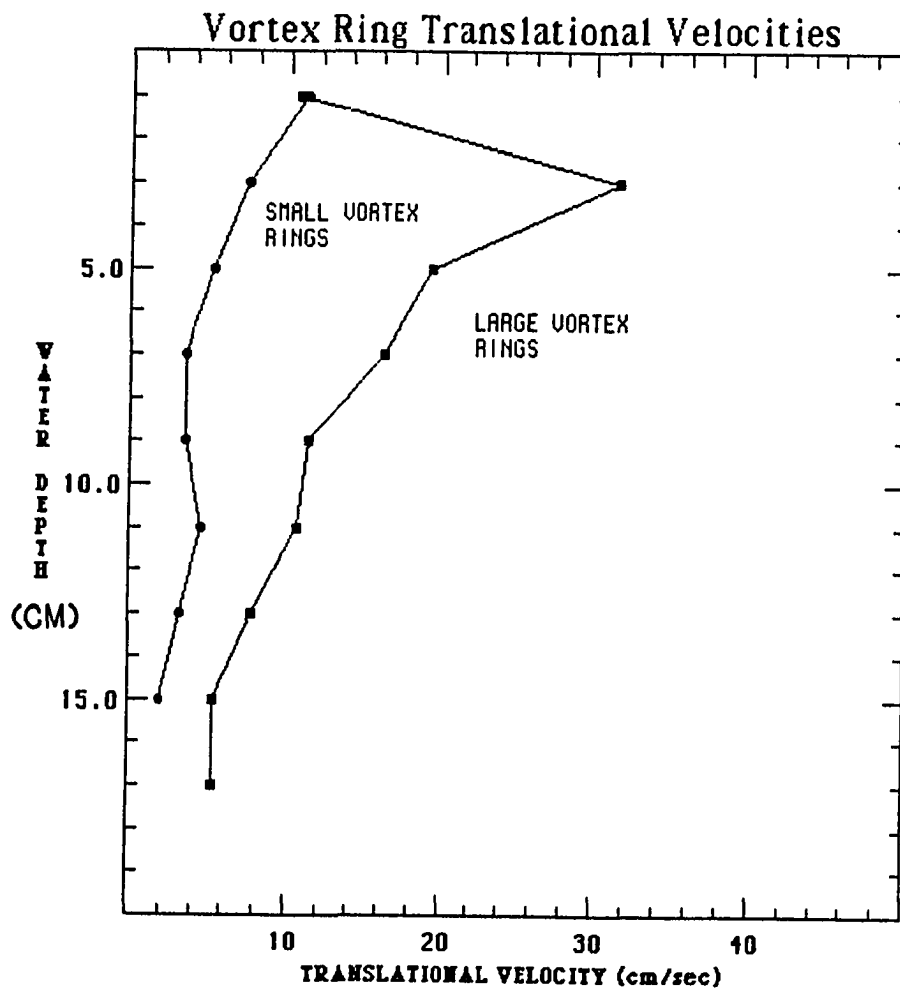


FIGURE 2-12. The average translational velocities of vortex rings produced by both both small and large drops, as measured from selected rings from Experiment 4. The low velocities of the larger rings at a water depth of about 1 cm is because at this depth the ring is still being formed as is not moving downward through the water column.



2-12). Translational velocities then decreased with depth. Below 6 cm the velocity average about 3.5 cm/sec.

The effect of receiving water temperature and drop height was not tested because of the problems in obtaining a representative sample of velocity profiles. The rings which could be measured were biased toward the better defined rings, and rings which had a moderate velocity. Other rings could not be detected on the video stop action. This limitation should be kept in mind when the velocity profiles are used in subsequent discussions.

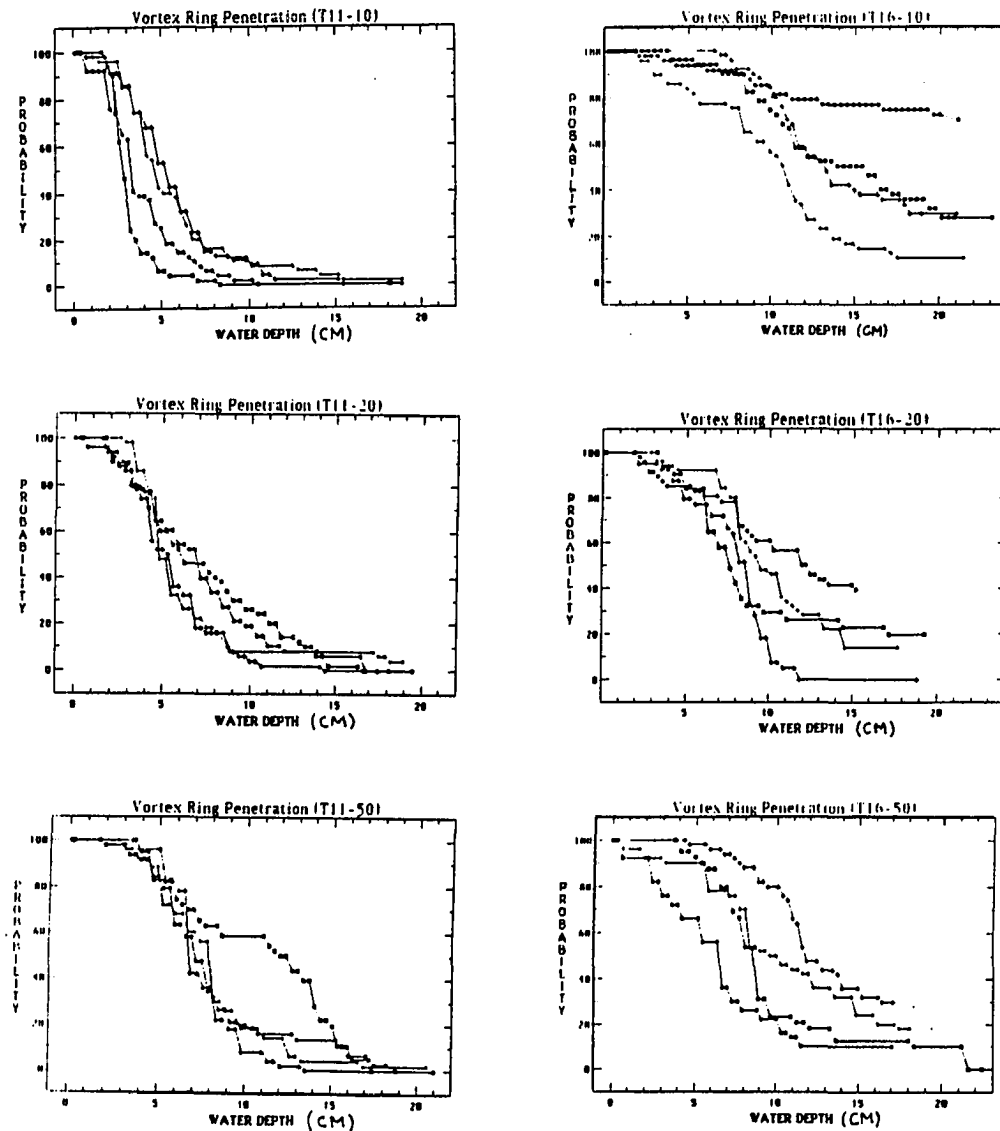
**Vortex Ring Penetration.** Vortex ring penetration is important because it gives the depth range for dissipation of the ring energy. Ring penetration was determined in Experiment 4, by noting the depth at which the ring stopped moving downward for each drop size, drop height and receiving water combination. Up to 50 rings were analyzed for each combination.

Ring penetration varied depending upon initial drop size. The vortex rings produced by the large drops, when the whole data set is considered, showed no effect of receiving water temperature. In general, the probability (P) of ring penetration was proportional to water depth (Figure 2-13). The penetration depth distribution of the rings formed by the large drops is expressed with the following linear regression equation (R-squared value of 58.9% with 367 degrees of freedom, df):

$$P = 1.03 - 0.0454 (z) \quad (2-4)$$

In contrast, the vortex rings formed by the small drops were influenced by temperature. These rings penetrated the water column as a hyperbolic function of water depth and linear function of temperature. As the receiving

FIGURE 2-13. The penetration of vortex rings is shown as a cumulative probability function of depth. The figures group penetration data by drop size and receiving water temperature. For a given drop size-temperature combination, each profile represents a specific drop height.



water temperature increased the penetration of the rings increased. The depth of penetration by the small rings is best explained by a multiple linear regression equation combining water depth and temperature. The observed probability distribution (P) as a function of depth (z), below z = 1cm, took the form:

$$P = \cosh^{-1} z = \ln (z + \sqrt{z^2 - 1}) \quad (2-5)$$

Combining the depth and temperature in the regression equation, the probability of ring penetration was

$$P = 1.42 - 0.461 [\ln(z + \sqrt{z^2 - 1})] + 0.0068 t_r \quad (2-6)$$

This relation was significant with an R-squared value of 79.6% with 324 df.

### **Discussion**

The purpose of the single drop studies were to develop a picture of the important factors controlling the transfer of rain drop energy through a shallow water column to a sediment covered bottom. This transfer process was believed to be vortex rings because of the ability of the splash central jet to create an organized vorticity of fluid which subsequently moved through the water column. By virtue of its transported mass the vortex ring contains momentum. This momentum is proportional to the size of the ring and the translational velocity.

The ring dimensions varied with initial drop size, as did the translational velocity of the ring. In general the velocity of the ring was greatest just

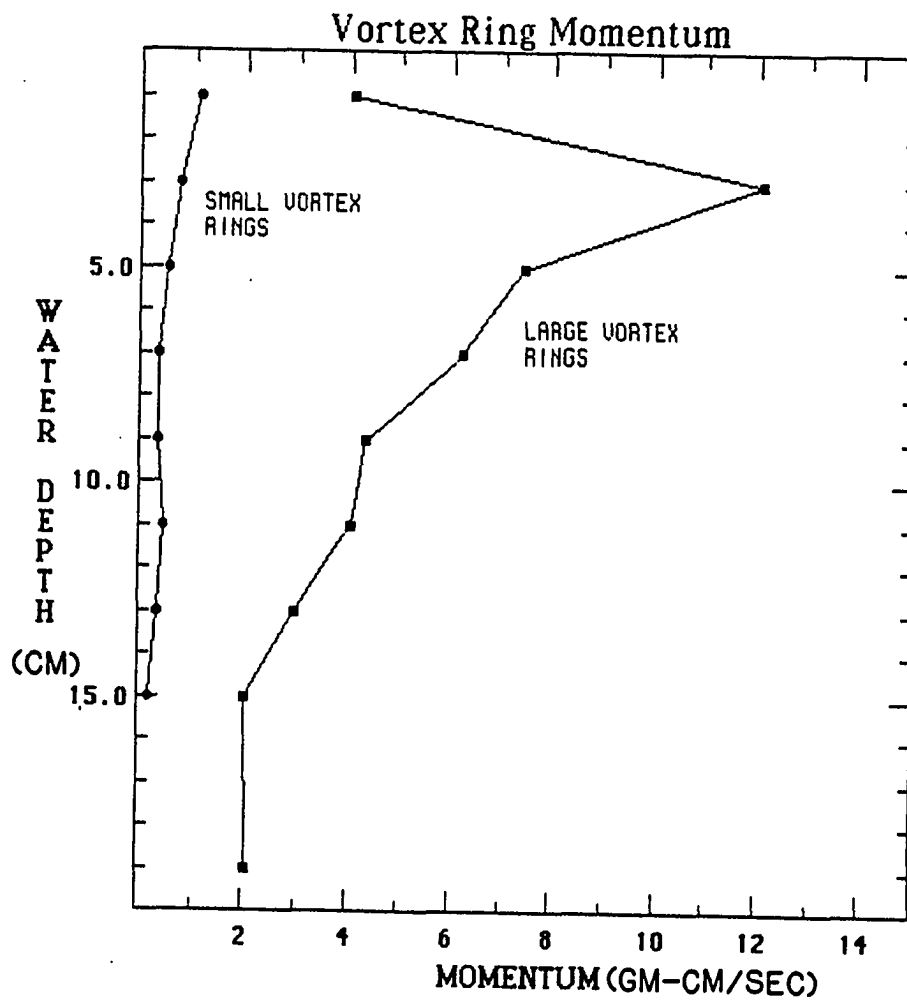
after a development period. The velocity then decreased with depth of penetration. Using the ring volume and the velocity, a momentum profile for single large and small rings can be constructed (Figure 2-14). The large rings contain one order of magnitude more momentum than the small rings. The greater momentum contained in the large rings suggests that these will be more important than the smaller rings for resuspending bottom sediment.

The greater energy within the ring will also allow the ring to survive turbulence in the ambient fluid surrounding the ring. Using the ring Reynolds number, the importance of inertial forces over viscous forces can be estimated. The Reynolds numbers of the large rings ranged from 1517 near surface to 259 at depth (17 cm). The Reynolds numbers of the small rings were much less, 366 near surface and 65 near bottom (15 cm). These Reynolds numbers are substantially less than the Reynolds numbers for vortex rings studied by Maxworthy (1977).

Lower than expected Reynolds numbers may have two important effects on the survivability of the vortex rings in the natural environment. The first is that wind waves in even 5 cm of water, have wave Reynolds number which are an order of magnitude greater than the largest drop formed vortex ring. The second is that viscous effects may have more importance in modifying the vortex ring. This is seen in the temperature dependence of the smaller rings to penetrate the water column. The smaller rings were better able to move through a water column, which was warmer than the raindrop.

Salinity effects were observed only by qualitative observations. When the receiving water column was well-mixed and contained saltwater with a salinity of approximately 25‰, there appeared to be little density effects on the size and translational velocity of rings produced by freshwater drops.

FIGURE 2-14. Profiles of vortex ring momentum as a function of depth for rings formed by the large and small drops used in Experiment 4. Momentum is defined as the inner core volume times the translational velocity.



This may be expected since the inner core volume of the ring is substantially larger than the original drop, and the inner core is produced by the central jet, which includes both drop water and surface receiving water. Thus the ring core is a mixture of fresh and salt water. A salinity effect was noted, when the receiving water was stratified with a low salinity surface layer of 2 to 5 cm thick and a high salinity bottom layer. In this case, the ring was formed with low salinity, near-surface water. As the ring moved through the density gradient, buoyancy became more and more important. Eventually, as the downward translational velocity decreased, buoyancy caused upward transport of the ring fluid to a depth intermediate between the surface and bottom layers (Figure 2-15).

The previous discussion of the physical properties of the vortex rings has not considered the effects of the rotational velocity within the ring. This velocity has the capacity to impart significant shear on bottom sediment at ring impact even though the translational momentum is small. The rotational velocity of the largest rings was estimated to be 50 to 75 cm/sec, substantially higher than the translational velocities. It may be this rotational fluid flow which has the greatest ability in resuspending bottom sediment.

The momentum available at any depth to be transferred to the water column is a function of both the momentum within the ring at the particular depth and the probability that a ring will penetrate to that particular depth. Combining Equations 2-7 and 2-9 with the ring momentum profile (Figure 2-16) gives an estimate of the momentum available to be imparted upon the bottom over a range of water depths (Figure 2-16). The large rings provide substantially more momentum at any given depth than the smaller rings. The vertical distribution of available momentum

FIGURE 2-15. Diagram illustrating effects of salinity stratification on vortex ring penetration.

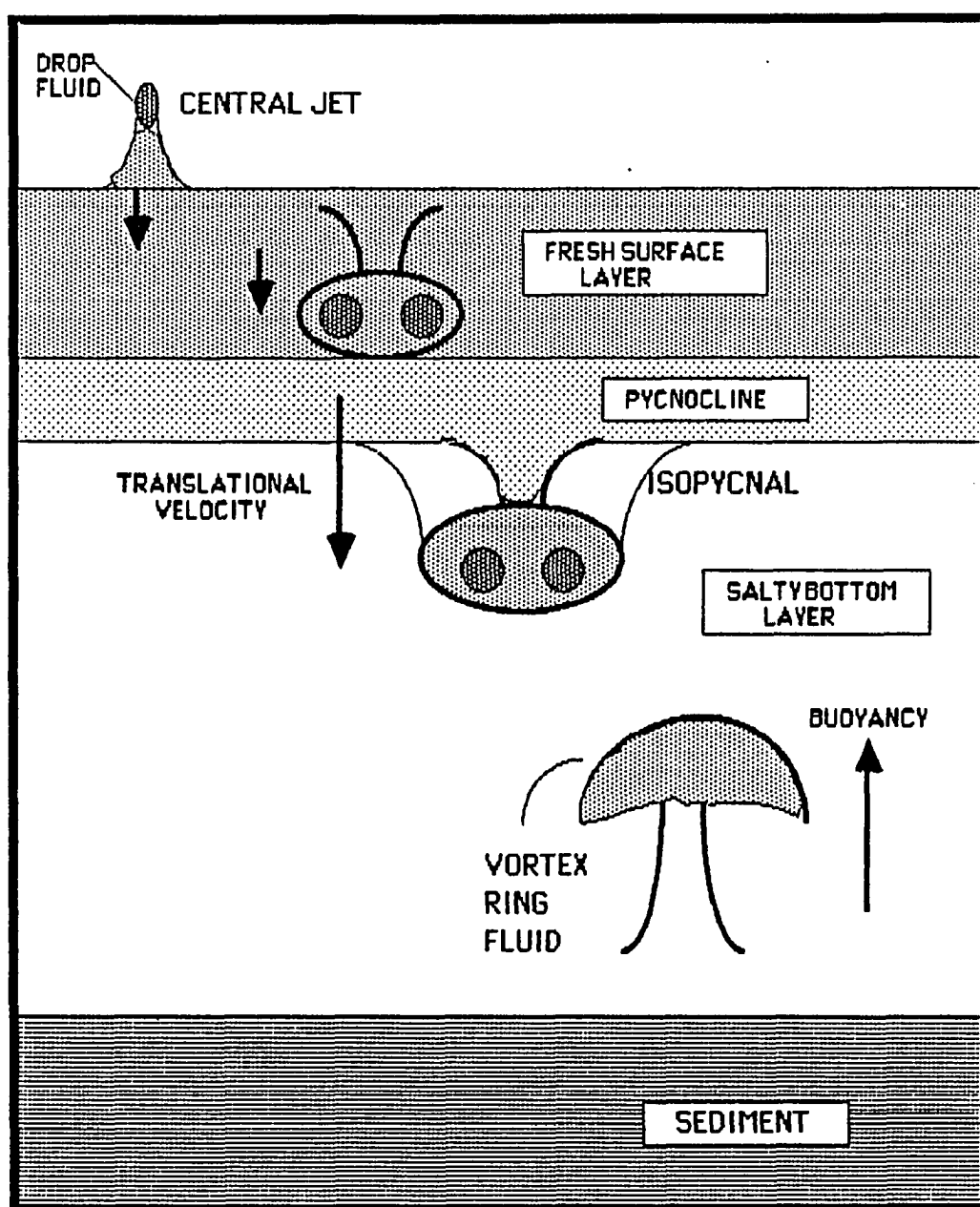
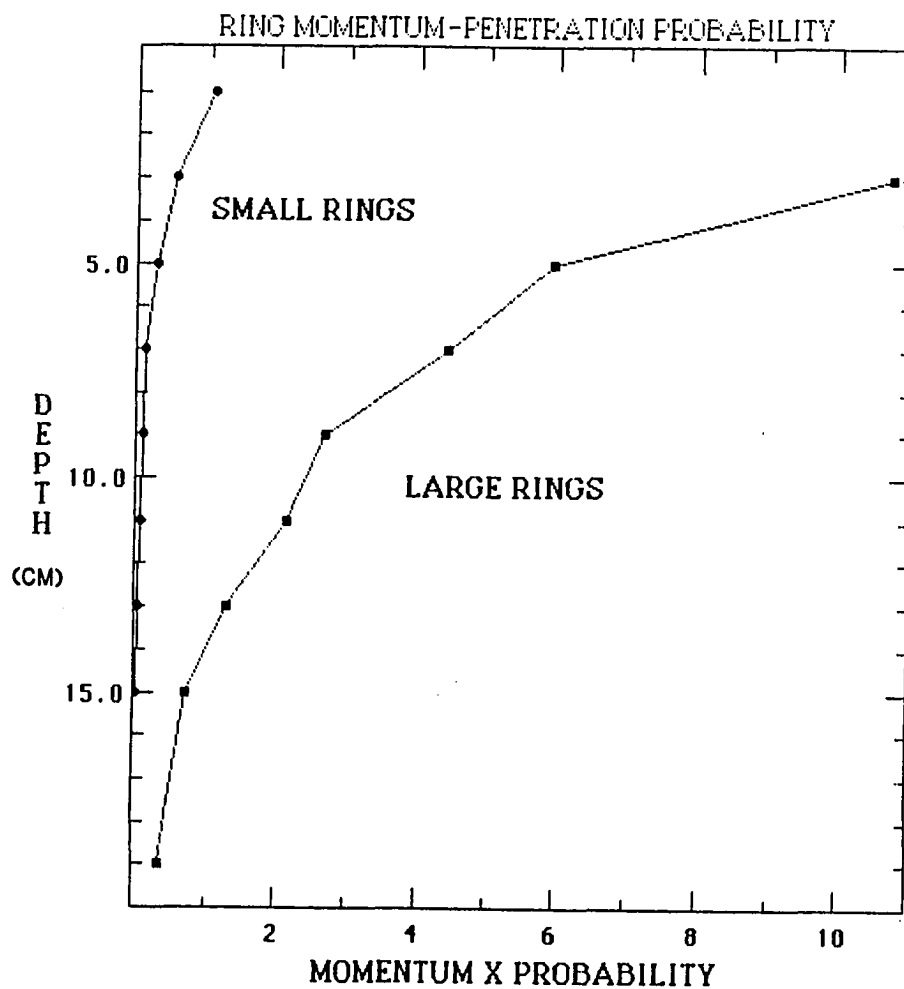


FIGURE 2-16. Profiles of available momentum from drop-formed vortex rings at water depths from 1 to 19 cm. The profile combines the vertical momentum distribution for single rings with the probability of penetration for large and small rings.



decreases rapidly with an inflection point at 9 cm water depth for the large rings and at 6 cm for the small rings.

The physical properties of drop formed vortex rings are controlled by the drop size, thus the impact energy. The rings produced by the larger drops have a larger mass and move through the water column faster than the rings produced by the smaller drops. The larger rings penetrate deeper in the water column than the smaller rings, and are less affected by the ambient water temperature. If rings initiate motion of bottom sediment, then the amount of resuspension or motion should be proportional to the physical properties of the ring. In the next chapter initiation of motion of non-cohesive, sand sized sediment by individual vortex rings will be documented.

## **CHAPTER 3**

### **RAIN-INDUCED INCIPIENT MOTION OF NONCOHESIVE SEDIMENT**

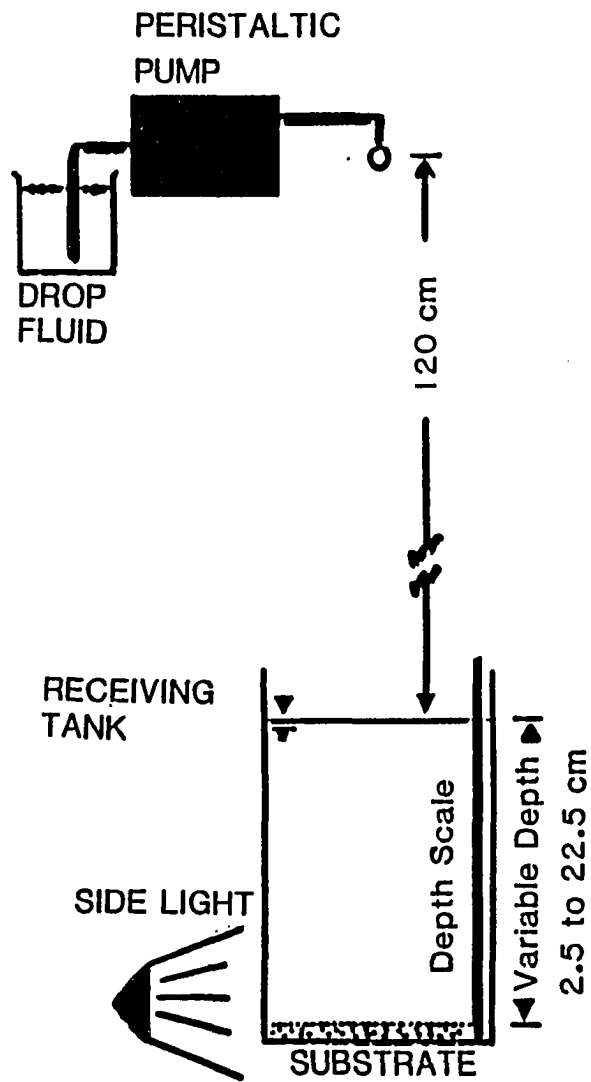
#### **Introduction**

The physical properties of drop-formed vortex rings suggest that they may be an important mechanism in initiating motion of bottom sediment. The translational momentum of the ring and the rotational velocity within the inner core of the ring, both appear to have sufficient energy to move sediment when the ring impacts the bottom. This chapter presents the results of a laboratory study designed: (1) to determine the probability of vortex rings initiating sediment motion for a range of water depths and substrate textures; and (2) to define the maximum depth for drop-induced incipient motion.

#### **Methodology**

Vortex rings were formed by drops of a fixed size falling into a receiving water tank with a maximum depth of 22.5 cm (Figure 3-1). Drops with a 0.535-cm diameter and a 120-cm fall distance were selected to represent an impact energy equivalent of a 0.36-cm drop-size falling at terminal velocity. The 0.36 cm drop size corresponds to one of the drops used by Green and Houk (1979). The dyed drops were generated as described in Chapter 2. Drop size was determined by weighing 25 drops, assuming a density of 1.0 gm/cm<sup>3</sup>, and calculating the equivalent spherical diameter.

FIGURE 3-1. Schematic diagram of the experimental set-up.



Water depths and substrate textures were varied for a specific drop size and height. Quartz- and feldspar-rich sediment was sieved to restrict the size range to 0.5 phi ( $\phi$ ) intervals. The sand substrates tested were very-fine (3.0 to 3.5  $\phi$ ; 0.125 to 0.088 mm), fine (2.0 to 2.5  $\phi$ ; 0.25 to 0.177 mm), medium (1.0 to 1.5  $\phi$ ; 0.5 to 0.35 mm), coarse (0.0 to 0.5  $\phi$ ; 1.0 to 0.71 mm), and very coarse (-0.5 to -1.0  $\phi$ ; 1.41 to 2.0 mm). To provide a hydrodynamically similar substrate, organic material was removed by treating the bulk sample with hydrogen peroxide, and mica was removed by agitating, then decanting the sample. The sediment was spread evenly over the bottom of the tank to form a smooth substrate approximately 0.5-cm thick. The receiving water depth was varied from 2.5 to 22.5 cm in 2.5-cm increments.

Triplicate sets of observations of 100 drops each were taken for each water depth-substrate texture combination. The results of this study are based on 12,900 observations (summarized in Appendix 3A). Data collection consisted of two sequential observations: (1) If a vortex ring was formed, did it penetrate to the substrate (tested on first 25 drops)? (2) Did the drop initiate sediment motion (tested on all 100 drops)?

Initiation of sediment motion occurred when the circulation within the inner core was sufficiently intense and when the vortex ring touched the sediment-covered bottom of the receiving water tank. The types of sediment motion was not differentiated in the analysis; however, it ranged from a few grains rolling radially away from the center of the vortex ring to numerous grains being lifted about 1 to 2-cm off the bottom. In the latter case, the grains were either ejected outside the influence of the ring and allowed to settle unhindered, or entrained within the flow pattern of the inner core and "deposited" at the center of the ring, where flow was directed

toward the bed (Figure 1-1). The dynamic nature of vortex-ring impact is shown in Figure 3-2, where the substrate was estuarine mud.

### Results

If raindrops strike a water surface and create organized vortex rings, which travel to the sediment/water interface, then sediment motion may be initiated. The vortex ring structure consists of a rapidly spinning toroidally-shaped inner core and a slowly circulating outer core (Figure 1-1). The ring moves through the water column at translational velocities observed to exceed 50 cm/sec. The rotational velocities within the inner core were not measured, but were observed to be 50-75 cm/sec. The inner-core diameter of these rings (normal to the direction of translation) was about 1.36 cm and did not change with depth.

Not all rings that touched bottom moved sediment. In general, these rings were moving too slowly downward and the rotational velocities within the inner core were too weak to entrain sediment. The percentage of vortex rings that touched bottom varied inversely with increasing water depth (solid line in Figure 3-3). In 22.5-cm of water, approximately one-third of all drops produced vortex rings that touched bottom.

Similarly, the probability of drops initiating sediment motion decreased with increasing depth for all sediment sizes (Figure 3-3). Most drops (94%) initiated motion in very shallow water (2.5 cm), but as the water depth increased, the percentage of drops that moved sediment decreased. However, even at the maximum depth tested (22.5 cm), 1 of every 10 drops caused sediment motion. An inflection point in the relationship was observed between the 7.5 and 10.0-cm depths (Figure 3-3).

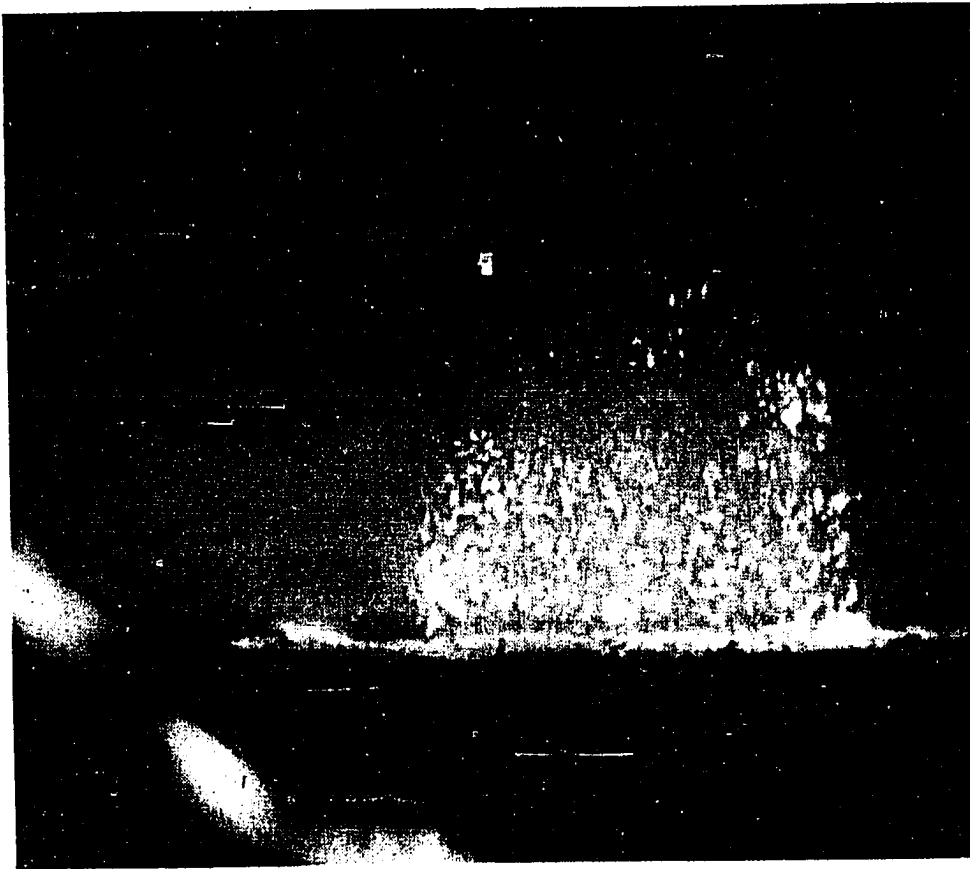
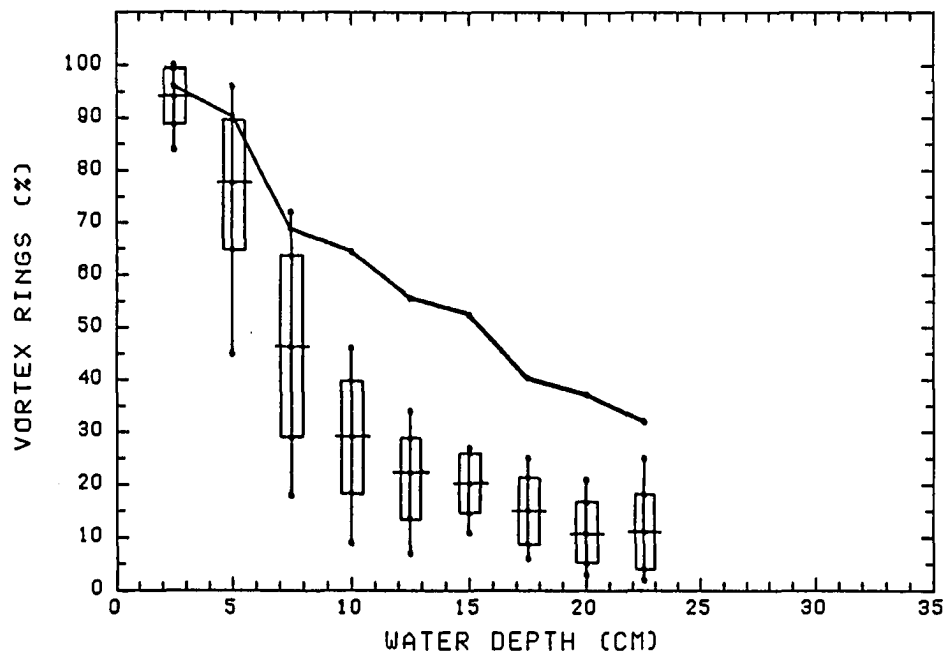


**FIGURE 3-2. Photograph showing a vortex ring impacting estuarine mud.**

FIGURE 3-3. Percentage of vortex rings that initiated sediment motion for each water depth including all substrate textures. Symbol represents maximum, minimum, mean, and +/- one standard deviation. The heavy solid line is the average percent frequency of vortex rings that touch bottom for each for each water depth.



The relationship between the number of drops initiating sediment motion and substrate texture was also tested. The percentage of rings causing movement of the very-coarse sand (27%) was significantly less (at the 95% CI) than the percentage of rings causing movement of the coarse to very-fine sand substrates (38%) at any specific water depth (Figure 3-4). There was no significant difference in the ability of drop-formed vortex rings to initiate motion within the coarse to very fine sand substrates. This experiment tested only sediment motion; that is, whether sediment did or did not move. A better relationship may exist between ring energy and a volumetric entrainment rate.

Since vortex rings produced by 0.535-cm drops initiated motion in all sediment sizes and water depths tested, an estimate of the minimum shear stress imparted to the sediment by the rings can be determined using the Modified Shields Diagram (Madsen and Grant, 1976). The use of this diagram requires the calculation of  $S^*$ , determining the Shields parameter ( $\Psi$ ) from the diagram and computing the bottom shear stress ( $\tau_o$ ) as follows:

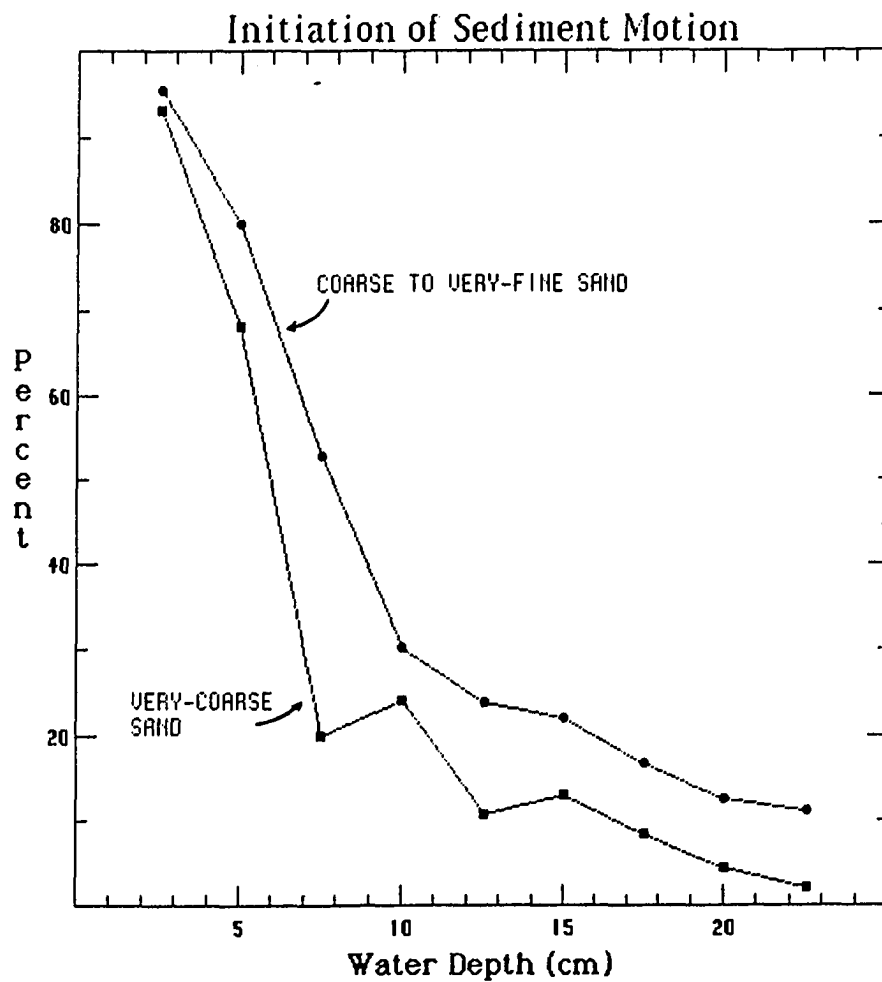
$$S^* = \frac{d_s}{4\nu} \sqrt{(s-1)gd_s} \quad (3-1)$$

and

$$\tau_o = \Psi(s-1)\rho g d_s \quad (3-2)$$

where  $d_s$  - diameter of the sediment (0.168 cm)  
 $\nu$  - kinematic viscosity (0.01 cm<sup>2</sup>/sec)  
 $s$  - specific gravity of the sediment (2.65)

FIGURE 3-4. The difference in the percent of vortex rings (the number of drops which formed vortex rings divided by the total number of drops in the set or 25) which moved very-coarse sand, and which moved coarse to fine sand. Both show similar changes in percentages with depth.



Incipient motion of very-coarse sand (1.68 mm) occurs at a critical shear stress of 11 dynes/cm<sup>2</sup>. This represents an approximate velocity of 36 cm/sec. using Shields bottom velocity curve as a function of quartz-sand size (Vanoni, 1977). Qualitative observations indicate that cohesive estuarine muds can also be resuspended by vortex ring impact. The material which appeared to be resuspended was the disaggregated surficial material.

### **Discussion**

This initial experiment has focused on the most simplistic end-member of the rain-induced sediment transport process, namely single vortex rings in a still-water laboratory environment. In this experiment drop-formed vortex rings were able to move non-cohesive sediments at all the depths tested. This included depths of 22.5 cm which was the limit imposed by the receiving water tank. A significant break in slope in the relationship between percent rings moving sediment and water depth was observed between depths shallower than 7.5 cm and depths greater than 10 cm. The results of this study were consistent with preliminary work by Anderson (personal communication) in which clay-sized material was resuspended by impacting vortex rings in water depths to 40 cm.

Water depths of 20 to 40 cm are significant, when studying the muddy intertidal. Rain falling on the exposed tidal flats can cause sediment transport by the same processes active in terrestrial environments. The methodology and techniques to assess the importance of these processes can be approached from essentially this soil erosion perspective (Moss and Green, 1983).

Rain-related sedimentation processes are also significant in the shallow (<50 cm) lens of water flooding over and ebbing from the tidal flat. In this

area, the shallow water depths limit wind-wave turbulence, and the broad expanse minimizes tidal current velocities. In a study by Anderson and Mayer (1984) of an intertidal flood front (15-cm deep), they determined that rainfall accounted for 46% of the observed variability in suspended sediments and the combination of wind and rain accounted for 72% of the variation.

Rain-formed vortex rings can influence estuarine sedimentation in several ways: (1) Ring impact with the bottom can initiate motion of sediment and inject sediment into the water column where it can be transported by currents. (2) When the vortex ring forms, low salinity water is incorporated with the rain into the inner core. Initially, surface water is transported downward; however, when buoyancy exceeds ring momentum, there will be subsequent upward mass transport of water and suspended material. (3) Rain action can also cause secondary effects on other physical processes; for example, dampening wave action, decreasing currents by creating a surface shear (Glass and Smerdon, 1967), increasing density stratification (Houk, 1975), and transferrring momentum to settling particles (Bhuiyan *et al.*, 1971).

Thus, the experiments in still water appear to be reasonable first approximations for understanding how rain causes resuspension in a shallow water column. However, interaction terms, such as multiple vortex-rings and turbulence due to currents and wind-waves, are probably significant when applying this process to natural intertidal environment. The determination of the importance of these interactions is the subject of Chapters 4 and 5.

## CHAPTER 4

### MULTIDROP EXPERIMENTS ON RESUSPENSION OF MUDDY INTERTIDAL SEDIMENTS

#### Introduction

Single-drop laboratory studies suggest that drop-formed vortex rings are an important mechanism in the rain-induced incipient motion of non-cohesive sediments (Shevenell and Anderson, 1985). These studies did not consider interaction effects, when numerous drops are concurrently striking a water surface. Rain induced surface waves may decrease the effectiveness of the splash central jet to form vortex rings. If formed, the ring penetration may be inhibited by water column density stratification in salt water, and/or by increased turbulence near the water surface (Houk, 1975). In addition, fine-grained cohesive sediment responds differently than non-cohesive sand-sized material. A portion of the sediment moved by the impacting rings will go into suspension, and the remainder will rapidly settle out, acting as saltation load. The suspended material with a very slow settling velocity may be entrained by subsequent ring motion, thus remaining in suspension.

Erosion of fine-grained cohesive sediments occurs when the entrainment forces, imparted by the overlying fluid, exceeds the ability of the sediment to resist motion, or from Ariathurai and Krone (1967)

$$\frac{dM}{dt} = R \left( \frac{\tilde{\tau}_a}{\tilde{\tau}_{ce}} - 1 \right) \quad (4-11)$$

where  $dM/dt$  = mass of sediment eroded per unit time  
 $R$  = erosion rate constant  
 $\tau_{ce}$  = critical shear stress for erosion  
 $\tau_a$  = applied shear stress.

The evaluation of a critical shear stress required to initiate erosion is very complicated because of (1) the problems in measuring instantaneous hydraulic shear (Sutherland, 1967); and (2) the many factors which influence the cohesive nature of the muddy intertidal sediments (Amos and Mosher, 1985). For example, it is known that there are many complicating factors in predicting the response of a specific sediment to an applied stress, including: compaction (bulk density), shear strength and antecedent stress; variations in grain-size and organic content; effects of desiccation (*e.g.* exposure time to the atmosphere, solar heating, and ground water influence); and effects of bioturbation and vegetative cover.

Extension of the cohesive sediment erosion process to rain-induced resuspension of muddy estuarine sediment requires an understanding of how rain energy is transferred to the bottom as an applied shear stress. The applied shear stress due to vortex ring impact is difficult to measure, but should be a property of the initial impulse mechanism forming the vortex (Sutherland, 1967), less the amount of momentum lost as the ring moves through the water column (Maxworthy, 1977). Therefore, the rain induced shear stress on the sediment should be related to the rate of energy transferred to the rings, the translational and rotational velocities in the ring at impact, and the ring impact frequency.

The purpose of the multi-drop experiments was to determine if rain could resuspend muddy intertidal sediments covered with a shallow water column; and if so at what water depth did this mechanism resuspend

significant sediment. The approach to the problem was to first conduct a series of laboratory experiments, in which the rate of rainfall energy and the receiving water depth could be controlled. The sediment erosion rate was determined by measuring the excess mass resuspended with time. This mass was determined by sampling the suspended sediment load in the overlying water then subtracting the baselevel concentrations.

It was felt that the tank side walls may affect the turbulent structure within the receiving water tank and consequently affect the amount of sediment resuspended by the artificial rainfall. Therefore, controlled field experiments where there were no side walls followed the laboratory work to confirm the water depth at which rainfall caused significant resuspension. The final phase of the study was observation during two storm events. These experiments were to put into perspective the effectiveness of rainfall as an erosion mechanism, when compared to other natural and man-made processes (e.g. wind and boat waves).

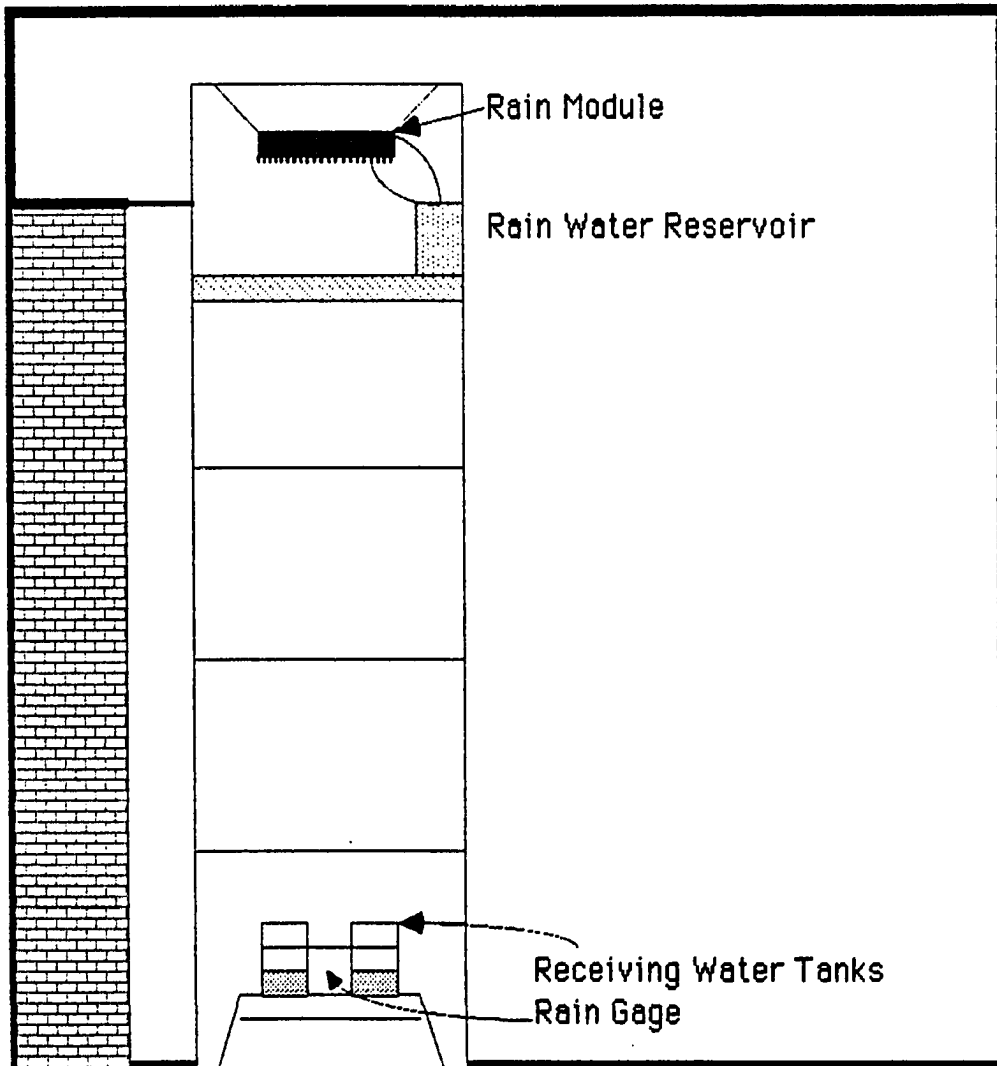
## **Methodology**

### **Field Methods**

**Tower.** A 7-m rain tower was constructed using metal construction staging to position the rain module at specific levels of up to 6 m above the receiving water tanks (Figure 4-1). The tower was encased in plastic sheeting to minimize drafting and to localize rainfall to directly below the module. The distances between the rain module and the receiving water tanks was varied by either lowering the module or raising the receiving water tanks. The tower was located adjacent to the Jackson Estuarine Laboratory (JEL) for the "laboratory" studies.

The same tower was used for both the laboratory experiments and the

FIGURE 4-1. Schematic diagram of the experimental set up for the multidrop experiment. The relative positions of the rain module and reservoir, and the receiving water tanks and rain gage are also shown.



insitu studies on the mudflat. Before the tower was moved to the mudflat, a wooden frame 1.5 by 2.5 m was constructed and mounted above the intertidal mud surface on 25 cm diameter concrete pilings (Figure 4-2). The pilings were pinned to and rested on a basal gravel beneath about 75 cm of estuarine mud. This provided a level and stable base for the 7-m tower, with minimal disturbance to the estuarine mud and water (Figure 4-2). A platform, cantilevered from the frame, provided a work area for sample collection and data monitoring. Plastic curtains were used to minimize wind effects on the falling drops. These were designed to be removed between experiments to minimize wind drag on the tower.

**Rain Module.** The rain module was designed to conform with the apparatus used by Houk (1976). It consisted of a 70 x 70 x 10 cm plexiglas box with the base perforated with 680 holes spaced on a 2.5 x 3.75 cm diagonal grid (Figure 4-3). Hypodermic needles (21 gage) were glued in the perforations to act as flow constrictors and to control drop size. Drops forming at the end of the needles were 0.375 cm in diameter. Plastic tubing 0.32 cm ID, placed over the needles created 0.545 cm drops.

"Rainwater" was pumped from a reservoir of freshwater into the rain module through a particulate filter (Ametek Model PS-S1). A constant head was maintained in the module by an adjustable drain, which returned the excess "rainwater" to the reservoir. The intensity of the rain was controlled by the water head in the module and by plugging alternate needles (Figure 4-3). Intensity was monitored using a Weathermeasure Model 6011-B rain gauge mounted between the two receiving water tanks. The analog output was recorded on a Bausch and Lomb VOM 5 stripchart recorder.

**FIGURE 4-2.** Photograph of the insitu experimental set up. The rain gage is located just under the rain module. The control sampler is set up to the left of the tower and the impact sampler is located in the center of the tower frame. Two wind curtains are set to isolate the rain from the local winds.

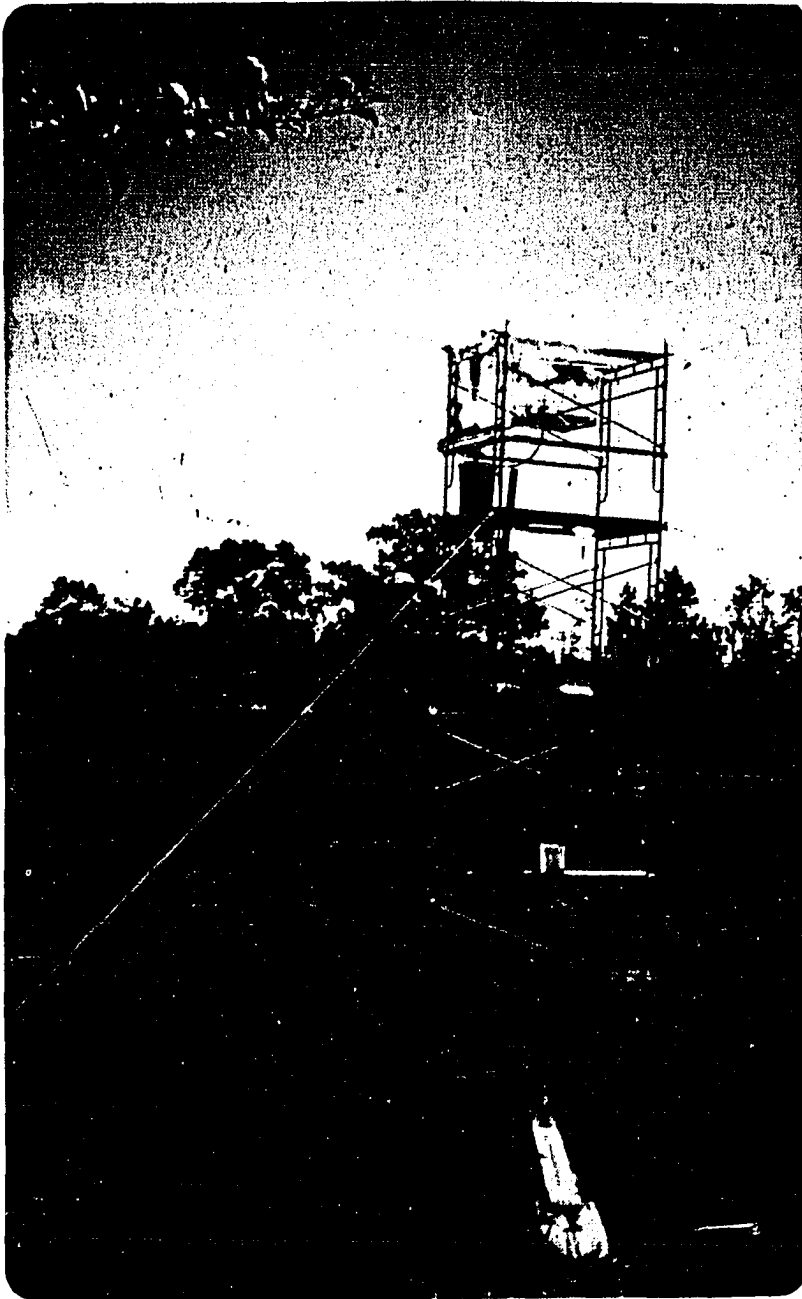
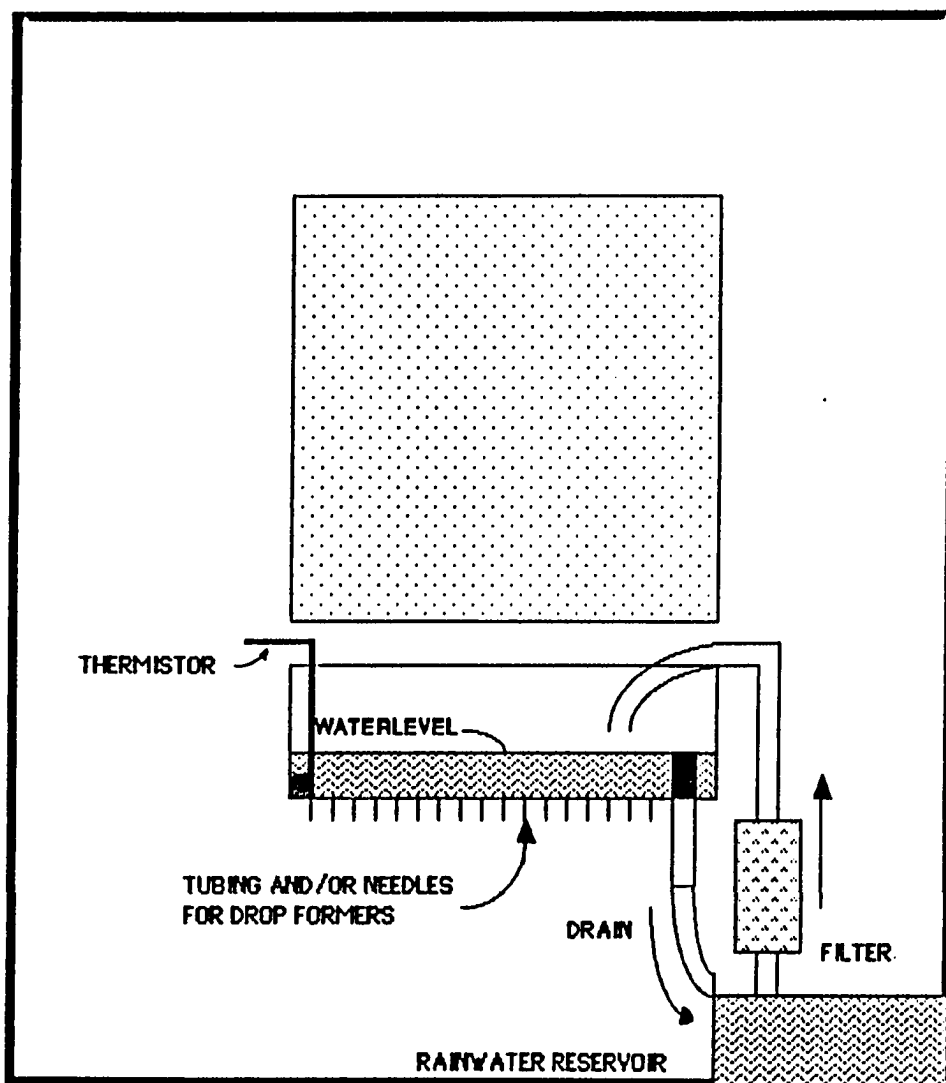


FIGURE 4-3. Schematic of the rain module and the rainwater reservoir system. The rain module consisted of 685 hypodermic needles on a diagonal grid with a 2.5 x 3.75 cm spacing. An in line sediment filter removed most of the suspended load in the rain water. The reservoir contained enough water for a complete run. The reservoir was filled and allowed to come to equilibrium with the ambient temperature before the start of the run. Temperature of the rain water was monitored with thermistor probe.



**Multidrop Experiment: Receiving Water.** Receiving water tanks consisted of two 20.5 cm diameter by 28 cm high translucent plastic tanks with removeable bottoms (Figure 4-4). The tank sidewalls flared slightly to minimize rain drop impact within 1.5 cm of the sidewalls. Water was added and sampled through 0.5 cm ID samplers fixed relative to the bottom (Figure 4-4). Water was taken from the JEL.seawater system and allowed to settle one hour before being siphoned into the receiving water tanks. The water depth in the tanks was controlled approximately by the height of the upper sampler (Figure 4-4). Filling the tanks prior to a run consisted of allowing settled seawater to flow into the tank through the near-bottom sampler, then when full, to flow out the near surface sampler. Typically surface tension lifted a layer of "sediment" off the bottom. Water was cycled until this material was removed.

Water depth and bottom topography in the tanks was measured at 32 locations on a systematic grid (Figure 4-5). These data provided the basis for computing the actual average water depth and water volume. Water depth at the start of the run was standardized by siphoning til dry from the upper sampler. Water depth was monitored at the beginning and end of each sample using a scale fixed to the outside of the tank. Receiving water temperature was monitored using a thermistor from a YSI Model 47 Scanning Tele-Thermometer mounted near the sediment surface.

Water samples were collected throughout the run by siphoning water from the near bottom and near top samplers into 300 ml sample bottles. The rate of sample collection was fixed to the rainfall intensity. The objective was to maintain a constant volume in the receiving water tank. All water, except incidental spillage and purging of the lines prior to each sample collection (about 25 ml), was retained for suspended load analyses.

FIGURE 4-4. Schematic of the receiving water tanks and water samplers. The water level at the start and end of each sample was read from the scale. Water was sampled from the two intakes, one near surface and one near bottom, by siphoning. Water temperature was monitored near bottom with a thermistor probe.

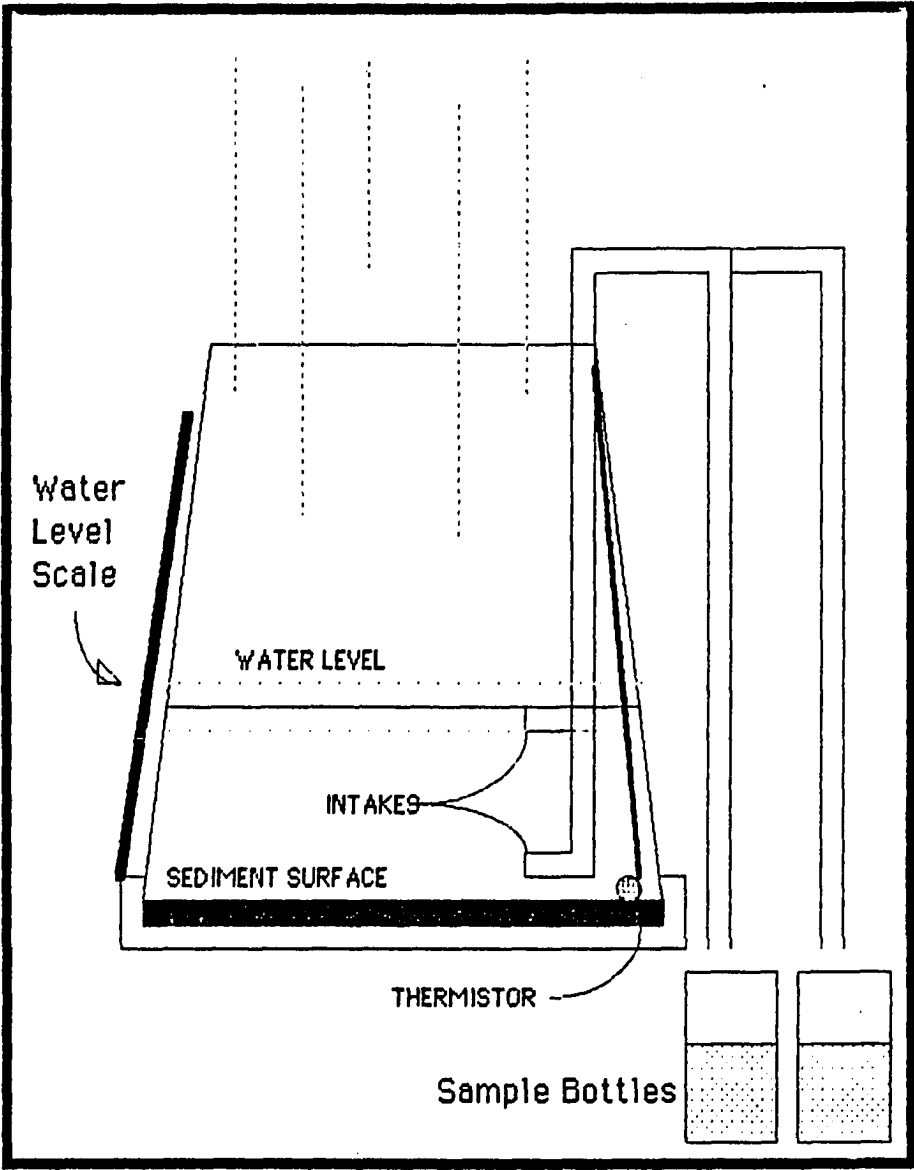
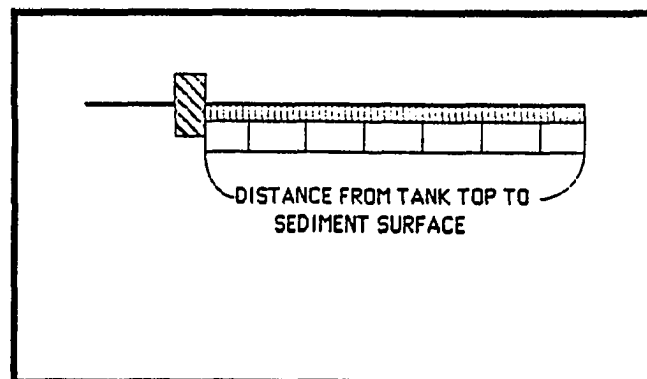
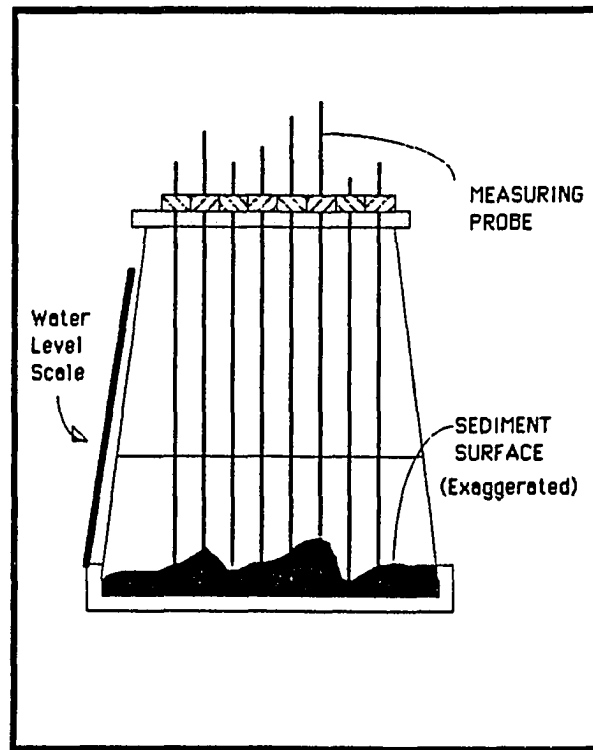


FIGURE 4-5. Diagram showing the methodology used to measure the sediment microtopography in the receiving water tanks. Each measuring probe was removed, length to sediment measured and the data averaged for the 32 points.



**Multidrop Experiment: Substrate.** Bottom substrate for each run was collected from the tidal flat in Adam's Cove near JEL. The receiving tank bottoms were carefully slipped horizontally beneath the sediment surface. The area around the cover was cleaned away and the cover with the undisturbed sediment surface was removed from the tidal flat (Figure 4-6). The sidewall of the tank was clamped into place making a water tight seal. Since the thickness of sediment and the microtopography varied with each collection, the surface was carefully measured relative to the tank top.

Surface samples for textural analysis were collected from most sediment surfaces. This sample was collected after the runs to minimize the disturbance of the surface. The sampling consisted of careful scraping the upper few millimeters of sediment from several random locations to obtain as representative sample as possible. The results from the analysis of these samples are presented in Chapter 6.

**Insitu Experiment.** The insitu experiment duplicated some of the rainfall characteristics used in the multidrop laboratory experiment. The receiving water was the ebbing estuarine water and the bottom sediment was the insitu estuarine sediment. The difference between the two experiments was that there were no confining sidewalls to concentrate turbulence. The effect of the rainfall was monitored by a pair of near-bottom ( $<1$  cm) samplers, one in the rain impact area and one in a control area. The samplers in the study area and the control site consisted of two sections of 0.5 cm ID tubing mounted horizontally and connected to a peristaltic pump (Figure 4-7). Water was pumped continuously during each experiment, and collected in 300ml sample bottles. The experiment was initiated when the falling water depth was about 30 cm, and continued until the tidal flat was exposed. The

FIGURE 4-6. Diagram showing the sediment collection technique, which minimized the disturbance of the sediment surface. The receiving tank bottom was carefully pushed under the sediment surface, keeping the bottom parallel with the sediment surface. The excess sediment was cleaned from the circumference so that the tank wall could fit into place.

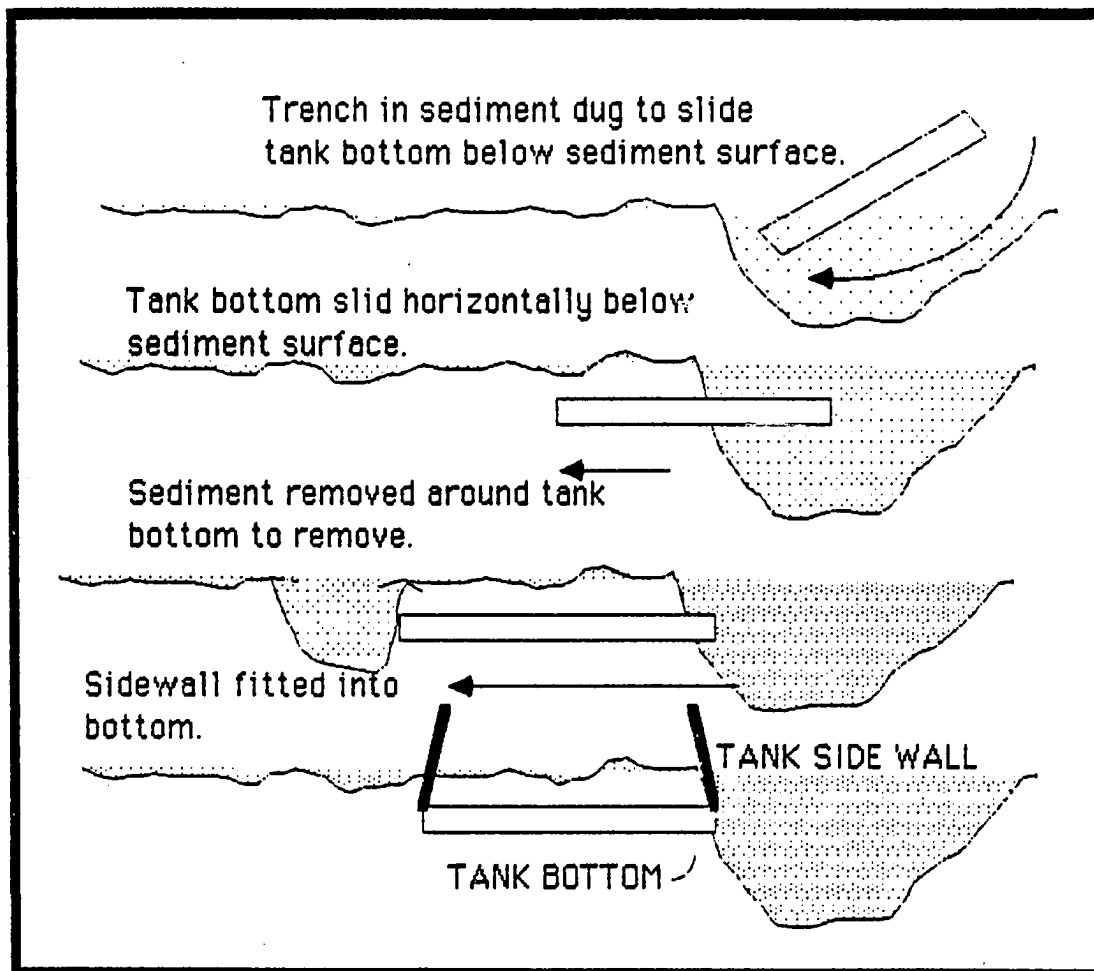
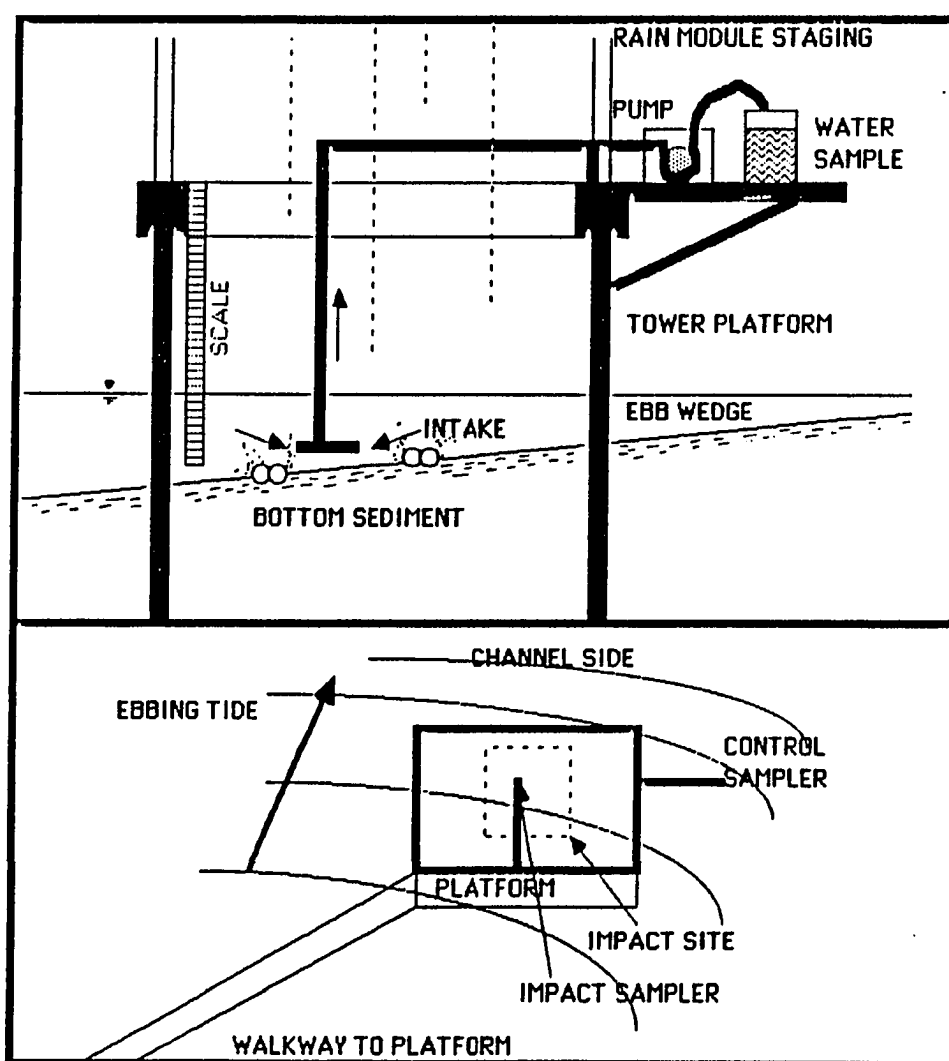


FIGURE 4-7. Schematic diagram showing the sample collection set up for the insitu experiment. The control pair of samplers was located outside of the tower platform. The impact pair of samplers were located inside the tower platform. The frame for the tower was high enough off the sediment surface so that it did not interfere with water movement during the sampling period. A peristaltic pump was used to draw water for the suspended load samples.



water depth and time was monitored for each sample. Field notes were made when an unusual disturbance occurred, such as boat wakes, wind waves or epibenthic animals passing through the study area.

**Storm Observations.** Two rainstorms were sampled using the same sampling and analytical procedures as in the insitu experiment. The location of the storm sampling was near the insitu rain tower at the head of JEL Cove. Water samples were collected in pairs about 1.1 cm above the sediment surface. Sampling was started when the water depth was about 20 cm and continued until the water was too shallow for sampling. Rain drop size distribution was sampled using the flour method (Robinette and McCool, 1985). Rainfall intensity was determined volumetrically, knowing the collection area and the time interval. A sediment sample was collected for textural analysis at the end of the second storm.

### **Laboratory Methods**

**Artificial Rainfall Characteristics.** The drop size from the rain module and during natural rainfall events was measured using the flour-pellet method (Robinette and McCool, 1985). In this method a pan of flour was held under the rain module for a several seconds to obtain at least 50 rain drops. The water from the drop was absorbed by the flour. Baking produced dough pellets which were proportional in weight to the original volume of water in the drop (Laws and Parsons, 1943). The pellets were sieved and weighed on a Cahn TA 450 balance, and converted to drop size using a calibration curve developed with known drop sizes (using the technique described in Chapter 2). The modal (by weight) pellet size was used as the characteristic rain-drop size.

Impact velocity of the drop was determined by measuring the distance from the tip of the drop formers to the water surface in the receiving water tanks. The results of Laws (1941) were then used to calculate the impact velocity for the specific drop size and fall distance.

**Physical Characteristics of Receiving Water.** The salinity of each sample was measured using an American Optics refractometer with an accuracy of  $\pm 0.5$  o/oo. Water density was computed from the measured temperature and salinity with a computer program based upon Knudsen's Tables.

**Suspended Sediment.** Suspended sediment was measured using the filtration method based upon Banse *et al.*, 1963). Glass fiber filters were used because of the ease of use, high number of samples per run and because it was consistent with the numerous studies conducted in the same study area by Anderson (*e.g.* 1983). Approximately 300 mls were filtered through pre-weighed filters, carefully washed with a solution of sodium sulfate and distilled water to remove the sea salts, and dried for about 12 hrs at 50°C. The dried filters were reweighed, along with control filters to determine the total dry weight of suspended sediment. The filters were then ashed at 500°C for 2 hrs and reweighed to determine the percentage of combustibles. Changes in filter weights, as determined by the controls, were accounted for in the data reduction.

## Results

### Multidrop Experiment

The purpose of the multidrop experiment was to determine, in a controlled, quiescent environment, the maximum water depth in which rain-induced resuspension is a significant mechanism. The single-drop studies suggested that drop-formed vortex rings could initiate motion of non-cohesive sand-sized sediment in quiescent water depths of at least 22.5 cm (Shevenell and Anderson, 1985), and motion of clay-sized material in water depth of 42 cm (Anderson, personal communication, using a similar experimental set-up and drop size). This study expanded the hypothesis to cohesive estuarine sediment and multiple drops.

There were both benefits and limitations in the laboratory study. The single-drop experiments illustrated the relatively complex physical processes involved in a rain drop causing sediment motion. The laboratory study could control some of the more important independent variables. However, the drop-formed vortex rings, the hypothesized mechanism for sediment resuspension, were quite sensitive to ambient turbulence in the receiving water. Experimental rain-induced turbulent motion is probably not similar to the turbulent scales in the natural environment, because of the presence of the tank side walls. One would suspect that the turbulent action in the tanks is more intense than in the natural environment because of reflection of surface waves by the tank sidewalls. This turbulent action may disrupt the formation of vortex rings, thus leading to an under-estimation by the laboratory studies of the importance of rainfall resuspension in shallow water.

The changes in suspended sediment concentrations in the receiving water were due to both conservative mixing between rain water and the

initial volume of seawater in the receiving water tanks, and nonconservative mixing with resuspended bottom sediment. The initial concentrations in the rain water and in the receiving water tended to be low ( 0.7 to 47 mg/l in the receiving water and 0 to 14 mg/l in the rain water). The suspended sediment data from the multidrop experiments were used to calculate the mass of sediment in suspension in the receiving water during the experiment. This mass ( $M_e$ ) was determined by first accounting for changes in suspended sediment concentration due to conservative mixing between the rain ( $C_r$ ) and the initial receiving water ( $C_b$ ). The difference between the conservative and the observed concentration ( $C_o$ ) was termed the excess concentration ( $C_e$ ), or

$$C_e V_r = C_o V_r - (C_r f + C_b(1-f))V_r = M_e \quad (4-2)$$

where  $f = (S_s - S_o)/S_s$  = fraction of freshwater  
 $V_r$  = receiving water volume  
 $S_o$  = observed salinity  
 $S_s$  = the base salinity ( at start of run).

Differences between the observed concentration and the computed conservative concentration which exceeded the accuracy of the suspended sediment method (about 1 mg/l), were assumed to be due to either settling of sediment out of the water column or due to erosion of sediment from the bottom.

A sample correction to the excess mass calculation was required, because the samples represented a relatively large volume of water compared to the receiving water volume. The amount of water removed was determined by taking the volumetric difference between the start and end

of sampling, and accounting for the rain volume. The receiving water volumes ranged from 0.71 to 2.65 l, while the sample volumes represented about 1.5 to 2.5 l per run. Thus the samples were a major suspended sediment removal mechanism.

The change in excess mass with time ( $dM/dt$ ) curve of each run was simplified by taking the first observation in the run (mean of 11.5 min) after the initiation of rain, the last observation in the run (mean of 50 min), and the difference between the two observations. The purpose was to use the observed data, rather than averaged data as the dependent variables in the statistical analyses.

Multiple regression analysis was conducted by first developing a linear correlation coefficient matrix between the independent variables and the resultant excess mass dependent variables. The number of independent variables was reduced by selecting only significant (at the 95% CI) linear correlations. This sub-matrix was further reduced by removing those independent variables which had a significant correlation with other independent variables. Selection at this point was based upon physical reasoning. Multiple regression analysis Ryan *et al.* (1976) was then performed on the remaining independent variables. Each variable was then evaluated based upon its contribution to the regression sum of squares in the analysis of variance. An F-test (at 95% CI) was conducted on the analysis of variance to determine the significance of the regression equation. R-squared valued (corrected for the degrees of freedom) were then used to make relative comparisons between subsets.

The 60 runs in the multidrop experiments were first divided into two groups. Those runs in which the excess mass exceeded the accuracy of the methodology (5 mg), and those in which only conservative mixing was taking

TABLE 4-1. Summary of multidrop runs identified as conservative mixing or nonconservative cases. The nonconservative cases are subdivided by the four cases illustrated in Figure 4-8.

RUN	CONSERVATIVE MIXING	NON-CONSERVATIVE MIXING			
		1A	2A	2B	3
10A					X
10B					X
11A			X		
11B		X			
12A					X
12B		X			
13A	X				
13B		X			
15A		X			
15B			X		
16A	X				
16B	X				
17A		X			
17B			X		
18A		X			
18B		X			
19A		X			
19B		X			
20A					X
20B			X		
21A		X			
21B		X			
22A		X			
22B		X			
23A			X		
23B		X			
24A					X
24B					X
25A			X		
25B		X			
26A					X
26B	X				
27A	X				
27B		X			
28A	X				
28B		X			
29A					X
29B	X				
30A	X				
30B	X				
31A	X				
31B	X				
32A	X				
32B	X				
33A				X	
33B	X				
34A				X	
34B					X
35A	X				
35B					X
36A			X		
36B					X
37A				X	
37B			X		
38A		X			
38B		X			
39A		X			
39B	X				
40A	X				
40B	X				

place during the experiment (Table 4-1). Conservative mixing occurred when the observed suspended load was explained (within the accuracy of the method) by mixing between only the rainfall and initial receiving water baseload. Those runs which exhibited non-conservative processes were then sorted into three different cases based upon physical reasoning to describe

the  $dM/dt$  curve (Table 4-1). Examples of runs for each case are shown in Figure 4-8.

Erosion of sediment occurs when the applied shear stress exceeds the critical stress for erosion of the sediment (Equation 4-1). When the applied shear stress is large, compared to the critical stress, sediment will be eroded at a continuous rate. As the applied shear stress decreases and approaches the critical stress, the slope of the excess mass versus time curve changes in an asymptotic fashion. When the applied shear stress equals the critical shear stress, then the slope of the excess mass versus time ( $dM/dt$ ) is zero, or in equilibrium. Figure 4-8C illustrates this concept.

Case 1A is where the applied stress is much greater than the critical stress, thus the  $dM/dt$  curve is linear and increasing with time. Case 1B is similar to case 1A in that the applied stress is greater than the critical stress. However, if the critical shear stress for erosion of the sediment is gradually increasing with time, then the slope of the  $dM/dt$  curve will decrease and approach equilibrium. Equilibrium is where the applied stress and the critical stress for erosion are balanced.

Case 2 represents runs where a step increase in excess mass occurred immediately upon initiation of rainfall. After the initial increase  $dM/dt = 0$ , in Case 2A, suggesting equilibrium conditions. After the initial increase  $dM/dt$  is negative in Case 2B, suggesting no erosion and particle settling. In

FIGURE 4-8. Examples from the multidrop experiments which illustrate the four basic cases in which the excess mass suspended in the receiving water column varies with time. Panel A shows examples of Case 1 A, where  $M_e$  increases linearly with time. Panel B is where an equilibrium is gradually reached (Case 1B). Panel C shows examples where equilibrium is reached right after initial resuspension (Case 2A). Panel D is similar except material settles out over time (Case 2B). Panel E shows examples where no material is eroded but suspended matter settles out with time (Case 3).

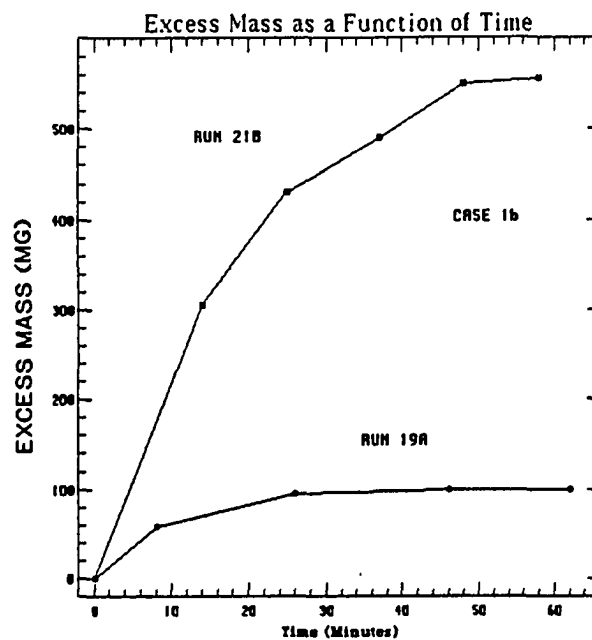
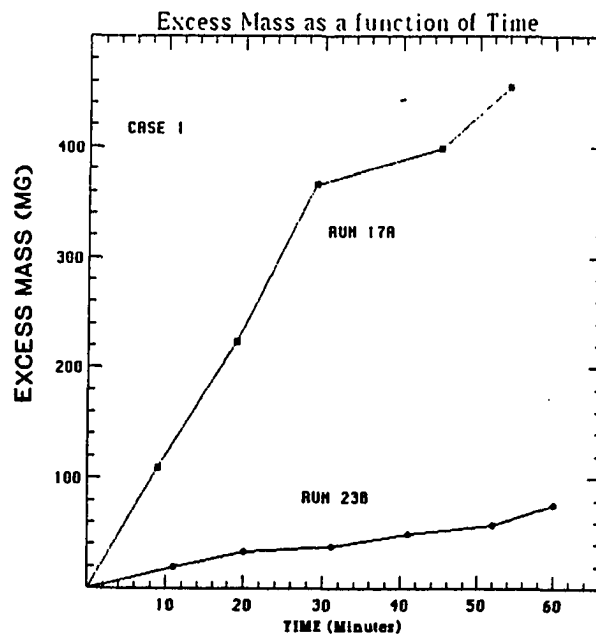
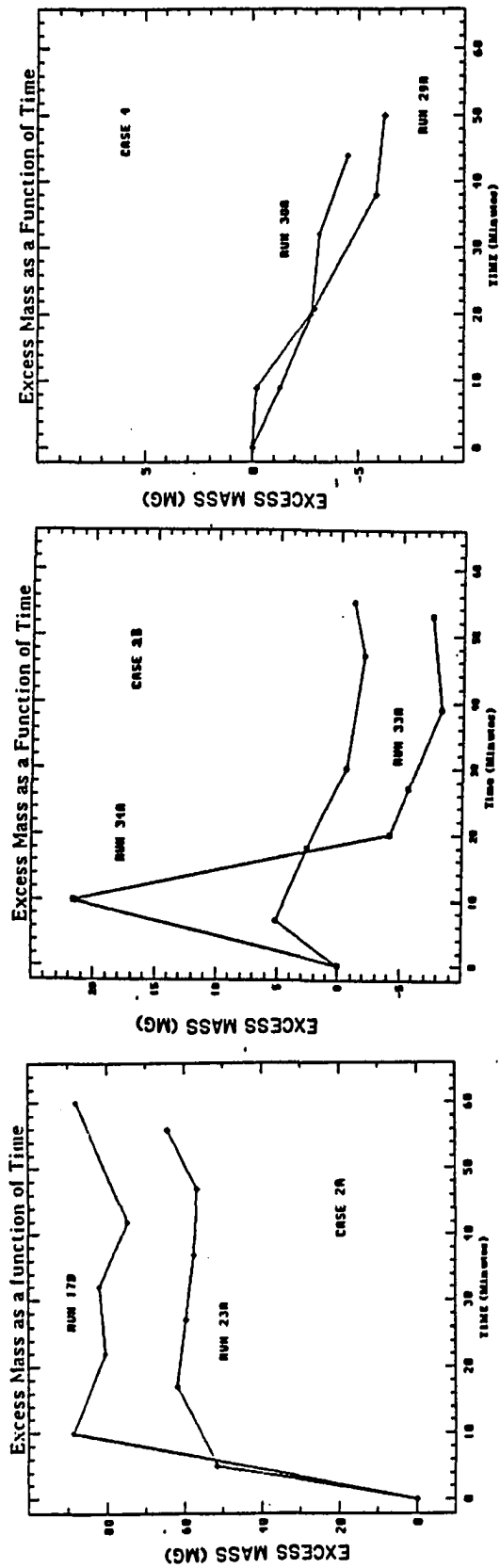


FIGURE 4-8. Continued.



these cases the material initially resuspended would have a low critical stress required for erosion, relative to the applied stress. However, the sediment surface, once this material was resuspended, required a relatively high shear stress for erosion. This suggests two distinct layers. The top layer would have had a relatively low antecedent stress history, thus requiring a low critical stress for erosion. The second layer would have had a relatively high antecedent stress history, thus requiring a high critical stress for erosion.

Case 3 represents no erosion of bottom sediment, thus the applied shear stress is less than the critical shear stress, resulting in a negative slope in the  $dM/dt$  curve. This case is different from the conservative mixing runs, in that significant amounts of material are settling out of the water column.

The above arguments for the three different cases have been made from the point of view of the sediment surface. A similar argument can be made using the energy input by the rain and the water depth through which the energy is transmitted. The applied shear stress may vary due to rainfall intensity, water depth and the penetration of vortex rings to the bottom. Resolution between the two points of view requires specific measurements stress applied to bottom and the critical shear stress for erosion of bottom material. Shear stress measurements at the appropriate scales were not made in this initial investigation, but the end products were observed.

The data set consisted of several independent variables which were measured during the course of the run. These variables have been divided into (1) rain, (2) water column and (3) bottom characteristics (Table 4-2). Multiple regression analysis was conducted on the matrix of independent

TABLE 4-2. Independent variables divided into rain, bottom sediment and water column characteristics. These groups of variables are further subdivided into groups which are similar from a physical point of view. Significant (at 95% CI) correlation coefficients for excess mass at 11.5 and 50 min into run.

INDEPENDENT VARIABLES	CORRELATION COEFFICIENTS							
	11.5 Min			50 Min.				
	1	2A	2B	3	1	2A	2B	3
<b>RAIN CHARACTERISTICS</b>								
Impact Frequency:								
Intensity								
No. Drops/min.								
No. Jets/min.								
Energy:								
Drop Size						.651	.804	
Drop Height	.539	.643		-.728	.473		.690	-.704
Drop $E_i$	.661	.828			.722	.795		
Drop $V_i$	.620	.827			.683	.836	.780	
Drop $E_i/A_i$	.542	.659			.505	.694	.762	
Dynamic:								
Rain Temperature								
Delta-t (Rain and Receiving)								.669
<b>BOTTOM CHARACTERISTICS</b>								
Resuspendables:								
Percent Mud								
Percent Organics in Mud								
Percent Total Organics								-.874
Lag Formers:								
Percent Sand								
Percent Org. in Sand								-.636
Percent Aggregates								-.808
Percent Total Organics								-.747
<b>WATER COLUMN CHARACTERISTICS</b>								
Density:								
Temperature								
Base Salinity								.711
Base Sigma-t								
Observed Salinity								
Stability:								
Delta-t (Rain and Receiving)								
Salinity Stratification								
Depth:								
Water Depth								.697
Topography	.421			.780				.675
Ratio Depth/Topo.								.808
								-.735

and dependent variables to determine the important factors controlling resuspension.

Multiple regression analysis was conducted by first developing a linear correlation coefficient matrix between the independent variables and the resultant excess mass dependent variables. The number of independent variables was reduced by selecting only significant (at the 95% CI) linear correlations. This sub-matrix was further reduced by removing those independent variables which had a significant correlation with other independent variables. Selection at this point was based upon physical reasoning. Multiple regression analysis Ryan *et al.* (1976) was then performed on the remaining independent variables. Each variable was then evaluated based upon its contribution to the regression sum of squares in the analysis of variance. An F-test (at 95% CI) was conducted on the analysis of variance to determine the significance of the regression equation. R-squared values (corrected for the degrees of freedom) were then used to make relative comparisons between subsets.

A linear correlation matrix was developed by subdividing the data by the four excess mass cases (Case 1, 2A, 2B and 3) then by correlating the excess mass at 11.5 min and 50 min after the start of a run with the range of independent variables listed in Table 4-2. The purpose of this analysis was identify the important groups of variables which may significantly affect the excess mass in the receiving water. Table 4-2 identifies those variables which exhibited significant correlation (at 95% CI) with changes in excess mass amounts.

The independent variables can be reduced, where there is a significant correlation between variables, by selecting the one which makes most sense from physical reasoning. Two approaches were used to identify the

important independent variables controlling changes in excess mass from run to run. The first approach was to take the individual independent variables and conduct a multiple linear regression analysis to determine the amount of variability in excess mass that was explainable by each independent variable, in a step-wise fashion. This was conducted for each case where excess mass exhibited non-conservative behavior.

The second approach was to identify interaction effects that might be important. This can be done by combining variables that make physical sense. The rainfall energy group of variables are most significant in controlling excess mass concentration. Therefore, an energy flux term ( $p$ ) which combined the intensity, the drop impact energy and drop size was considered, where

$$p = \rho f_d (I v_i^2 / 2) \quad (4-3)$$

where  $I$  = rainfall intensity  
 $f_d$  = drop size efficiency factor (defined below).

This is in agreement with Houk (1975) who found that the depth of mixing due to rain is proportional to power. In addition Houk (1975) observed that drop size was important when  $P > 75 \text{ gm/sec}^3$ . The physical reasoning for a drop dependence given by Houk (1975) was that larger drops created larger turbulent eddies, which are more efficient in mixing. In our experiments, power ranged from 139 to 1292  $\text{gm/sec}^3$ .

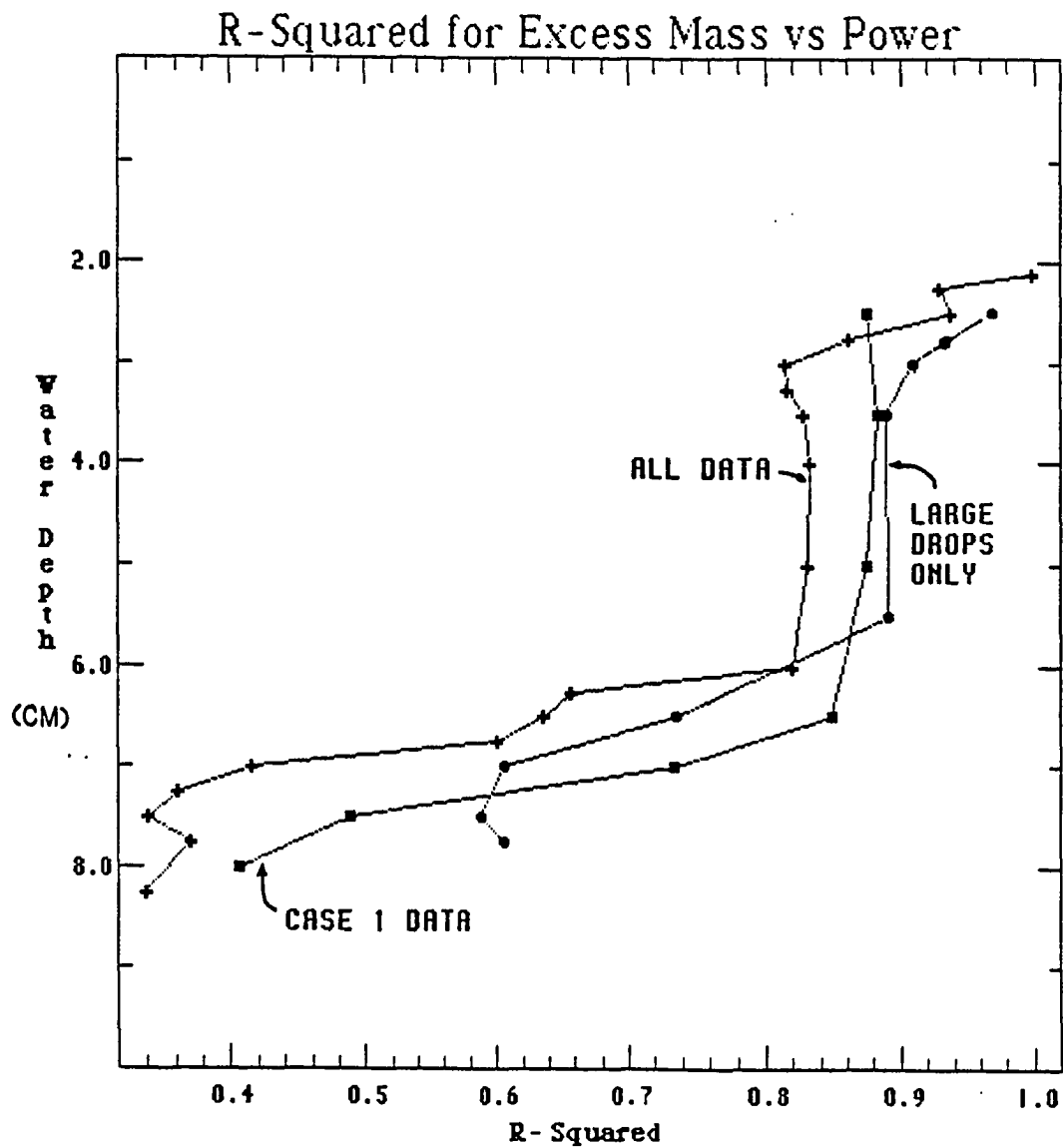
The efficiency factor ( $f_d$ ) used to test this conclusion was 1 for the 0.274 cm drops and 4 for the 0.513 cm drops. These coefficients were based upon the ratio between the ring volumes produced by the large and small drops. The small drops (0.01077 cc/drop) produced a ring with an inner

core volume of 0.0971 cc. The larger drops (0.07069 cc/drop) produced vortex rings with core volumes of 0.384 cc. Thus if turbulent mixing is proportional to ring volume, then larger drops would create about 4X more mixing than the smaller drops.

The depth dependence of bottom sediment resuspension was tested by ranking the data by depth then regressing the excess mass at 11.5 min into the run against the power term (no efficiency factor was used). Sequential subsets were generated by including data from increasing depths at 0.25 cm intervals starting at 2.1 cm depth. The R-squared, adjusted for the degrees of freedom, was plotted with depth to identify major changes in the relationship between power at the water surface and resuspension of bottom sediment (Figure 4-9). This depth dependent analysis, when using all data, suggests that as the water depth increases, the importance of rain-induced power at the surface decreases as a resuspension factor. If all data are considered, there is a significant (at 95% CI) correlation between power and excess mass. There appear to be three important zones: (1) less than 3 cm; (2) 3 to 6 cm depths; and (3) greater than 7 cm depths (Figure 4-9).

When only Case 1 is considered the R-squared values indicate a stronger relationship at each depth (Figure 4-9). When only the runs with the larger drops are considered, the R-squared values are similar to Case 1, except in the deepest water (7.5 to 8 cm). The R-squared values of the large drop runs remain relatively strong throughout the depths tested. When only runs with the small drops are used, kinetic energy flux at the surface shows no significant relationship with the observed excess mass. For the small drops the significant independent variable was the inverse of rainfall intensity. In addition this relationship was significant only when the receiving water depth was greater than 5 cm deep.

FIGURE 4-9. Vertical distribution of R-squared for linear regression between excess mass at 11.5 minutes into the run and rain power. The three plots consider all data, only Case 1 data, and only the large drop data. All R-squared values are significant at the 95% CI.

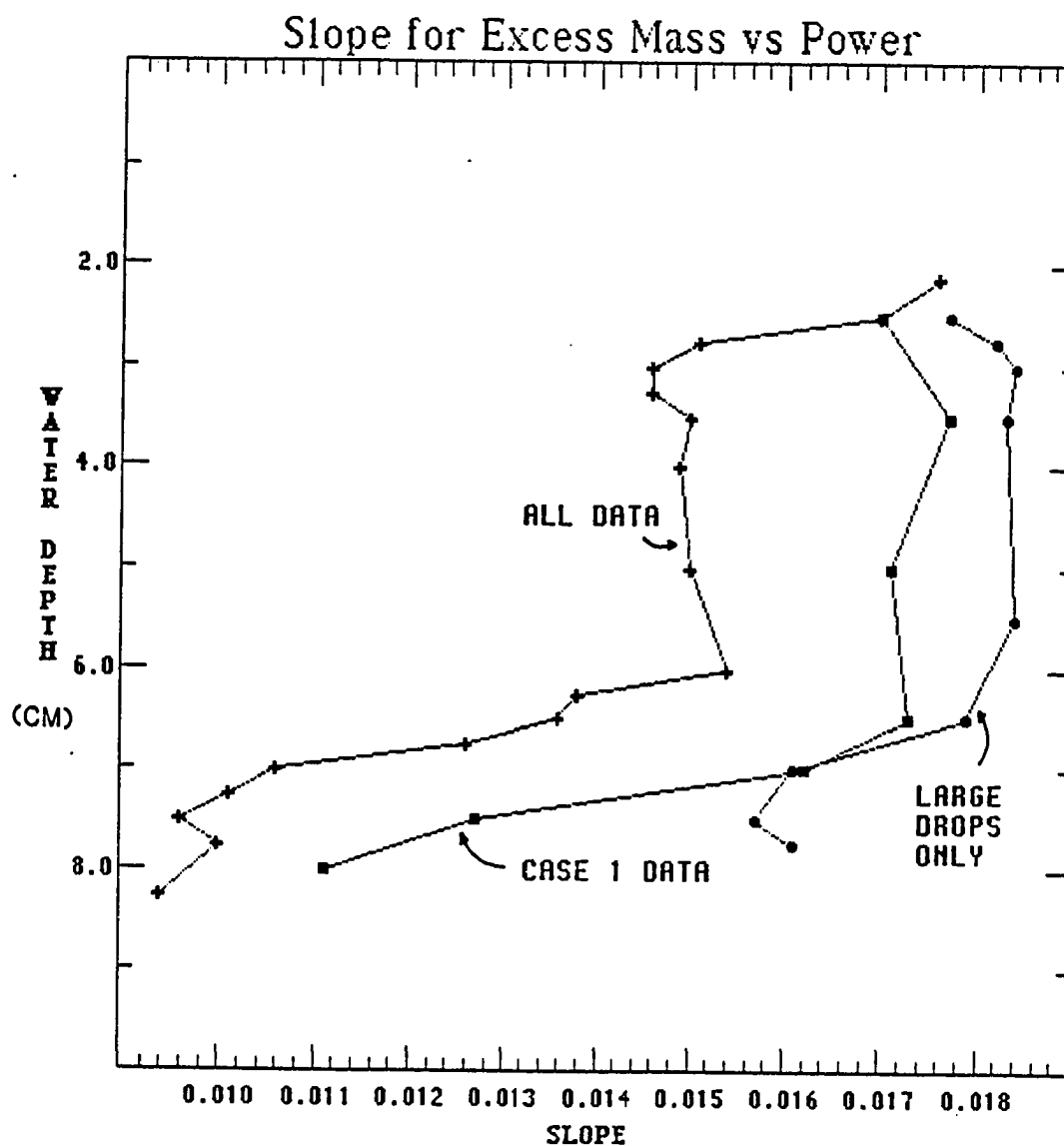


The response by the small rings makes sense, if ring momentum is the critical factor in maintaining the ring integrity as it moves through the water column. The smaller drops produce relatively weak vortex rings. These rings do not penetrate if there is substantial turbulent mixing due to the rainfall intensity. If the rainfall intensity is relatively light, thus the turbulence is low and rings can penetrate to the bottom and resuspend sediment. This would explain the inverse relationship with intensity and why resuspension occurs only when the water is relatively deep.

The larger drops produce larger rings with much greater momentum than the smaller drops. The larger rings are able to move through the turbulent water column and strike the bottom, resuspending sediment by both translational impact and shear created by the rotating fluid in the inner core. As the rainfall intensity increases the number of rings formed also increases, thus resuspending more sediment. As water depth is increased the ring momentum at impact with the sediment is less because of the lower translational velocities. The results of this experiment suggest that there is a transition zone at water depths between 6 and 7 cm, where either less rings are touching the bottom or the rings have less rotational velocity to resuspend sediment. It is important to note that even at the greatest depths studied, there is significant bottom material resuspended by the rings.

As power to the water surface is increased, a response should be seen in the excess mass of suspended sediment observed in the water column. The slope of the linear regression equation defines the amount of change in excess mass per amount of change in power; therefore changes in slope would occur if more (or less) power is needed to resuspend the same mass of excess sediment. When the slope is plotted with respect to the depth of the overlying water column, it decreases as water depth increases (Figure 4-10).

FIGURE 4-10. The vertical distribution of the slope from the linear regression between excess mass at 11.5 minutes into the run and power. The three curves represent all data, only Case 1 data, and only data from the large drop runs. The water depth is in cm.



A transition zone is observed at water depths of 6 to 7.5 cm when all data and Case 1 data are considered.

### **Insitu Experiment**

The insitu experiments were conducted to test the observation that artificial rainfall could resuspend significant amounts of estuarine sediment in a shallow water column. The limitations of the laboratory experiments included potential problems with boundary effects due to the receiving water tank walls. A second potential problem was modification of the sediment surface during collection, transport to tanks and filling the tanks with receiving water. A second purpose of the insitu experiments was to compare the amount of sediment resuspended by the artificial rain with other resuspension events including wind and boat waves, and epibenthic organisms tracking across the sediment surface.

The insitu experiments were conducted when the ebbing tide occurred early in the morning so as to minimize the probability of wind and boat waves encroaching upon the experimental site. The purpose was to isolate the artificial rain effects from the other resuspension mechanisms. Since ideal conditions were not always present during the experimental run, it was possible to make comparisons between the resuspension signature for the artificial rain and the other mechanisms. The objectives of this study were (1) determine the water depth at which significant amounts of sediment were resuspended by artificial rain; and (2) compare the magnitude of resuspended material by rainfall with the other observed resuspending mechanisms.

Several assumptions were made when analyzing the results of this experiment. The paired samplers in the rain impact site were located in the

center of the rain, about 1 cm off the bottom. The rain impact area was about 75 by 75 cm. Although there was a slight current due to wind and the ebbing tide ( $\ll 2$  cm/sec), it was assumed that the water samples were representative of the impact area. The control site was always located away from (about 1.5 m) and up current from the tower platform and the rain impact area. It was assumed that the control area represented natural conditions at the site and was not influenced by the artificial rain. On occasional runs, epibenthic organisms (hoheshoe crab and green crab) tracked through either or both sampling sites. These occurrences were noted. No measurements of wave characteristics were made, except to differentiate between wind waves, boat waves, and calm conditions.

The effects of waves versus rain resuspension on the suspended sediment signature of the trailing edge as water ebbs off the tidal flat was differentiated in this experiment. Wave action affected suspended load at both the control and impact sites (*e.g.* Figure 4-11). A broad and gradual increase in suspended load was observed as water level decreased, when either wind waves or wind generated swell was present in the study area throughout the sampling period.

Boat waves and faunal tracking tended to cause short term spikes in the suspended sediment signature (*e.g.* Figure 4-11). Boat wakes differed from wind waves in that they were relatively short term pulses of increased energy. It was interesting to note, that concentrations decreased after the effects of boat wakes decayed (Figure 4-11). This suggests that much of the material resuspended settles out rapidly. This observation is consistent with work by Anderson (1971) on boat wave resuspension at the same site.

Elevated concentrations were observed only in the impact area and not in the control area, when artificial rain was the important resuspension

FIGURE 4-11. In situ suspended sediment concentrations within the rain impact area and in the control site. Each panel shows how the suspended sediment concentrations (PM) vary with different resuspension mechanisms. The mechanisms are labeled when observed. Water depths are in cm.

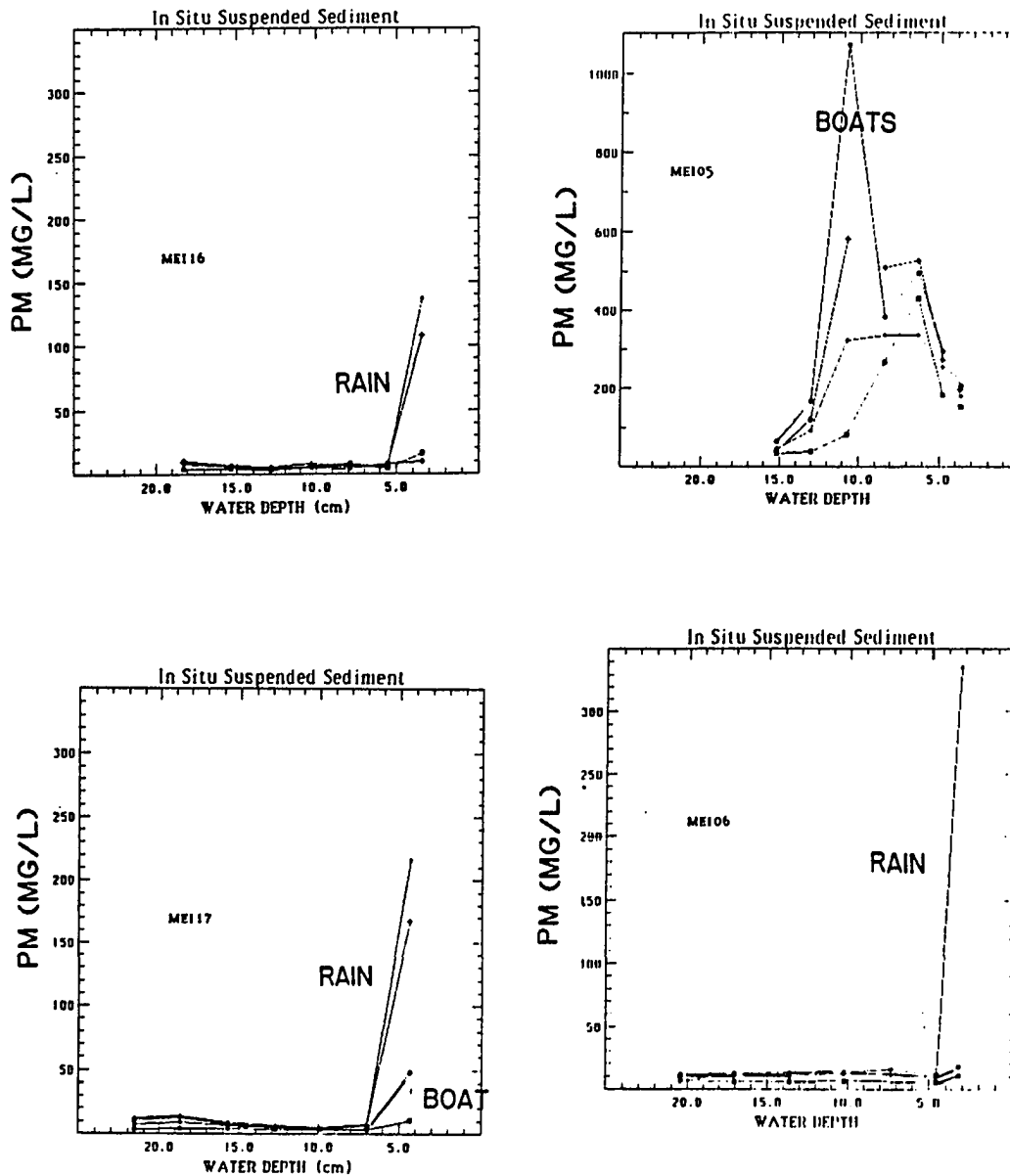
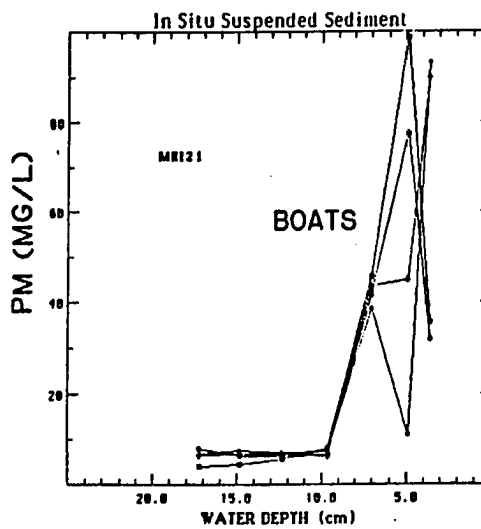
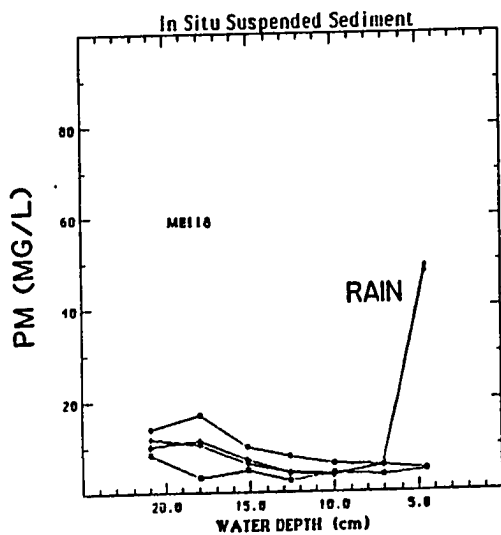
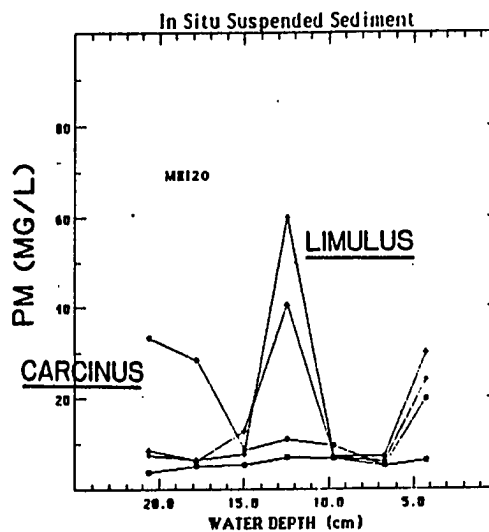
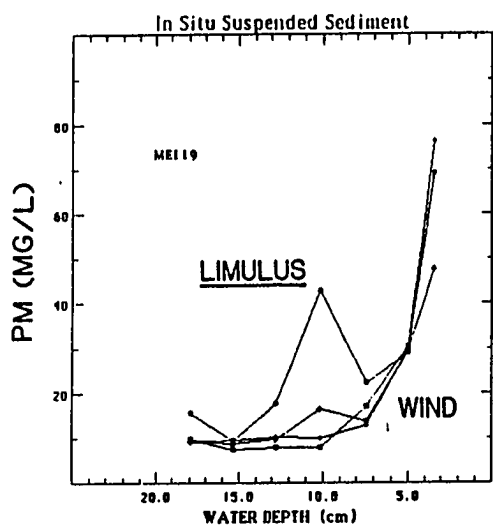


FIGURE 4-11. Continued.



mechanism (e.g. Figure 4-11). Rain enrichment of suspended sediment concentrations was determined by taking the ratio of concentrations between the impact and control areas. The impact area concentrations were significantly elevated over the control site when the enrichment ratio exceeded two standard deviations of the average (after those outliers were removed). The runs in which significant rain resuspension was observed, and where no organisms were observed in either site are listed in Table 4-3. The rain enriched concentrations were observed during these runs, when the average (over the sample collection time) water depth was 3.25 to 5.1 cm. Therefore the ability of artificial rain to significantly increase the suspended load was limited water depths to 5 cm. Rain effects may have occurred in deeper water, but this conclusion is limited due to sampling methodology. The range of average water depths for the samples prior to the rain-enriched samples was 4.6 to 7.1 cm. If one optimistically assumes resuspension started at the beginning sampling, the maximum water depths in which an observed rain influence may have occurred was about 7 cm. Rain-formed vortex rings may be resuspending bottom sediment in deeper water, but the rain effect could not be isolated from the natural variability in suspended sediment concentrations observed on the muddy tidal flat. However, this depth compares favorably with the results of the multidrop laboratory studies where resuspension due to rain was observed at the maximum depth tested (8 cm).

Each resuspending mechanism affects the suspended sediment signature of the trailing edge of intertidal water as it ebbs off the mudflat. Wind waves, if continuous during the ebb period, tend to increase concentrations as the water depths get shallower (Figure 4-11). This effect continues until a critical depth (about 7 cm), at which time the

TABLE 4-3. Resuspension mechanisms observed in the suspended sediment concentration.

RUN	RAIN	BOAT	WIND	ANIMAL
1	X			
2		X	X	
3		X	X	
4				
5		X		
6	X			
7	X			
8	X	X		
9		X	X	
10			X	
11		X	X	
12	X			
14	X	X		
15		X		
16	X			
17	X			
18	X		X	
19			X	X
20				X
21	X	X		

concentrations decrease with decreasing water depth. The reason for this decrease may be due to the "larger" waves being filtered out by the shallow depth. Bottom material resuspended by wave action appears to rapidly settle out of the water column as previously observed (Anderson, 1971).

### **Storm Observations**

On August 29, 1985 rainfall occurred throughout the day. Rainfall intensity varied from intense thundershowers to light drizzle. During the study period (5:00 to 6:00 pm) the intensity averaged 0.5 cm/hr. Drop-size distribution was measured several times during the storm. Figure 4-12 presents the drop-size distribution, as a function of volume, at five times prior to sampling, and once during sampling. At this time the modal drop size by volume was 0.262 cm.

The suspended sediment concentrations, in general, increased as the water depth decreased during the ebbing tide, from 25 to 7 cm (Figure 4-13). The concentrations ranged from 93 to 301 mg/l in water depths of 25 to 15 cm. In water depths between 7 and 15 cm, concentrations jumped to 529-711 mg/l due to wind wave action. As the water depth decreased below 7 cm the concentrations decreased slightly to 465 mg/l at 1.1 cm depth.

The suspended sediment concentration, as a function of ebbing water depth, varied in a manner similar to that observed during the insitu experiments, when wind waves were present. The high concentrations observed in water depth less than 7 cm made it impossible to identify a rain induced component.

On September 2, 1985, observations were made as the water ebbed from the tidal flat during a less severe, early morning, rainfall event. The

FIGURE 4-12. Histograms of the measured drop size distribution during the two storm observations. One sample was collected during Storm 1 and three samples were collected during Storm 2. Measurements were based upon the flour technique. The drop diameters are in cm.

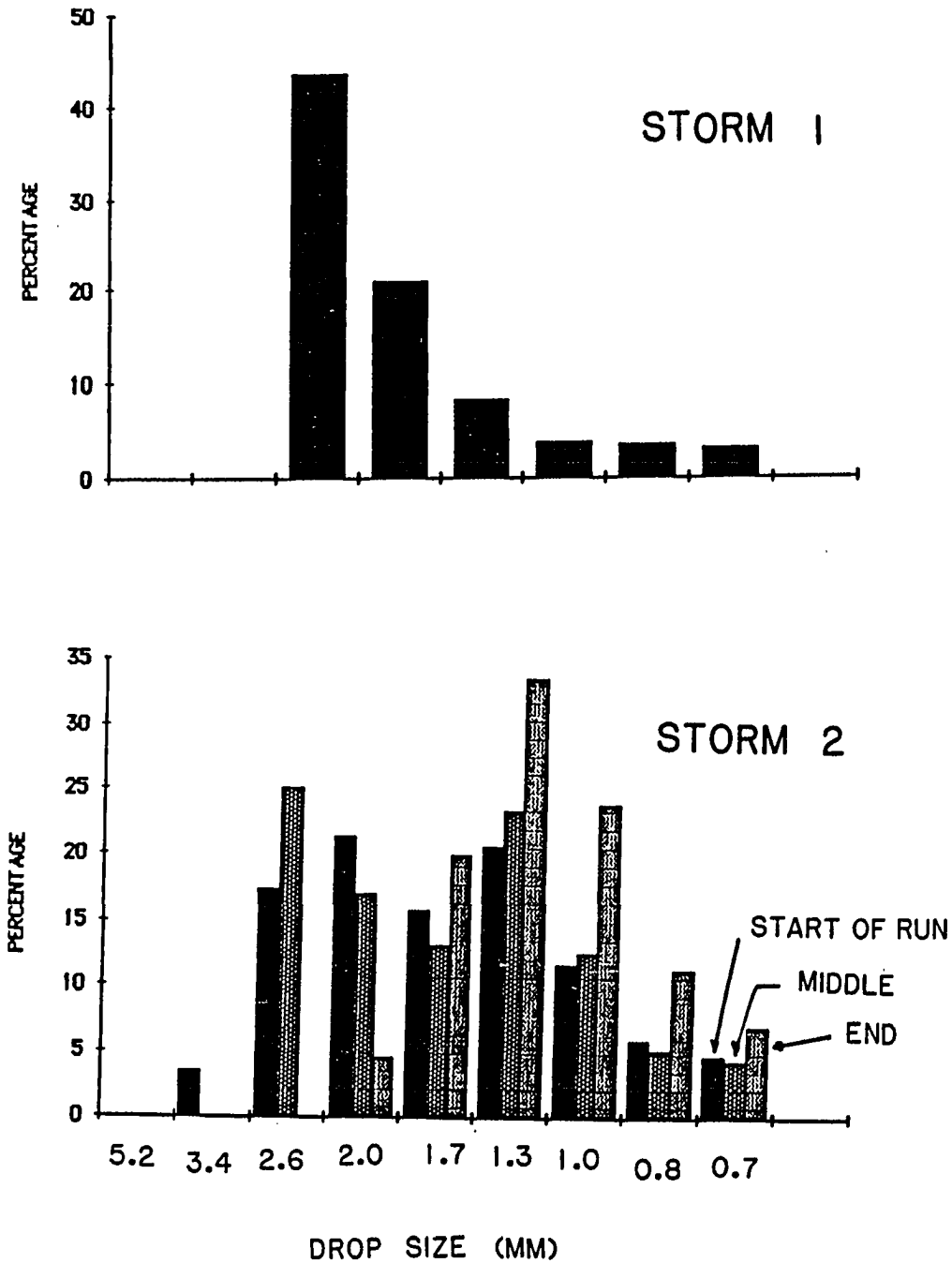
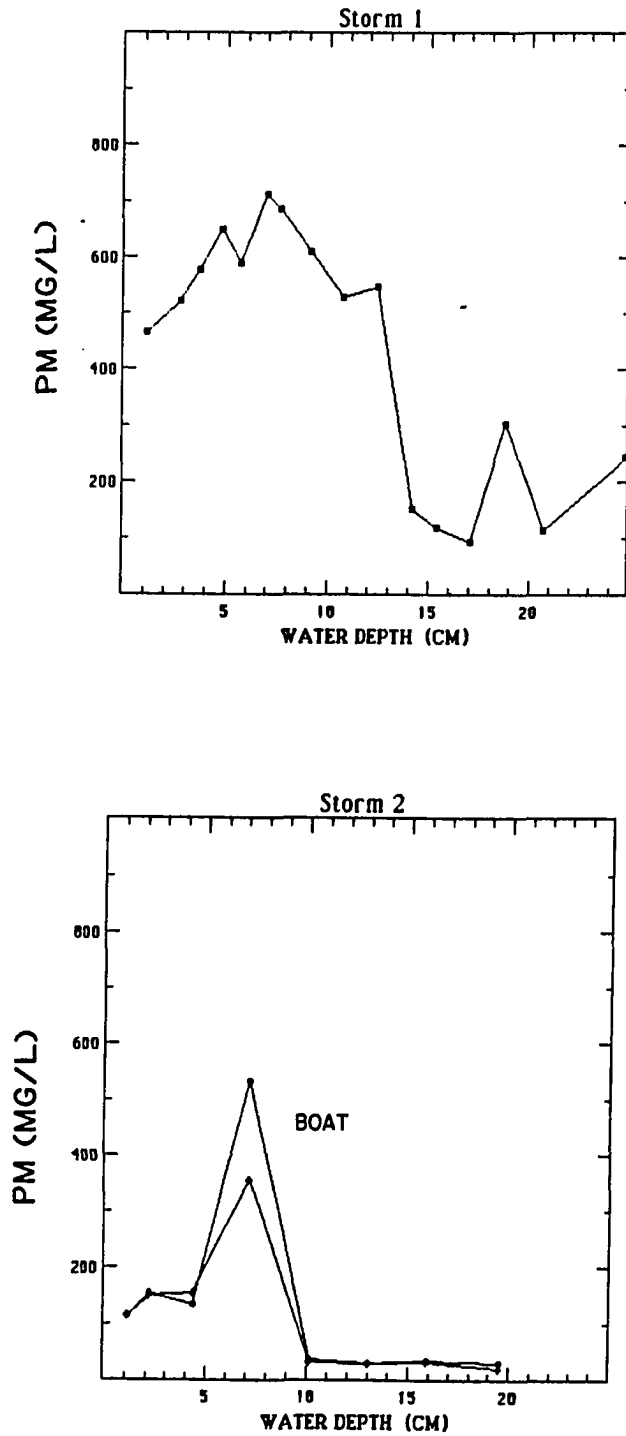


FIGURE 4-13. The observed suspended sediment distribution with time during the storm period when the water level at the sampling site decreased from about 30 cm to about 1 cm water depth.



rain intensity during the study period (7:15-7:45 am) was 0.05 cm/hr. The drop size distribution was measured at three times during the study. The modal drop size (by volume) was 0.13 cm, when the water depth was less than 7 cm. Drop sizes, as large as 0.34 and 0.26 cm were observed in the rain samples when water depths ranged from 22 to 7 cm.

In water depths from 22 to 10 cm, the suspended sediment concentration was low, 21 to 38 mg/l. When the water depth was about 7 cm, boat wakes encroached on the study area, resuspending significant sediment, 357 to 534 mg/l. The bulk of this material settled out rapidly after the wave train passed. Within 4 minutes the concentrations decreased to 127 to 136 mg/l. The suspended load remained above 116 mg/l. until the water was too shallow for sampling.

The distribution of suspended sediment with time and depth during the rainfall event, varied in a manner similar to that observed during the insitu experiments. With no wind waves the observed suspended sediment load remained at low concentrations. Boat wake resuspension can cause significant resuspension; however, the bulk of the material rapidly falls out of the water column. Again it was not possible to determine if rainfall maintained elevated concentrations, in depths less than 7 cm, as the water ebbed from the study area.

### **Discussion**

The insitu studies point out the importance of rain induced resuspension in the shallow intertidal water column. The results of the insitu and multidrop experiments indicate a resuspension depth (5 to 8 cm), much less than the single-drop studies (20 to 40 cm). This may be due to salinity or density stratification, or due to the increased ambient turbulence

in the water column, when many drops are impacting the water surface concurrently. However, rain caused enrichment of 3 to 34 times the background suspended load. This represented excess concentrations due to rain of 40 to 318 mg/l (Table 4-4). Rain resuspension was important in water depths less than 7 cm, and increased in importance as the water depth decreased. Therefore the rain is acting in a complimentary fashion to the wind waves. As the influence of waves is diminished in water depths less than 7 cm, the effect of rain resuspension is enhanced.

The observations during the insitu experiment lead to an interesting conclusion, which previously has only been qualitatively observed (Anderson, 1983). It has been noted that there appears to be higher suspended sediment concentrations during storms in which there is both wind and rainfall than windy days in which there is no rainfall. An explanation for this observation can now be presented. As water ebbs from the tidal flat, a portion of the suspended sediment due to wind wave action at the trailing edge settles back out onto the tidal flat. If it is raining then material which would normally settle out in the shallow trailing edge is resuspended, and rain induced mixing maintains the material in suspension as it ebbs off the tidal flat into the channels of the estuary.

TABLE 4-4. Summary of data from insitu experiments where rain showed an effect on the excess mass concentration (as determined between the impact area and control area). The physical characteristics of the artificial rain are given, as well as the water depth in which the rain effect was first observed.

RUN	DEPTH (cm)	$E_{Ratio}$	$PM)_I$ (mg/l)	$PM)_C$	Excess Mass	Drop Size	Intensity (cm/hr)	Power (gm/s <sup>3</sup> )
6	3.25	18.6	335.6	18.0	317.6	3.08	6.21	495.5
10	4.20	3.2	57.6	18.0	39.6	5.46	1.61	175.1
12	3.65	33.7	138.3	4.1	134.2	5.38	2.47	267.5
14	5.10	15.3	81.2	5.3	75.9	5.70	5.32	582.3
16	3.45	13.8	136.6	9.9	126.7	5.33	2.45	203.3
17	4.40	15.4	167.6	10.9	157.7	5.60	5.34	478.1
18	4.55	10.2	47.8	4.7	43.1	5.25	5.32	426.0
21	3.60	2.9	93.3	32.0	63.3	5.43	3.22	89.8

## **CHAPTER 5**

### **MULTIDROP EXPERIMENT ON BEDLOAD TRANSPORT OF MUDDY INTERTIDAL SEDIMENTS**

#### **Introduction**

The multidrop experiments in Chapter 4 focused on the suspended sediment component of transport of muddy intertidal sediment due to rain action. However, a significant portion of the muddy intertidal is relatively coarse grained (Rust, 1980). This material includes fecal pellets, organic detritus and sand-sized mineral grains and rock fragments. Fecal pellets represent an important component of the surface sediment, since by weight they comprise over 20% of the sediment in the study area (Rust, 1980).

Chapter 3 illustrated that coarse grained sediment can also be moved by the impact of drop-formed vortex rings. A simple experiment was conducted to estimate the amount of estuarine sediment which may be moved as bedload (in this study movement by saltation was considered as bedload), due to impacting vortex rings. The purpose of this experiment was to identify the magnitude of the bedload component relative to the suspended load. Since fecal pellets represented a major portion of the coarse fraction, and are some of the largest particles on the sediment surface, these pellets were tested for density, composition and settling velocity. A detailed discussion of pellet sedimentological properties is presented in Appendix 5.

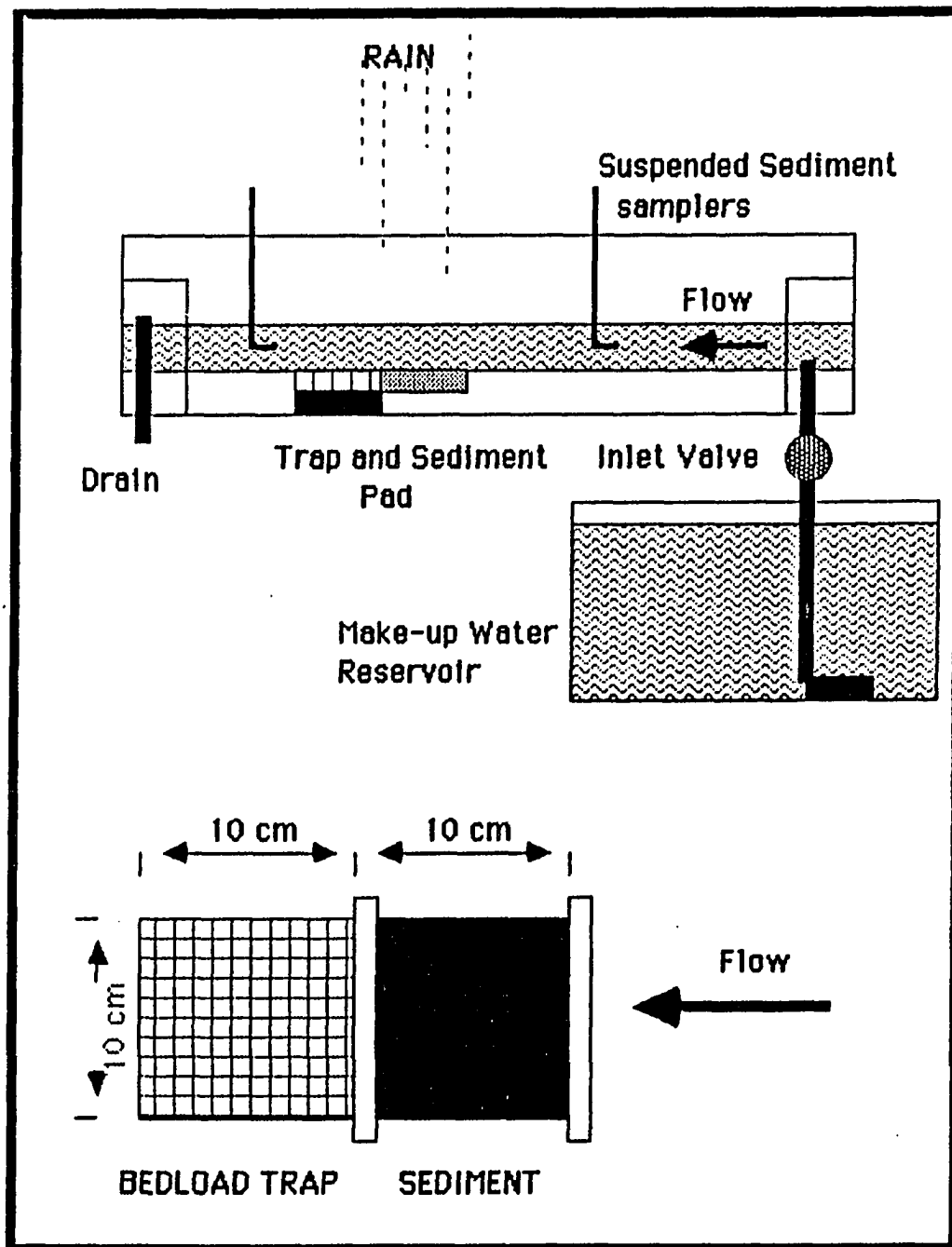
### **Methodology**

A 110 by 15 cm plexiglass flume was used to allow a slow (3 cm/sec) and shallow (3 to 4 cm) flow of seawater to move over an estuarine mud surface (Figure 5-1). The seawater was drawn from a stilling basin, where the coarsest suspended matter had been allowed to settle out for one-hour before the run. This was pumped into one end of the flume and the rate was controlled by an in-line valve. The water passed through a baffle to allow development of a uniform flow. Water exited the flume and was discarded. The flow rate was measured by dye injection, and was less than 3 cm/sec at the water surface in the center of the flume channel. The change in reservoir volume during the run was used to calculate an average flow rate through the flume.

The sediment pad was located near the center of the flume just upstream from a baffled bedload sampler (Figure 5-1). Suspended sediment samplers were located along the flume centerline, upstream and downstream of the sediment pad. Water was siphoned from these intake points, with the draw off rate controlled to collect a single integrated sample during the 20 minute run.

The sediment pad consisted of a 9.5 x 10 cm box with 2-cm wide flanges to minimize turbulence at the pad edges (Figure 5-1). Estuarine mud was collected by randomly placing a frame on the mud surface. The sample was collected with care not to disturb the sediment surface and placed in the sediment pad. The pad was then placed in the flume in a frame which held the bedload sampler. A false bottom was placed upstream and downstream of this frame to allow the flow to pass over the sediment without a depth change. The bedload sampler consisted of a partitioned tray positioned

FIGURE 5-1. Experimental set up for the flume study.



underneath a 10 x 10 cm baffle with 1.2 cm square holes (Figure 5-1). The thickness of the baffle was about 0.9 cm. Dye injection into the bedload sampler indicated that the baffle was adequate to keep turbulence in the flow from impinging upon the collection tray.

Rain drops were generated by 16 drop formers placed in a 4 x 4 grid and covered a 9 x 9 cm area. The drop size was 0.54 cm and the drop height was fixed at 75 cm above the water surface. Rainfall intensity was controlled by changing the head of the rainwater reservoir. Intensity was measured volumetrically at the start and end of each run; an average intensity was used for data analysis.

Each experiment consisted of two 20-minute runs. The first run was with water flow only. The bedload sampler tray was removed and the collected material removed. The second run was with rain and flow. The material caught in the tray was removed with pipette. The tray was partitioned so that the amount of sediment caught as a function of distance from the sediment pad could be measured. The sediment amounts in the flow-only runs were so low only a total sediment load could be determined.

Total sediment by weight and percent organics were determined using the procedures described in the previous chapters. Sediment samples were collected from the pad after being subjected to rainfall and the slow current. A control pad, collected at the same time as the run pad, was also sampled for textural analysis.

## **Results**

The bedload transport due to rain was estimated in the flume studies. The results of this study can then be used to compare with the suspended load as determined in the multidrop experiments discussed in Chapter 4.

The rate of bedload transport was computed by taking the difference between the sediment mass in the trap, observed with unidirectional flow and the mass observed with combined rain and flow. The erosion rate of estuarine mud ranged from 4.0 to 9.0 gm/m<sup>2</sup>/hr with an average rate of 5.83 gm/m<sup>2</sup>/hr (Table 5-1).

The range in rainfall intensity causing this level of erosion was 14.2 to 91.1 cm/hr. The water in the flume was 3.6 cm deep and flowing at an average of 2.1 cm/sec (Table 5-1).

The material collected in the bedload sampler was viewed under the microscope. The largest particles were fecal pellets of *H. filiformis* organic detritus and sand were also common. This material was typically observed at the sediment interface. The transport rate of bedload material can be compared with the excess mass of sediment resuspended by rainfall. The excess mass results from the multidrop experiments were converted to erosion rates by dividing the observed mass by the unit time and the area of the sediment surface. The excess mass at 11.5 minutes after the start of rainfall was selected for comparison with the flume study, which ran about 20 minutes. Excess mass erosion rates ranged to 14.2 gm/m<sup>2</sup>/hr and averaged 2.8 gm/m<sup>2</sup>/hr (std. dev. of 3.63; n = 33) for the cases in which an increase in excess mass was observed in the first 11.5 minutes. Thus the amounts moved by resuspension and bedload are on the same order of magnitude with the average resuspension rate about half the average bedload rate of 5.8 gm/m<sup>2</sup>/hr.

The important point is that vortex ring impact not only resuspends the finer-sized material on the estuarine sediment surface, but also initiates motion of the coarsest fraction. The predominant component of this coarse

TABLE 5-1. Summary of the flume study results, including the amount of bedload sediment (mg) caught in the trap, the rainfall intensity and power, the flow velocity through the flume, and the erosion rate.

RUN	TIME (Min)	BEDLOAD			RAIN		FLOW (cm/s)	EROSION RATE
		Rain	Flow	Net	Intensity	Power		
4	20	15.8	(4.5)	11.3	69.9	872	2.1	4.19
5	20	15.8	(4.5)	11.3	91.1	1136	2.5	4.19
7	17.3	14.6	1.4	13.2	59.5	742	2.3	5.64
9	20	29.7	7.2	22.5	23.0	287	1.9	8.33
11	20	20.8	5.0	15.8	29.2	370	1.7	5.85
13	20	15.4	4.6	10.8	22.8	285	1.8	4.00
15	20	28.5	4.1	24.4	25.2	314	1.8	9.04
16	20	19.1	4.6	14.5	18.5	243	2.4	5.37
MEAN				15.5	42.4	531	2.1	5.83
STD. DEV.				5.2	25.3	339	0.31	1.93

NOTES: Bedload in grams.  
Intensity in cm/hr.  
Power per unit area in gm/sec<sup>3</sup>.  
Erosion rate in gm/m<sup>2</sup>/hr.

fraction was fecal pellets, which could be analyzed for their sedimentological characteristics (Appendix 5).

### Discussion

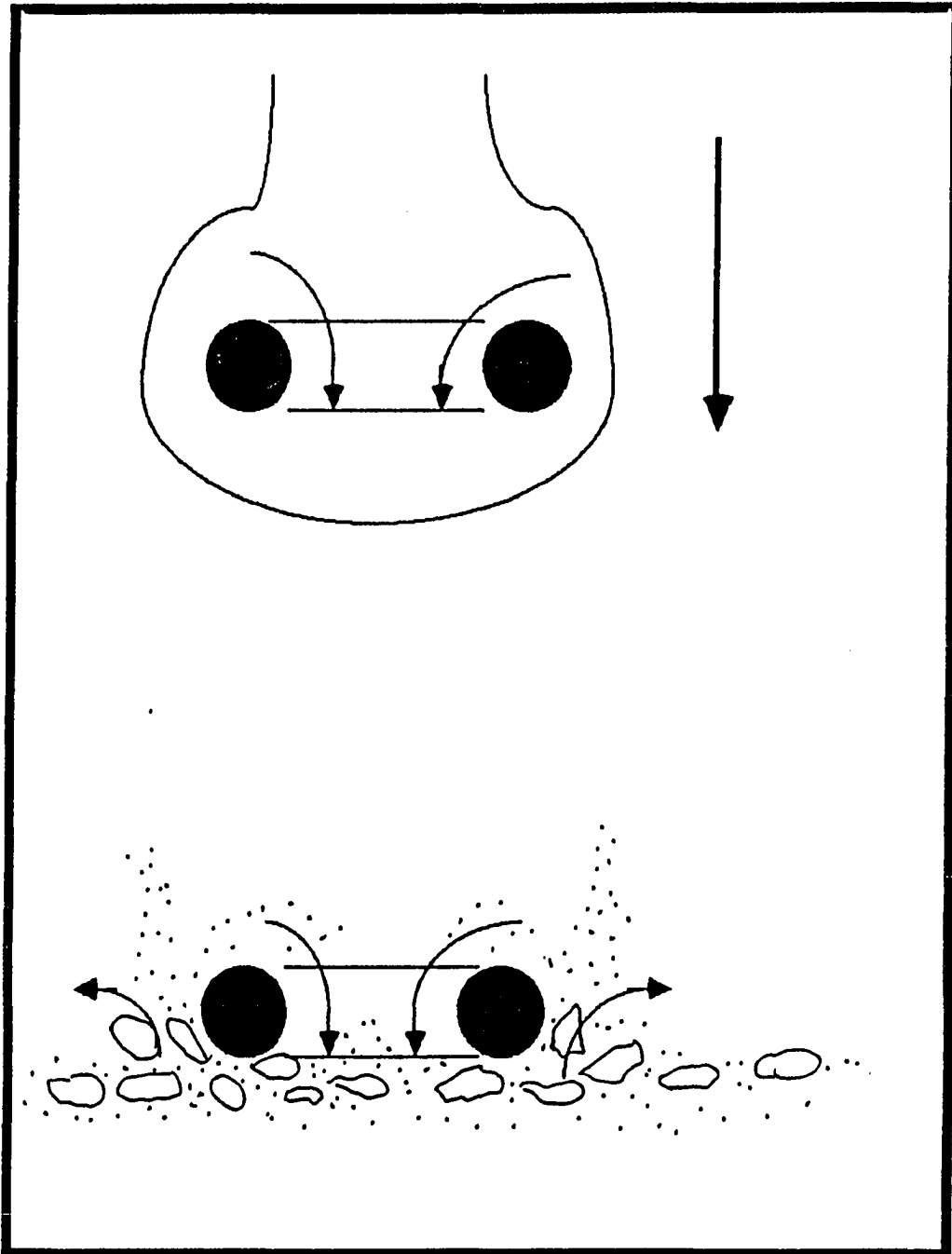
Impact of drop-formed vortex rings initiated motion of bottom sediment, as observed in the results presented in Chapters 3 and 4. Based upon these results, the shear stress, which can be imparted by the rings, probably exceeds 11 dynes/cm<sup>2</sup>. Material moved by this force may remain in suspension if the settling velocity is relatively low or immediately return to the bottom, after it is thrown from the region influenced by the ring. This would happen to the larger and denser particles. Consequently rain-induced vortex rings may cause both suspended load and bedload transport if it is accompanied by advection due to other processes, such as tidal currents..

The flume study investigated the bedload component of sediment transport. The average near-surface currents of 2.1 cm/sec would impart a shear stress of 0.046 dynes/cm<sup>2</sup> on the bottom (see Appendix 3 for calculation). This is too low to initiate motion of the *H. filiformis* or *M. balthica* pellets, which require a calculated critical shear stress of 1.14 dynes/cm<sup>2</sup> (Appendix 3). However, rain-induced vortex rings contain sufficient shear energy to move the pellets and the entire coarse fraction on the sediment surface.

Thus motion of a substantial amount of material may be initiated by vortex rings. The flume experiments, when compared to the results of Chapter 4, suggest that bedload transport due to rain action in a slow current may be twice the rain-induced sediment resuspension in quiescent water.

A conceptual picture of this process is illustrated in Figure 5-2. The muddy intertidal sediment surface is composed of a mixture of "coarse"

FIGURE 5-2. Conceptual diagram of how an impacting vortex ring initiates motion of coarse material on the sediment surface, and resuspends the fines into the water column.



detrital organic particles and fecal pellets interspersed with silt and clay-sized particles. The finer particles may be in the form of a light dusting on the coarser material. As a vortex ring impacts the bottom, there is sufficient shear velocities to (1) roll the coarsest particles away from the impact area, and (2) eject other material into the water column within 1 to 2 cm of the bottom. This ejected material may either quickly settle out in close proximity to the ring impact area, acting as bedload, or may stay in suspension long enough to be incorporated by subsequent turbulent action, and move upward into the water column. The dusting of finer silt and clay residing on the larger particles would be shaken off in the process and go into suspension. If this dusting were the only fine sediment activated by the ring impact, then subsequent rings will cause bedload movement, but no further resuspension.

The sediment involved in rain-induced sedimentation appears to be only the layers closest to the surface. The conclusion is consistent with the work of Green and Houk (1980). In order to determine if there is a significant change in the sediment texture due to rain action in a shallow water column required sampling of the very surface of the sediment. Sediment samples were collected from the upper 3 mm of the sediment surface in the multidrop and insitu experiments, and the flume study. The results from these samples will be the topic of Chapter 6.

## CHAPTER 6

### CHARACTERISTICS OF THE MUDDY INTERTIDAL SEDIMENTS USED IN EXPERIMENTS

#### Introduction

The texture and composition of the muddy intertidal sediment reflect seasonal and spatial processes, which control erosion and deposition on the mudflat (Rust, 1980). The effects of rain resuspension may or may not be noticeable in the measured texture of sediment subjected to this process. The purpose of this chapter is to evaluate the textural data collected from several experiments. The first objective is to describe the textural composition and natural variability. The second objective is to test if rain-erosion significantly alters the surface texture.

All the sediments used in the experiments came from JEL Cove. Subsamples of bottom sediment were collected as part of the insitu rainfall experiment, and flume study. These samples were analyzed to define the typical composition and to identify any significant differences between experiments.

#### Methodology

Sediment texture was determined using the rapid sediment texture analysis technique described by Anderson *et al.* (1981). The methodology determined the percent gravel (typically organic detrital material), sand,

mud and aggregates (fecal pellets). Each component was ashed at 500°C to determine the combustible fraction. The sample collection techniques have been described in the previous chapters.

## **Results and Discussion**

### **Description of Sediment Texture**

The surface sediment used in the three experiments was predominately mud (59.5 to 67.1% by weight). Sand represented 3.4 to 11.9% of the total sediment. Fecal pellets, or sand-sized aggregates, make up 18.2 to 23.5%, while very coarse material, commonly organic detritus, is only a small fraction (0.4%) of the total sediment (Figure 6-1). The general sediment textural composition was similar to that observed by Rust (1980) in a study of the same tidal flat.

The compositional data from the sediment used in each experiment was analyzed to determine if there were significant differences between sediments (Table 6-1). In general the multidrop experiment sediments had more sand-sized and total organic material and less inorganic mud than sediments used in the insitu experiments and the flume study (Table 6-1). The sediments used in the flume study and the insitu experiments were generally similar. Minor differences were observed in the organic mud fraction and total aggregates, which were slightly lower in the flume study (Figure 6-1).

### **Rain Effect on Sediment Texture**

The sediment data collected in the insitu experiment and the flume study were paired samples, one a control and one influenced by rain.

FIGURE 6-1. Histogram showing the percent composition of the sediments used in the multidrop and insitu experiments and the flume study.

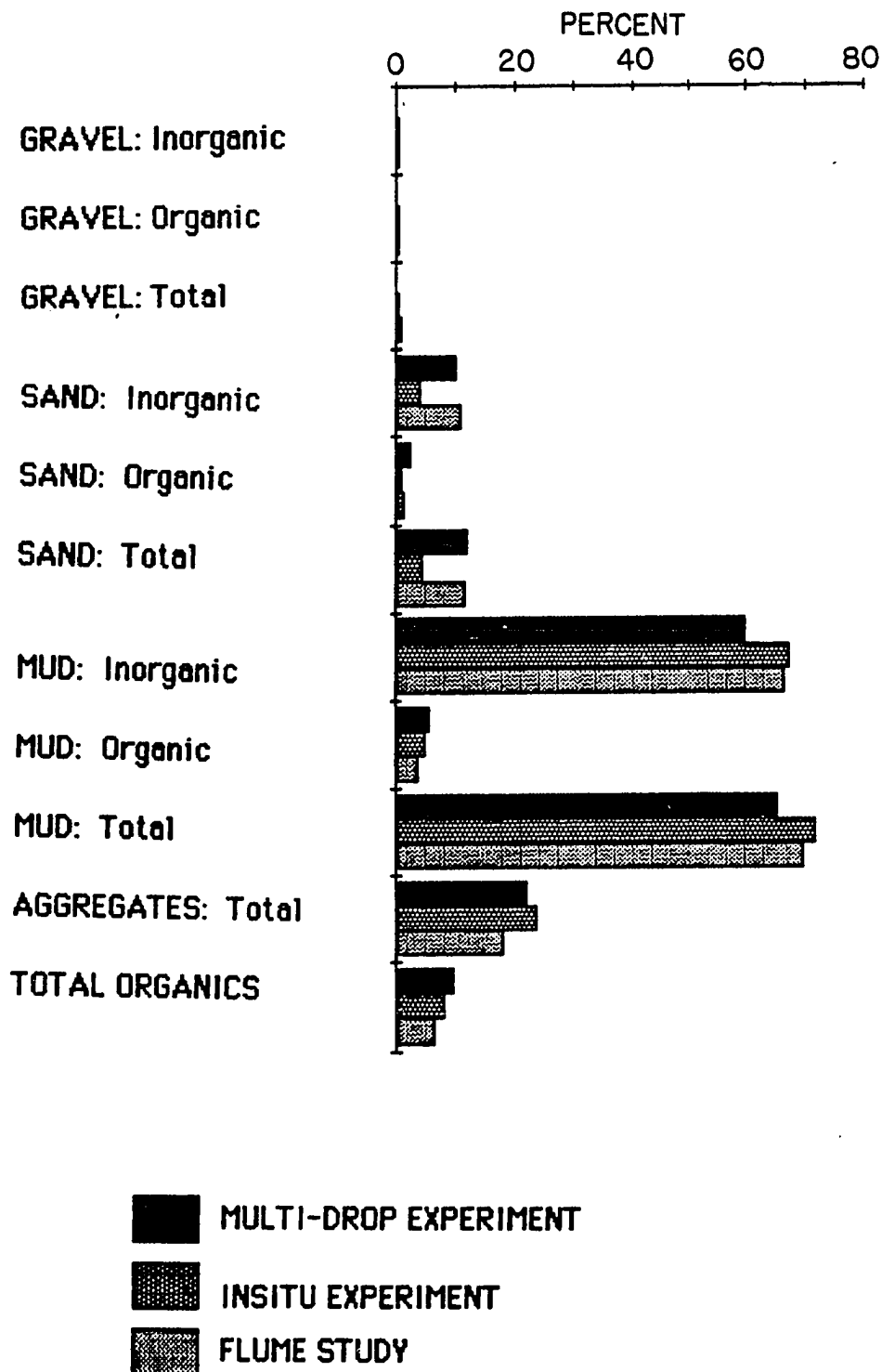


TABLE 6-1. Results of analysis of variance testing on the paired samples from the insitu experiment and the flume study. Comparison among the three experiments using estuarine sediment is also included.

TEXTURAL COMPONENT	INSITU EXPERIMENT		FLUME STUDY		EXPERIMENT		
	Significance of F-Ratio	Impact Area Higher/Lower	Significance of F-Ratio	Rain High/Low	1	2	3*
GRAVEL:							
Inorganic	70%	Higher	---				
Organic	90	Higher	70	Lower			
Total	70	Higher	---				
SAND							
Inorganic	---		---		X	Z	X
Organic	70	Lower	---		Z	X	X
Total	---		---		X	Z	X
MUD							
Inorganic	70	Higher	---		Z	X	X
Organic	70	Lower	---		X	X	Z
Total	---		---		Z	Y	X
AGGREGATE							
Total	---		70	Lower	X	Y	Z

\* X,Y,Z represent statistically different populations.

Therefore, it was possible to use these data to determine if rain had an effect of rain on the texture.

Analysis of variance using a F-ratio test indicated that the flume sediment subjected to low flow in conjunction with rain was significantly lower (at the 70% CI) in percent organic gravel-sized material, and in percent total aggregates (Table 6-1). This is reasonable in that the typical composition of the bedload samples, which represented scouring from the surface, was predominately organic detritus and fecal pellets. The fecal pellets were primarily from *H. filiformis* a few *M. balthica* pellets were observed. The organic detritus included eel grass fragments. Loosely bound aggregates of silt and sand-sized organic debris was also observed, as was inorganic sand grains.

The paired samples from the insitu experiment represented one from a control site, which was not influenced by the artificial rainfall, and one from the rain impact area. The sediment texture observed in the rain impact area represented the effects of both rain falling on a shallow column of water and rain impacting the exposed sediment surface. Although the experiment was designed to examine underwater resuspension effects on the ebbing tide, by the time the experiment terminated the trailing edge of the tidal wedge had left the impact area. This exposed the sediment surface to direct impact by the rain drops.

Analysis of variance testing of these data sets indicated that the sediment in the impact area was higher than the control area in gravel-sized material and inorganic mud, and lower in total organics. This difference in sediment texture suggests winnowing of the finer and lighter particles leaving a "coarse lag" deposit at the surface.

The two data sets suggest that different processes are influencing the sediment texture. For the flume experiment the coarse fraction was being removed in bedload, while in the impact study it was being left behind as a lag deposit. This was probably due to different experimental constraints. In the flume study a small isolated sediment surface was used. The sediment surface was subjected to rain indirectly through a water column. Therefore, as material was mobilized and moved downstream, there was no source of sediment upstream to move onto the sediment surface. Consequently a loss of the particles susceptible to bedload transport was observed. In contrast, the insitu experiment, direct impact of rain and subsequent rill and sheetwash movement of rainwater from the impact site caused erosion of the finer particles on the sediment surface, leaving a coarsened lag deposit.

One might speculate that the sediment surface under a shallow water column subjected to rain action, would respond as did the sediment in the insitu experiment. Vortex ring impacts would jar the larger particles and resuspend the fines, which either coated the aggregates and detritus, or resided in the pore spaces between the larger particles. This process would strip the fines, leaving a lag deposit of the larger particles. As the effects of rain resuspension diminished due to increasing water depth or decreasing rain intensity, the fines already in suspension would settle, recoating the larger particles and filling the pore spaces. In the estuarine environment, the system as just discussed would not be closed, because lateral advection would move some of the rain resuspended fines from the shallow edge of the tidal wedge into deeper water over the tidal flat and/or into the channel. Likewise, water from the channel, not containing rain resuspended fines could move onto the tidal flat. Therefore, the net result is that it may be

very difficult to identify changes in texture because of the dynamic nature of the surface.

The ability to detect rain effects on sediment texture can be investigated from a different point of view. Present sampling technology allows for sampling of approximately the upper 3 mm of sediment. Average net erosion rates due to rain action was about 8.6 gm/m<sup>2</sup>/hr (2.8 gm/m<sup>2</sup>/hr suspended load and 5.8 gm/m<sup>2</sup>/hr bedload). Using a bulk density of 1.7 gm/cm<sup>3</sup>, layer  $5 \times 10^{-3}$  mm removed each hour, or 0.17% of the minimum thickness, which was sampled. This is probably why no significant change was observed in the finer material in the flume sediments, and why, given existing sampling technology, it is difficult to determine rain effects by looking for changes in sediment texture.

## CHAPTER 7

### A TECHNIQUE TO OXYGENATE AQUACULTURE TANKS

#### Introduction

Entrainment and subsequent downward transport of air by drop-formed vortex rings is a mechanism to oxygenate subsurface water. The ability of vortex rings to incorporate air-bubbles during formation was noted as early as Rodgers (1858). Blanchard and Woodcock (1957) observed air bubbles in drop-formed vortex rings. The larger drops (0.22 cm) carried bubbles to 2 to 4 cm depth. The point of air-entrapment to form the bubbles is in dispute. Blanchard and Woodcock (1957) felt entrapment occurred with initial impact of the drop. Carroll and Mesler (1981) observed air entrapment when the pinched off jet drop impacted with the collapsing central jet.

Rohatji *et al.* (1979) studied the mixing effects of vortex rings produced by an impulse generator. They concluded that vortex rings mixed with energy efficiencies of 9 to 30%. The efficiency is the ratio of energy required to operate a mixing mechanism and the theoretical amount of energy required to mechanically mix the system. This is substantially higher than energy efficiencies of impellor mixing. They also expanded this concept and tried to mix an oxygen depleted layer in Hamilton Harbor, Ontario, using 2-m diameter vortex rings.

The purpose of this pilot study was to apply the ring mixing concept to drop-formed vortex rings. The specific application identified to test was with oxygenation of aquaria used in biological toxicity testing. Typically in

this type of test a 45 l aquarium, fitted with drain, is used (Figure 7-1). Sediment with the suspected toxic elements is placed in the bottom of the tank and covered with water. Water, relatively rich in dissolved oxygen, is added to the tank at the surface in a single stream, and the tank water from near the bottom is drawn from the tank by the drain to maintain a constant volume. Air is also bubbled into the tank to balance the oxygen demand of the sediment and maintain an oxygenated water column. Unfortunately this air if bubbled too vigorously also turbulently mixes the tank and may resuspend bottom sediment.

The objective of this study was to test if the same volume of new water, if introduced at numerous drop points, could oxygenate the tanks as efficiently as bubbling air. The hypothesis was that drop-formed vortex rings would entrain air bubbles and oxygen-rich surface water, then transport this water to depth in the inner core of the ring and release the oxygen rich water and bubbles. This would cause mixing with water near the sediment surface, which is depleted in oxygen, thus maintaining an oxygen saturated water column.

The benefits to a vortex ring oxygenation process are (1) costs could be saved by not requiring air bubbling, and (2) test procedures could be improved by gently mixing the water column. This pilot study represents a feasibility study, and is therefore a first step in determining the practical applicability of the process.

### **Methodology**

The experiment consisted of four aquaria with a 3 cm layer of fine-grained sediment (from JEL Cove) on the bottom (Figure 7-1). Tank 1 was the standard, where seawater and air were added at rates consistent with

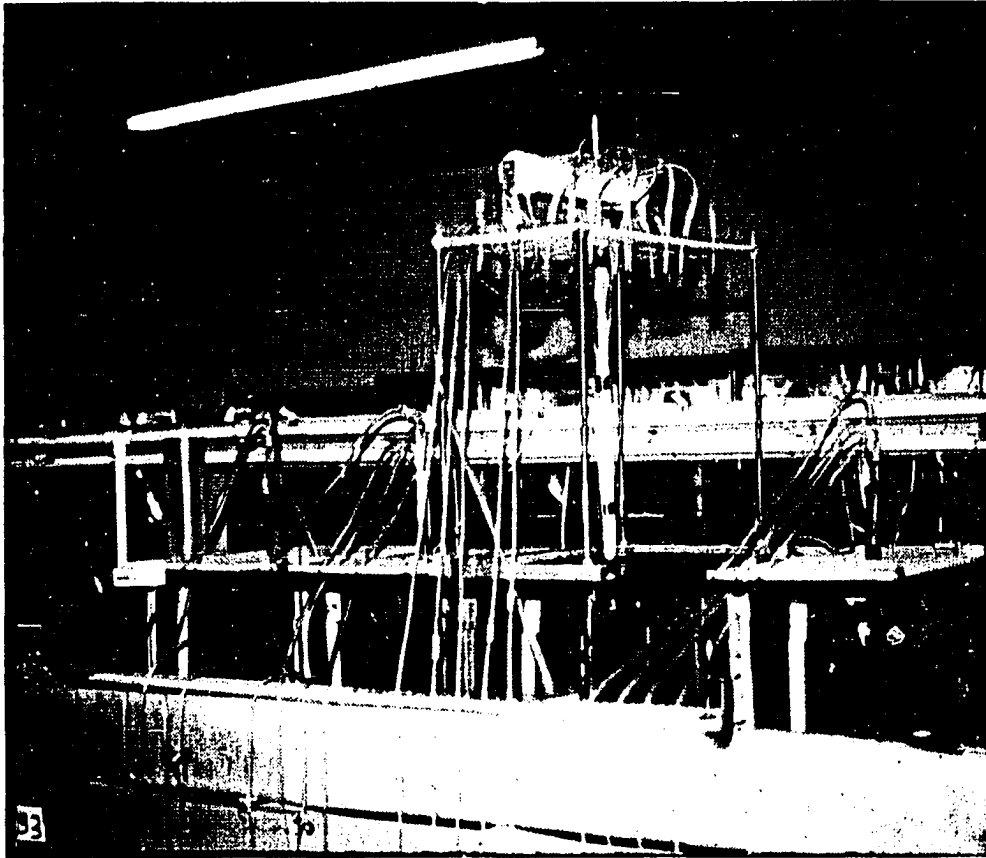


**FIGURE 7-1. Experimental set up for the vortex ring oxygenation experiments.**

the toxicity testing. Tank 2 was the vortex ring model, where the same amount of new seawater was dispersed over 20 drop points. No additional air was added to this tank. The water formed 0.54 cm drops at each point, and fell about 50 cm to the tank water surface. The drops were formed as described in Chapters 1 and 2. Tank 3 was a second control tank in which only water was added. No bubbled air was added to the tank. Tank 4 was considered as the static control, where no bubbled air or water was added.

Water samplers were located in the center of each tank and set at approximately 0.5, 5, 10 and 15 cm off the bottom (Figure 7-1; Table 7-1). Seawater was added to the tanks several days prior to the run to allow a natural oxygen depletion by the sediment. The water volume in Tanks 1 to 3 was about 33 l (Table 7-1). Tank 4 was filled with 48 l to allow for draw-down, when dissolved oxygen (DO) samples were collected. New seawater was gravity fed from a common cistern to each tank. The DO, temperature and salinity of this water was monitored throughout the run. The new water flow rate into Tanks 1 and 3 was measured volumetrically at the start of the experiment. The volume of water from the drop-formers of Tank 2 was measured volumetrically at the end of the experiment.

Each tank was monitored for six hours. A baselevel sampling was conducted for each tank prior to the start of the experiment. Once baselevel sampling was completed in a tank, the new water addition and air bubbling was started. Each sampling consisted of sequentially siphoning water from each of the four samplers in the tank starting with a near-surface and ending with a near-bottom sample. The samples were immediately processed for DO, temperature, and salinity. Sampling in this step-wise fashion, resulted in nine sets of data for each tank over the six hour period.

TABLE 7-1. The water characteristics and sampling depths for each tank used in the oxygenation experiment.

Water Tank Dimensions and Sampling Points:

TANK	START LEVEL	VOLUME	SEDIMENT THICKNESS	SAMPLING LOCATIONS			
				1	2	3	4
1	18.8 cm	34.9 l	3.6 cm	0.5cm	5.6	10.4	14.9
2	17.1	31.8	3.5	0.4	4.7	9.6	14.3
3	18.0	33.4	3.3	0.6	5.6	10.4	15.2
4	25.8	47.9	3.2	0.5	5.4	10.7	15.3

Baselevel Water Conditions:

TANK	TEMPERATURE (°C)	SALINITY (‰)	DISSOLVED OXYGEN (ml/l)
1	20.8	20.5	4.02
2	20.8	20.5	3.20
3	20.2	20.5	3.38
4	20.4	24.0	3.01

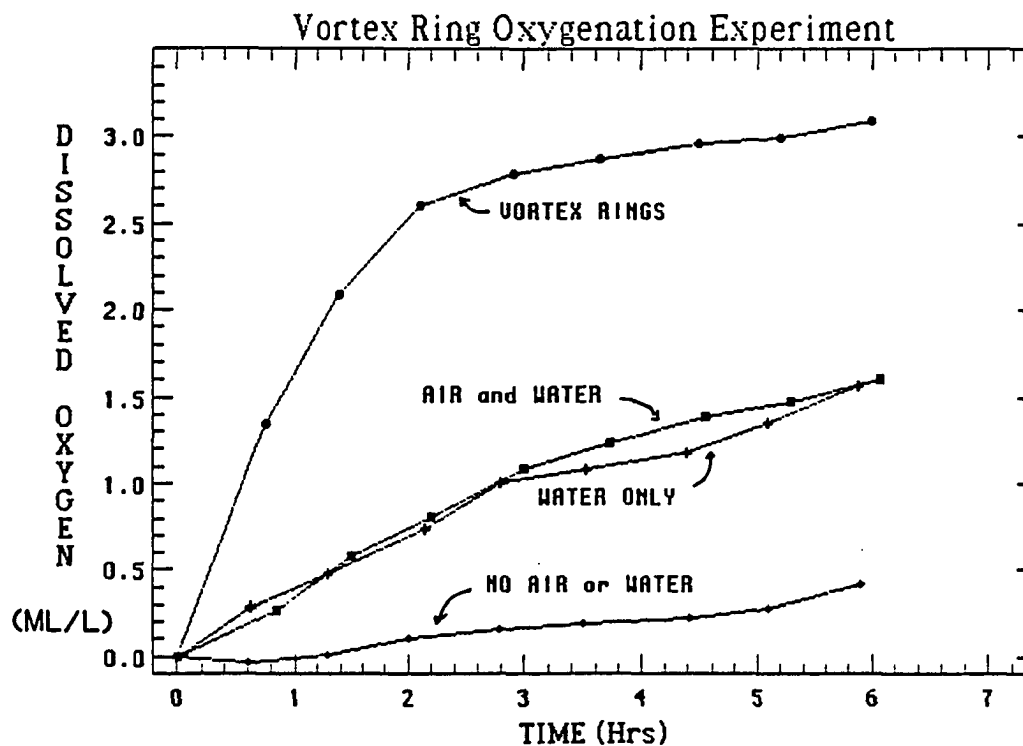
Dissolved oxygen was measured using a YSI Dissolved Oxygen and Temperature Meter. The DO probe was calibrated with saturated air at the start of the experiment. Probe drift was measured by comparing the probe reading at the start of the experiment in saturated air (6.47 ml/l or 100.8% saturation) and at the end of the experiment (6.74 ml/l or 103.4% saturation). No drift correction was made to the data set. Temperature was measured using the DO meter thermistor, where an accuracy of  $\pm 0.5^{\circ}\text{C}$  was assumed. Salinity was measured with an American Optics refractometer ( $\pm 0.5$  ‰). Percent saturation was calculated by comparing the observed DO with the predicted DO for 100 % saturation at the measured temperature and salinity.

### Results

The water in the tanks when the baselevel measurements were made had water temperatures of 20 to 21°C, salinity of 21.5 ‰, and gradients of dissolved oxygen ranging from 2.53 ml/l near bottom to 4.36 ml/l near surface (Table 7-1). The make-up water, which was added to the tanks after the baselevel sampling, had salinities of 22 to 23 ‰, temperatures of 18.5 to 16°C, and DO concentrations of 5.0 to 5.3 ml/l.

All four tanks showed an increase, on average, in the dissolved oxygen content in the volume of water overlying the fine-grained sediment bottom. However, there were significant differences in the amount of oxygen added to each tank (Figure 7-2). Tank 4, in which no water or bubbled air was added to the system, showed only a 0.4 ml/l increase in dissolved oxygen over the 5.9 hr period. This increase in oxygen may be artificial due to drift in the DO probe, or it may be due to a balance between oxygen uptake by the

FIGURE 7-2. Relative changes in the dissolved oxygen content of the four tanks during the study period. The baselevel dissolved oxygen content was subtracted from each of the DO values to illustrate how the added oxygen varied within each tank. The vortex ring mixed tank shows the greatest addition of dissolved oxygen. Bubbled air does not appear to be a significant contributor to the dissolved oxygen content in Tank 2 (air plus water curve). Addition of new water (water only curve) increases the oxygen content significantly over static conditions, where no water nor bubbled air was added. The dissolved oxygen concentrations are in ml/l.

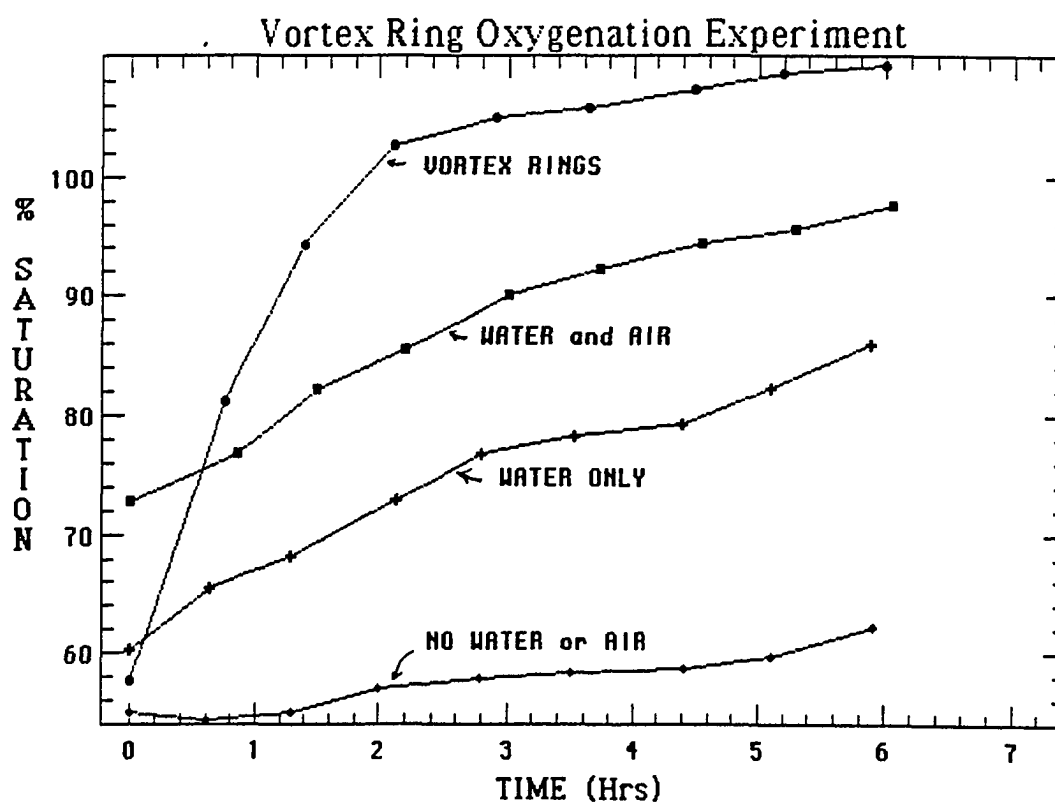


sediment and diffusion of oxygen into the water across the air-water interface. If the increase is real then there was only a minor change in DO due to these processes.

Addition of new water, which is relatively enriched in oxygen, and bubbled air increases the dissolved oxygen content of the tanks (Figure 7-2). It is interesting to note that bubbling air at the rate typically used in the toxicity experiments does not add a significant contribution to the dissolved oxygen in the tank. The rate of diffusion of air from the bubbles as they rise through the water column must not have been significant compared to the amount of oxygen brought to the tank by the new water. Where either water only or water and bubbled air was added to the tank (Tanks 1 and 3), 1.6 ml/l increase in DO was observed over the 6 hour period. This is a 400% increase over the static water condition in Tank 4. This increase must be due to the addition of new water to the tank.

Tank 2, where water was added as falling drops, was the most oxygenated after the experimental period (Figure 7-2). The oxygen in this tank increased rapidly during the first 1.5 hours of the experiment. A rate of oxygen addition of about 1.5 ml/l per hour was observed. The rate of oxygenation decreased once the water reached 100% saturation (Figure 7-3). Over the 6 hour period 3.1 ml/l of oxygen was added to this tank. This increase in oxygen is 775% greater than the static condition and 194% greater than the increases due to bubbling air and addition of make-up water at a single point. Only Tank 2 reached saturation in the time period of the experiment (Figure 7-3). The rate of oxygen saturation increase in the two tanks receiving oxygenated make-up water was similar. The static tank showed only a minor increase in percent saturation (Figure 7-3).

FIGURE 7-3. Oxygen percent saturation with time into the experiment is plotted for each tank. Only the vortex ring mixed tank shows supersaturation of dissolved oxygen. Addition of just water or water and air significantly increases the percent saturation over the static condition, but did not supersaturate the water during the time period of the experiment.



## Discussion

The purpose of this experiment was to evaluate the efficiency of drop-formed vortex rings in oxygenating a water column in an aquaculture application. The results of this initial experiment are quite encouraging. The vortex-ring-mixed tank rapidly (< 2hrs.) achieved 100% saturation, and maintained a supersaturated state over the course of the experiment.

In this experiment the oxygen demand from the sediment was not great, as determined from the oxygen content of the static tank (Tank 4). However, vortex ring mixing seems to be more efficient in oxygenating the tanks than bubbling air. This is probably because the rings not only transport air bubbles downward, but also entrain oxygen saturated surface water within the inner core and carry this fluid to depth. This mechanism probably increases the circulation within the tank. A much greater volume of water is transported to depth than just the volume of new water. This may explain why the vortex ring mixed tank achieves saturated level quite rapidly compared to the other tanks where water was added as a single stream. Increasing the air bubbling rate to improve the dissolved oxygen content was not tested. However, this may cause stirring up of the fine-grained bottom sediments.

The conclusions reached in this preliminary experiment can be expanded to other applications. Water drops falling on a shallow water column can significantly increase the oxygen content of that water column. This has implications for aeration techniques in which water is pumped through a nozzle and sprayed into the air to increase oxygen content. If the spray is controlled to produce drops of relatively large size, these drops may produce vortex rings, which can efficiently mix the water column. By generating vortex rings a much larger volume of surface water participates

in the downward mixing. Oxygenation of the surface waters due to rain storms may occur by the same basic principals. Drop-formed vortex rings entrain oxygen saturated surface water, as well as air bubbles, and transport this fluid to depth.

## **CHAPTER 8**

### **RAINFALL AND ESTUARINE SEDIMENTATION**

#### **A DISCUSSION**

##### **Introduction**

The effect of rain on intertidal estuarine sediment transport has been investigated through single- and multi-drop laboratory studies, controlled field experiments, and storm observations. The literature has been extensively reviewed to identify parallel research in other scientific disciplines, which can be used to understand how rain drops may be acting as a sediment transport mechanism. The results of these investigations lead to the conclusion that rainfall is an important component of storm related sedimentation processes on the estuarine intertidal.

In this concluding chapter, the results of the research are used in a discussion to speculate on the importance of rainfall in resuspending intertidal sediments. Areas of future research are delineated to focus on questions not answered by this research. A summary of the findings of this thesis research follows this chapter.

##### **Discussion**

###### **Erosion by Rain**

The ability of rainfall to initiate sediment motion, which lies beneath a shallow column of water, can be summarized by using the conceptual framework of the "Universal Soil Loss" equation (Wischmeier and Smith,

1960). Soil erosion (E) by direct impact of rainfall has been empirically defined as

$$E = R K L S C P_c \quad (8-1)$$

where R - erosion potential of rainfall in area  
 K - soil erodibility factor  
 L - length of flow in the supply area  
 S - land slope  
 C - cropping factor  
 P<sub>c</sub> - type of conservation practice.

This equation is typically applied to regions by developing regression equations, which define the variability in the parameters, for specific watershed areas (Vanoni, 1977). The equation can be modified for our application by grouping parameters to make physical sense in the intertidal area, which is covered by a shallow column of water,

$$E = [(R)(LS)][(K)(CP_c)] \quad (8-2)$$

where (R) - erosion potential of rainfall in the area  
 (LS)- tidal flat slope, width and depth of overlying water, as a function of the tide  
 (K) - erodibility of the intertidal sediment surface  
 (CP<sub>c</sub>)- biological, chemical and physical modifications of the surface, which modulate erodibility.

The erosion potential of rainfall (R) is the same on the estuarine water surface as it is on the land surface. The ability of the rainfall energy to penetrate the shallow column of water over the intertidal is controlled by rainfall intensity and drop size (i.e. kinetic energy flux or power) as shown in Chapter 4 and by Green and Houk (1980). Studies of rainfall erosion by impacting rainfall directly on soil surfaces is also controlled by kinetic

energy flux (Ekern 1950 and 1953; Wischmeier and Smith, 1960; and Bubenzer and Jones, 1971), or by momentum flux (Rose, 1960). The physical properties of the tidal flat surface (LS), such as dimensions, slope, and depth of overlying water during the rainfall event, have an effect in controlling the amount of rainfall energy which reaches the sediment surface. The properties of the sediment surface ( $K$  and  $CP_c$ ) affect how the sediment will respond to the rainfall energy or momentum which does reach the sediment surface. Thus it is possible to use the general form of this equation to show how the various aspects of the research interrelate in the erosion process and to estimate the importance of rain resuspension of intertidal sediments for an estuary, such as the Great Bay.

### **Erosion Potential of Rainfall**

The erosion potential of rainfall is related to drop size and rainfall intensity. In Chapter 2 we showed that the central jet characteristics changed systematically with drop impact energy. This energy is directly related to drop size because larger drops have greater mass and higher impact velocities than the smaller drops. The collapse of this central jet produces the vortex rings. Research by Maxworthy (1977) and others summarized in Chapter 1 show that the properties of vortex rings are proportional to the properties of the "impulse slug" used in ring generation. The splash central jet is the impulse slug analog in drop-formed vortex rings. In our vortex ring studies we saw a direct relationship between drop size and the ring properties. The larger drops produced rings with larger dimensions, and with greater translational velocities, than rings produced by smaller drops. These larger rings have substantially more momentum and penetrate deeper into the water column than the smaller rings.

The ability of the larger drops to transfer more energy to greater depths is reduced by two factors. The first is bubble formation. If a drop strikes a water surface with too much impact energy, the splash crown is thrown high off the water surface and forms a bubble due to surface tension. By interfering with the formation of the central jet (and consequently the vortex ring) the bubble confines the rainfall energy to very near the water surface.

The second factor is that in natural rainfall events, a broad spectrum of drop sizes are created. The maximum observed drop size is about 0.6 cm in diameter (Laws, 1941). Drop size distribution varies with geographical area, storm type and rainfall intensity (Bubenzer, 1979). For example, in storms reported by Bubenzer (1979), which had intensities less than 2.5 cm/hr, the percentage of total rainfall volume represented by drops larger than 0.4 cm ranged to 6.3%. It should be noted that there is relatively little information on drop size distributions, especially during short high intensity rainfalls (Quimpo and Brohi, 1984).

Rainfall intensity controls the impact frequency of the raindrops. The higher the intensity, the greater number of drop impacts occur per unit area. In addition, the drop size spectrum shifts towards the larger drops with higher intensities. Therefore, erosion potential is a function of not only the number of rainfall events in a geographical location, but also the maximum intensity of these events.

Erosion potential of rainfall on the shallow intertidal water column is controlled not only by the intensity and drop size distribution, but also the timing and the horizontal extent of the rainfall event. High intensity storms, such as thundershowers, occur over short time periods. To be effective these storms must occur as the leading (or trailing) edge of the tidal prism is

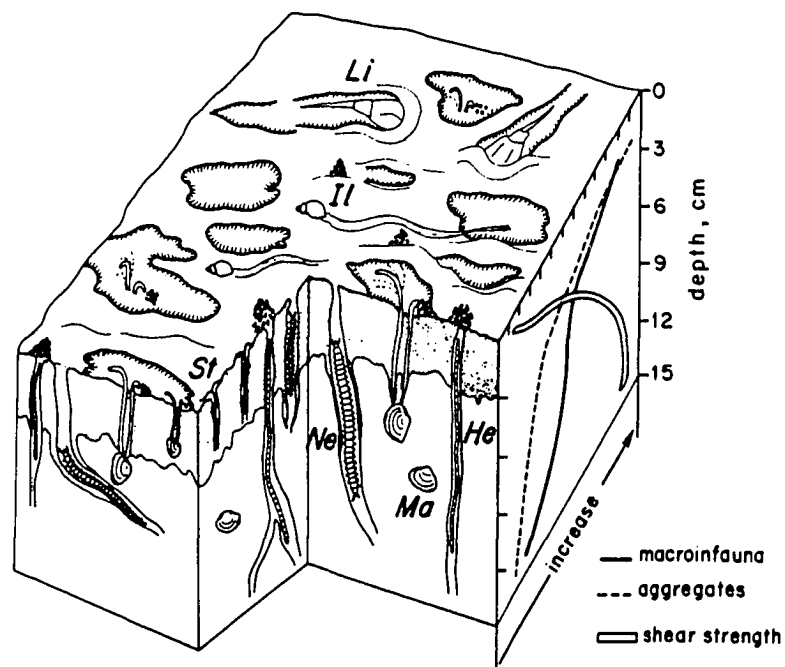
crossing the mudflat. The spatial extent of the high intensity rainfall is also important because rain resuspension is only one component of storm-induced resuspension. For example, if the rainfall is confined to small isolated squal lines, then the total amount of rain-resuspended sediment in a broad estuary may be quite small compared to wind wave action.

### **Physical Properties of the Tidalflat**

The duration of rainfall induced erosion will be controlled by the physical dimensions of the tidalflat environment. Rain falling on a shallow water column may initiate sediment motion in depths as great as 40 cm (Anderson, personal communication). In Chapter 3 drop-formed vortex rings moved non-cohesive sediment in all depths tested, including 22.5 cm. In Chapter 4 multidrop experiments showed resuspension of estuarine mud in all depths tested, including 8 cm. The insitu experiments indicated that rainfall could cause observable resuspension in water depths less than 7 cm. Therefore, the tidalflat slope and microtopography will control the area which can be affected by rain resuspension.

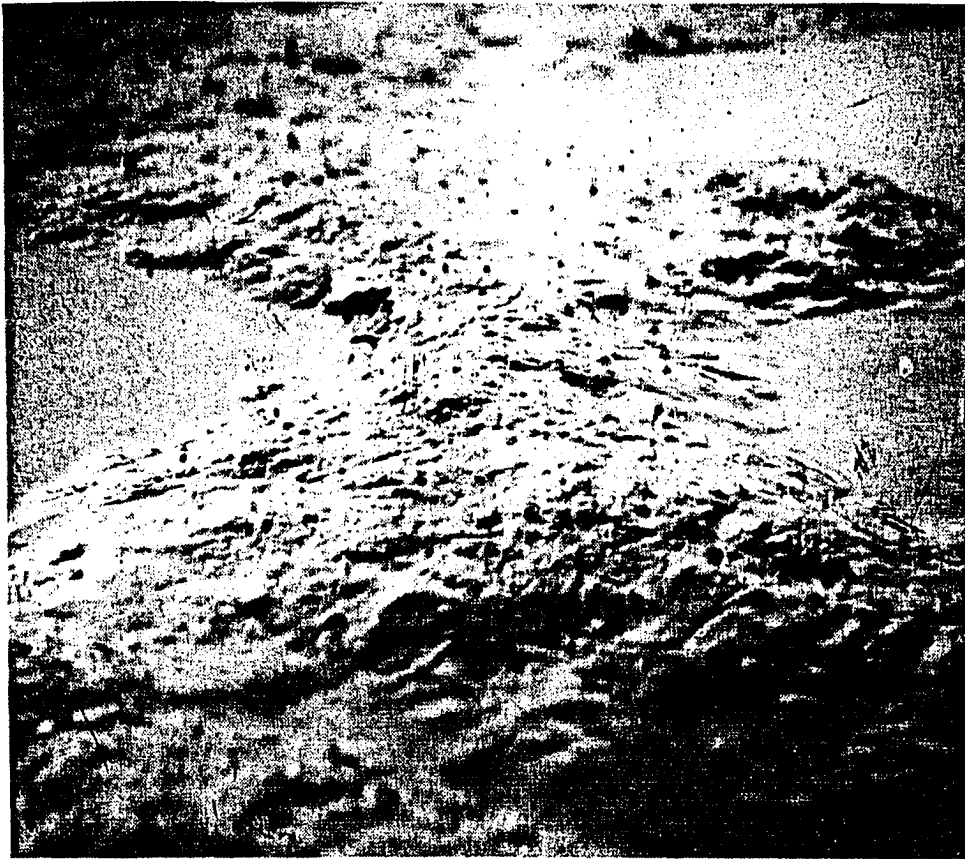
Figure 8-1 illustrates the complex nature of the muddy intertidal sediment surface (Jaramillo, personal communication). The microtopographic relief can be several centimeters from the bottom of pits produced by the hoeshoe crab to the interpit highs (Figure 8-2). The general slope of the tidal flat varies with tide range. In the Great Bay measured slope range from 0.2 to 1.0° (Anderson, 1980). A wedge of intertidal water 40 cm deep on the channel side, would be 10 to 115 m wide given the above range in slopes. Thus as the water floods and ebbs across the intertidal area, a

FIGURE 8-1. Diagrammatic representation of the sediment surface showing the interrelationships between the organisms in the sediment and the microtopography of the sediment surface as interpreted by Jaramillo (personal communication).



*Li: Limulus polyphemus*  
*Ma: Macoma balthica*  
*St: Streblospio benedicti*

*Il: Ilyanassa obsoleta*  
*Ne: Nereis diversicolor*  
*He: Heteromastus filiformis*



**FIGURE 8-2. Photograph showing the microtopography of the sediment surface. The complexity of this surface needs to be considered in interpreting erosion rate predictions for the muddy intertidal.**

relatively wide swath is exposed for rain induced resuspension. Seaward of this swath, the water is too deep for drop-formed vortex rings to impact the bottom. Landward of this zone rain is impacting the mudflat surface directly. Significant amounts of sediment can be eroded by the direct impact of rain and transported to the estuarine water's edge by subsequent sheetflow. This is a very important component of storm-induced sediment erosion; but was not addressed by this study. The effects of direct rain impact on the mudflat surface is the topic of future research efforts.

The amount of time a unit area of mudflat surface is exposed to rain induced resuspension is a function of the tide range and the location. For a 2-m tide, typical for the Great Bay Estuary, the geometric mean rate for water to fall 40 cm (during mid-tide to low tide) is one hour. Thus for any given square centimeter, the mudflat surface can be exposed to rain action for a one-hour period, while the water column decreases from 40 to 0 cm (on the ebb tide), or increases from 0 to 40 cm (on the flood tide).

### **Erodibility of the Sediment Surface**

In Chapters 4 through 6 the resultant erosion by rainfall was hypothesized to vary depending upon the antecedent stress history and the nature of the sediment surface. A sediment surface subjected to high antecedent stress is resistant to additional erosion by rain-induced vortex rings. This can result in very little resuspension of fines into the water column. In contrast, if the sediment surface was dominated by depositional processes just prior to the rainfall event, relatively little shear stress is needed to resuspend the freshly deposited fine sediment. In this case rain-induced vortex rings could resuspend significant amounts of fine sediment.

In either extreme, the vortex rings penetrate only the upper few grain layers (Chapter 6, and Green and Houk, 1980). The sediment surface at this scale is highly variable in texture and composition (Figure 8-3). The fines on the sediment surface are commonly bound into fecal pellets and pseudofeces (Figure 8-3). Sand and gravel-sized organic particles are present and may be covered with a dusting of fine clay and silt particles. Fines are also observed in the interparticle spaces. How these particles respond to turbulent bursts, such as vortex ring impacts, is very difficult to measure or predict for quantification of the erodibility of the sediment surface.

The following hypothesis may conceptually describe the sediment surface's response to impacting vortex rings. As a ring impacts the bottom, the translational momentum and the rotational shear velocities within the inner core eject some of the coarse fecal pellets and organic debris a short distance (<1 cm) into the water column. These coarse particles rapidly settle to the bottom in close proximity to the ring impact area, but downstream in the direction of any advective flow. Other coarse particles, too heavy to be lifted off the bottom are rolled radially away from the impact area. In the course of this movement, clay and silt-sized particles are shaken from the coarse material and resuspended by the turbulent action of the impacting rings. Because of the slow settling velocities of the particles, the fines remain in suspension and may also be mixed upward by the turbulent velocity gradient in the water column. The amount of fines readily available for resuspension will control the amount of material resuspended by the vortex rings. Subsequent rings may move the coarser particles as bedload but not resuspend any fines, because the dusting had been removed

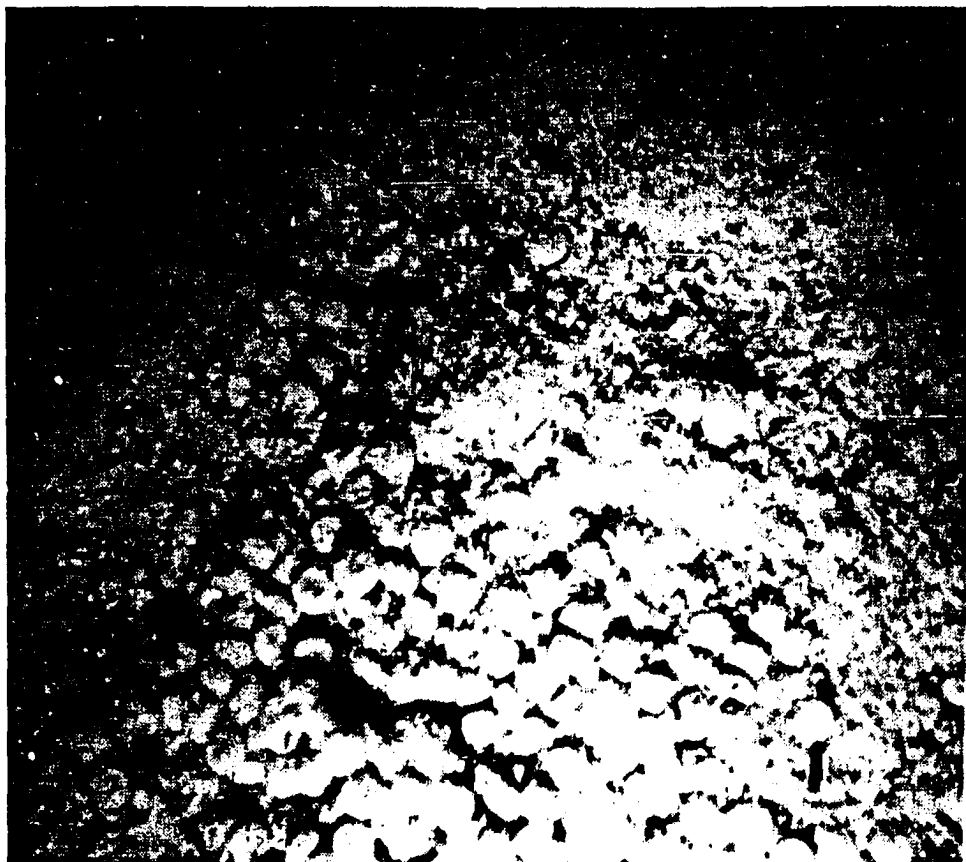


**FIGURE 8-3.** Photograph showing the sediment surface under the microscope. The predominance of fecal pellets and pseudofeces is quite evident at this scale. The *M. balthica* pellets in the picture are about 0.05 cm in length.

at the onset of ring impacts. The coarse particles cleaned of fines will essentially armour the bottom precluding additional resuspension.

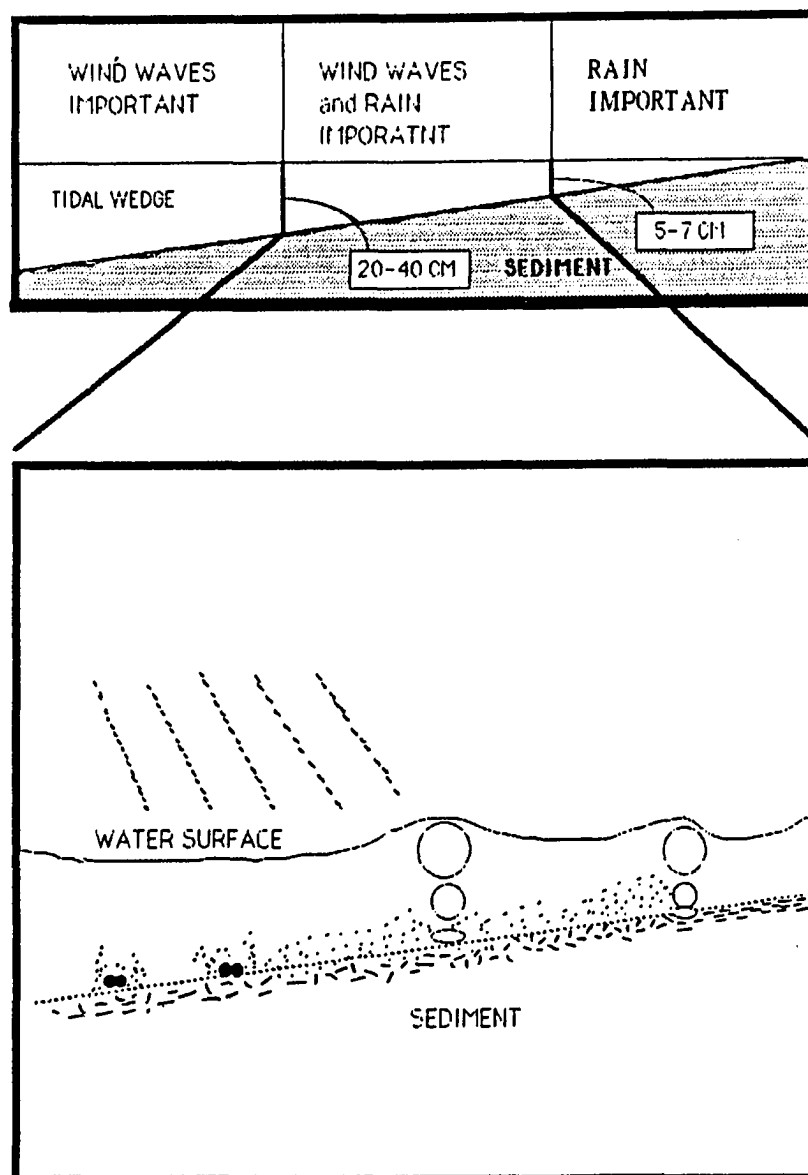
### **Modification of Surface Erodibility**

Numerous factors can control the erodibility of the sediment surface. These factors are summarized in Chapter 1, but were not part of this study. One of the more important factors, wave action, was investigated in the insitu experiment (Chapter 4). Waves due to wind or boats can cause substantial sediment resuspension. Suspended load due to wave action was observed to increase as the water depth decreased to a depth of about 7 cm, then concentrations decreased. The decrease in concentration may be due to the decrease of wave energy available for resuspension. Most of the wave energy may have been frictionally dissipated as the water moved across the shallow tidal flat (causing sediment resuspension) in the deeper water. When the water column was shallower than 7 cm, this filtering allows only the smallest waves to resuspend sediment.

Rain effects were just the opposite; rain resuspension increased as the water depth decreased below 7 cm. Thus rain may be a mechanism, which indirectly enhances wind wave erosion. Rain mixing may cause sediment, which had been resuspended by the wind waves and would normally settle out of the water column, to remain suspended in the water column for a longer period of time. In addition, rain-induced vortex rings may be resuspending bottom sediment, which had just settled to the bottom (Figure 8-4).

This process can be summarized as follows. Sediment is initially resuspended by wave action, a portion settles out in the shallow tidal wedge, rain action resuspends this recently deposited material, and maintains that

FIGURE 8-4. Cartoon on how waves and rain interact in the shallow intertidal wedge. The waves exert significant shear stress mobilizing the bottom sediment surface. Much of this material rapidly settles out and provides surfaces upon which the fines subsequently settle. Rain-induced vortex rings impact this recently deposited material, resuspending the fines and causing the coarse particles to be moved about.



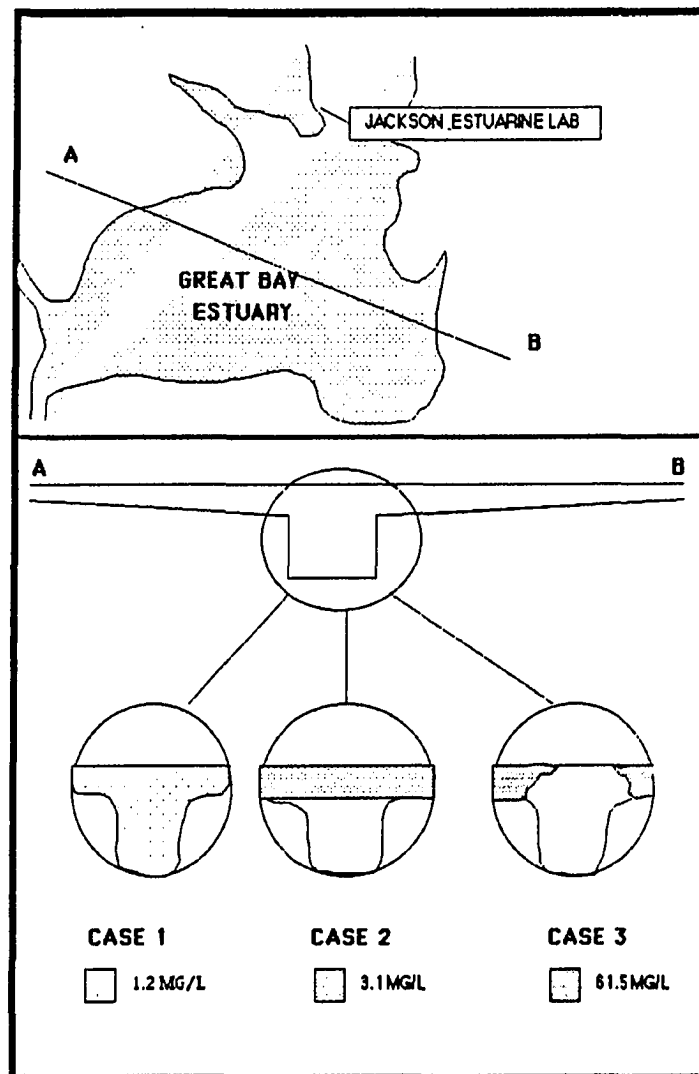
material already resuspended by the waves. The two processes, by acting in complimentary manner, perhaps extend the residence time of the resuspended load in the intertidal water column. If this occurs on the ebb tide then the sediment will be transported off the mudflat and into the channel. If it occurs on the flood tide, then the material will be moved higher onto the tidal flat for deposition, assuming lateral advection doesn't carry the material into the channel. There may be differences in the nature of the sediment surface between the flood and the ebb tide. As water floods the tidal flat, the surface has been exposed to subaerial processes, such as desiccation. In addition, rain effects may be felt through the shallow wedge of overlying water, before relatively large wind waves can act on the sediment surface. In contrast, on the ebb tide these larger waves will be acting on the surface before the rain action.

The ability of rain to compliment wind wave action in the shallow tidal prism may explain why storm events combining wind and rain seem to put more material into the estuarine channels, than that observed during wind events.

### **Importance of Rainfall**

Rust (1980) calculated sediment concentrations within the estuary based upon erosion rates of the intertidal area and concluded that all of the sediment in suspension in the estuary could be due to tidal flat erosion. The importance of rainfall as a tidal flat sediment resuspension mechanism can be estimated by a simple model. This model represents the concentrations of suspended sediment in the low tide volume of the Great Bay portion of the estuary (Figure 8-5). Three cases are considered. Case 1 is where all the rain resuspended sediment is completely mixed with the low tide volume of

FIGURE 8-5. Diagram illustrating the three cases in the simple model which describes the distribution of the rain-induced suspended sediment concentration in the Great Bay estuary at low tide.



the Great Bay. This case is the most conservative and probably the least realistic; however, the calculated concentration can be compared with observations by Loder *et al.* (1983).

In this case the area of Great Bay is 12.08 km<sup>2</sup> and 52.3% of the area is intertidal mudflat. If we have a rainstorm, which erodes 2.8 gm/m<sup>2</sup>/hr (Chapter 4) by rain-induced resuspension, then 17.7 x10<sup>6</sup> gm would be washed into the low tide volume of the Bay. This assumes that the rain acts uniformly over the entire tidalflat area, that the bottom sediments are exposed to a water column falling from 40 to 0 cm in one hour, and that there is complete mixing in the low tide volume. The average concentration due to rainfall resuspension would be 1.2 mg/l where the low tide volume is 14.6 x 10<sup>6</sup> m<sup>3</sup>. Typical low tide concentrations in the Great Bay channel, as measured by Loder *et al.* (1983) over a three year period from 1976 to 1978 range to 70.2 mg/l and average 12.2 mg/l with a standard deviation of 14.0 mg/l. Consequently rain-induced underwater erosion can account for 1 to 10% of the total suspended load in the Great Bay at low tide just after a rainstorm with characteristics similar to those used in the multidrop experiments.

However, this case does not realistically model what is observed as intertidal water ebbs off the tidalflats. Typically the distribution of suspended sediment concentrations observed at the channel edge of the intertidal water has relatively high concentrations near surface (<0.5 m), which slowly mixes in the vertical and in the horizontal with the channel water. These turbid "plumes" are commonly seen close to the channel edge and in the surface layer. This is probably because the intertidal water is less saline and warmer (in the summer) than the channel water. Case 2 of the simple model can be considered where the rain-induced suspended sediment

is dispersed in only the upper 1 m of the low tide volume in the channel. This assumes that there is complete horizontal mixing across the channel. In this case the concentration due to rain would be 3.1 mg/l. Case 3 would be where the intertidal water plume is confined to the edge of the channel with minimal horizontal and vertical mixing. In this case the plume is confined to the upper 1 m and to 5% of the low tide surface area. Concentrations due to the rainstorm in this case would be 61.5 mg/l.

The concentrations calculated for Cases 2 and 3 are relatively high for concentrations in the channel, even at low tide. However, the plumes of turbid water are commonly seen in the estuary during storm events. There is no question that wind wave action is the most important erosive factor in intertidal sedimentation. However, this study has shown that rain-induced underwater resuspension of sediment is a significant component in storm-related erosion of intertidal sediments that acts in a complimentary manner with wind wave action.

### **Areas for Future Research**

This research has identified several areas for future examination. The more important areas are as follows:

1. How rain influences the settling rates of particles in the water column needs to be investigated to improve our sedimentological knowledge of rainstorm effects.
2. The ability of rain-induced vortex rings to entrain the surface microlayer and transport this fluid to depth needs to be studied. In experiments presented in Chapters 2 and 7 we observed drop fluid and oxygen bubbles entrained in the inner core of the ring. Whether or not the microlayer fluid is also incorporated was not possible to determine. This

may be an important pathway for organic pollutants to be removed from the microlayer and linked to settling particles.

3. How rain induced vortex rings act as a vehicle to transport nutrients and oxygen away from the surface layer to depth where they can be utilized by planktonic organisms in an environment much less harsh than the microlayer. These two areas would be important to the chemical oceanographers and microbiologists.

4. The ability of vortex rings to act as efficient mixers was investigated in a preliminary fashion. Further work in using this knowledge in spraying applications may identify areas to improve operation efficiencies.

5. More work needs to be done on quantifying the effects of rain as a sediment resuspending mechanism in the natural environment. This study has identified the processes, and developed spatial and energy limits, which will allow subsequent studies to focus on rain effects in storms.

6. This study focused on the effects of rain on a shallow intertidal water column. It was observed that substantial erosion can occur if the tidal flat is exposed to direct rain impact. Research has been initiated (Anderson, personal communication) and should be expanded to quantify this component of storm activity in the estuary.

## SUMMARY AND CONCLUSIONS

1. The existing literature has shown that rain drops can form vortex rings, which are not only a mechanism for downward mixing of surface water, but also a potential mechanism for resuspending bottom sediment.

2. The areas in the estuary where rainfall will be an important mechanism is the shallow wedge of water (depths  $<7$  cm), which ebbs and floods across the intertidal sediment. In this zone, wind waves are moderated by the shallow water depths.

3. Vortex ring formation is controlled by both the impact energy and drop-shape oscillation. Below a specific impact energy per unit threshold, all drops form a central jet, which is a prerequisite to form vortex rings. Because of the drop shape oscillation, not all drops in this energy range will form energetic vortex rings.

4. The dimensions of the central jet are primarily related to impact energy. Jet cross-sectional area and average jet diameter increase with increased impact energy per unit area. Temperature has more effect on the jets produced by the smaller drops than on the jets produced by the larger drops.

5. The size of the vortex rings ranged from 0.9 to 1.36 cm in horizontal length of the dyed inner core. The larger rings were produced by the larger drops. Translational velocities of the rings ranged to 98 cm/sec for the larger rings and 11 cm/sec for the smaller rings.

6. Penetration of the vortex rings was affected by the size of the ring and the receiving water temperature. The probability of ring penetration

was inversely proportional to water depth. Viscous effects were observed in the penetration of smaller rings.

7. Salinity was observed to affect ring penetration, only when a surface layer of low salinity water thicker than 2 cm was present. If the receiving water was well-mixed, then vortex rings appeared to move as easily through salt water as fresh water.

8. The vertical distribution of available momentum (due to inner core mass and translational velocity) decreases rapidly with depth with an inflection point at 9 cm of water depth for the larger rings and 6 cm for the smaller rings.

9. Vortex rings initiated motion of non-cohesive sediments in all water depths tested to 22.5 cm (limit due to tank depth). An inflection point in the relationship was observed between the 7.5 and 10 cm depths.

10. Multidrop experiments showed that muddy estuarine sediments could be resuspended by artificial rainfall in water depths up to 8 cm. The amount of material resuspended was related to the energy flux due to rain at the water surface. The strength of this relationship decreased with increasing water depth to the sediment surface. A transition zone was observed from 6 to 7.5 cm. Excess mass ranged to 14.2 gm/m<sup>2</sup>/hr and averaged 2.8 gm/m<sup>2</sup>/hr.

11. Similar multidrop experiments conducted on the mudflat showed that rain effects could be observed when the ebb water reached depths of 7 cm. The magnitude of rain resuspension was comparable to resuspension by wind waves, boat wakes and epibenthic faunal disturbances.

12. Storm observations illustrate the problem of isolating rain effects from wind wave effects. In general, the water depths in which rain was

observed to be increasingly important are the same water depths in which wind wave effects were modulated by the shallow water column.

13. Vortex ring impacts can cause bedload transport if there is a slow current over the sediment surface. The coarser particles, such as fecal pellets and organic debris, were moved by the ring impacts. The erosion rate averaged  $5.8 \text{ gm/m}^2/\text{hr}$ .

14. The sedimentological properties of the fecal pellets, the dominant coarse particle on the sediment surface, required a critical shear stress of  $1.14 \text{ dynes/cm}^2$ . The shear stress of  $11 \text{ dynes/cm}^2$ , calculated for impacting vortex rings is sufficient to move the pellets.

15. Textural characteristics of the estuarine sediment did not significantly change due to rain resuspension. This is because the existing sampling technology is not refined to isolate the upper few grain layers which are affected by impacting vortex rings.

16. Vortex rings are also efficient water column mixers. Results of an intercomparison in aquaculture tanks used for toxicity testing suggest that vortex rings are more efficient than air bubbling to oxygenate the aquaria.

17. Rain may contribute 1 to 10% of the observed suspended load in the low tide volume of Great Bay after a rainstorm.

## REFERENCES

- Anderson, F.E. 1972. Resuspension of estuarine sediments by small amplitude waves. *J. Sed. Petrol.* 42:602-607.
- 1973. Observations of some sedimentary processes acting on a tidal flat. *Mar. Geol.* 14:101-116.
- 1975. The short term variation in suspended sediment concentration caused by the passage of a boat wave over a tidal flat environment. Technical Report No. 2, Jackson Estuarine Laboratory, University of New Hampshire. 45p.
- 1980. The variation in suspended sediment and water properties in the flood-water traversing the tidal flat. *Estuaries.* 3(1):28-37.
- 1983. The northern muddy intertidal: A seasonally changing source of suspended sediment to estuarine waters -- A review. *Can. J. Fish. Aquatic Sci.* 40 (Suppl. 1):143-159.
- 1984. Observations of some sedimentary processes acting on a tidal flat. *Mar. Geol.* 14:101-116.
- , L. Black, L.M. Mayer and L.E. Watling. 1981. A temporal and spatial study of mudflat texture. *Northeast. Geol.* 3(3/4):184-191.
- and L.M. Mayer. 1984. Seasonal and spatial variability of particulate matter of a muddy intertidal flood front. *Sedimentology.* 1:383-394.
- Ariathurai, R. and R.B. Krone. 1967. Mathematical modeling of sediment transport in estuaries. p. 98-106. In: M. Wiley (ed.) *Estuarine Processes; Volume II: Circulation, Sediments and Transfer of Material in the Estuary.* Academic Press. 428p.
- Bagnold, R.A. 1966. An approach to the sediment transport problem from general physics. *U.S. Geol. Survey, Prof. Paper* 422-J.
- Baird, M.H.I., T. Wairegi and H.J. Loo. 1977. Velocity and momentum of vortex rings in relation to formation parameters. *Can. J. Chem. Eng.* 55:19-26.

- Banerji, S.K. and R.V. Barave. 1931. On Oberbeck's vortices. *Phil. Mag. Ser. 7* 11(73):1057-1081.
- Banks, R.B. 1978. Accelerations and terminal velocities of raindrops. *ASCE Proc.* 104(EE3):527-531.
- Barfield, B.J. 1968. Studies of turbulence in shallow sediment laden flow with superimposed rainfall. Ph.D. Thesis, Texas A&M University, 106p.
- Batchelor, G.K. 1967. *Introduction to Fluid Dynamics*. Cambridge University Press.
- Beard, K.V. and D.B. Johnson, 1984. Raindrop axial and backscatter ratios using a collisional probability model. *Geophys. Res. Letters*. 11(1):65-68.
- Berry, E.X. and M.R. Pranger. 1974. Equations for calculating the terminal velocity of water drops. *J. Appl. Meteor.* 13:108-113.
- Bhuiyan, S.I., E.A. Hiler and E.T. Smerdon. 1971. Effects of rainfall on settling velocity of suspended sediment in quiescent water. *Water Res. Research*. 6:810-817.
- Black, L.F. 1980. The biodeposition cycle of a surface deposit-feeding bivalve, *Macoma Balthica* (L.), 389-402. In: V. S. Kennedy (ed.) *Estuarine Perspectives*, Academic Press, New York.
- and F.E. Anderson. 1978. What is the role of pellet producers in estuarine tidal flat sedimentation. *Geol. Soc. Am. Abstr.* 3:367.
- Blanchard, D.C. and A.H. Woodcock. 1957. Bubble formation and modification in the sea and its meteorological significance. *Tellus*. 9:145.
- Bubenzer, G.D. 1979. Rainfall characteristics important for simulation. *Proc. of the Rainfall Simulation Workshop*. U.S. Dept. Agr. Pub. ARM-W-10:22-34.
- and B.A. Jones. 1971. Drop size and impact velocity effects on the detachment of soils under simulated rainfall. *Trans. ASAE*. 14:625-628.

- Bursinger, J.A. 1965. Eddy diffusion and settling speed in blown snow. *J. Geophys. Res.* 70(14):3307.
- Caldwell, D.R. and W.P. Elliott. 1971. Surface stresses produced by rainfall. *J. Phys. Oceanogr.* 1:145-148.
- Carroll, K. and R. Mesler. 1981. Part II: Bubble entrainment by drop-formed vortex rings. *AIChE Jour.* 27:853-856.
- Chase, R.R.P. 1979. Settling behavior of natural aquatic particulates. *Limnol. Oceanogr.* 24(3):417-426.
- Chapman, D.S. and P.R. Critchlow. 1967. Formation of vortex rings falling drops. *J. Fluid Mech.* 29:177-185.
- Chen, C.J. and L.M. Chang. 1972. Flow patterns of a circular vortex ring with density difference under gravity. *J. Appl. Mech.* 39(4):869-872.
- Davies, A.G. 1985. Field observations of the threshold of sediment motion by wave action. *Sedimentology.* 32:685-704.
- Dillon, W.P. 1964. Floatation technique for separating fecal pellets and small marine organisms from sand. *Limnol. Oceanogr.* 9:601-602.
- Dingle, A.N. and Y. Lee. 1972. Terminal fallspeeds of raindrops. *J. Appl. Meteor.* 11:877-879.
- Dyer, K.R. 1976. The measurement of bed shear stresses and bedload transport rates, p. 124-135. In: M. Wiley (ed.) *Estuarine Processes; Volume II: Circulation, Sediments, and Transfer of Material in the Estuary.* Academic Press, 428p.
- Einstein, H.A. 1950. The bed-load function for sediment transportation in open channel flows. U.S. Dept. Agr., Soil Conserv. Ser., T.B. No. 1026.
- Ekern, P.C. 1950. Raindrop impact as the force initiating soil erosion. *Soil Sci. Soc. Proc.*, 7-10.
- 1953. Problems of raindrop impact erosion. *Agr. Eng.* 34:23-25.
- Ellison, W.D. 1947. Soil erosion studies--Part I. *Agr. Eng.* 28:145-146.

- Emery, K.O. 1958. Rapid method of mechanical analysis of sands. *J. Sed. Petrol.* 39:777-780.
- Engel, O.G. 1964. Crater depth in fluids impacts. *J. Appl. Phys.* 37(4):1798-1808.
- , 1967. Initial pressure, initial flow velocity, and the time dependence of crater depth in fluid impacts. *J. Appl. Phys.* 38(10):3935-3940.
- Escudier, M.P. and T. Maxworth. 1973. On the motion of turbulent thermals. *J. Fluid Mech.* 61(3):541-552.
- Falco, R.E. 1977. Vortex ring/wall interactions in still and moving ambients. *Am. Physical Soc. Bul.* 2292:1277.
- Filloux, J.H. 1973. Tidal patterns and energy balance in the Gulf of California. *Nature.* 243:217-221.
- Fowler, S.W. and L.F. Small. 1972. Sinking rates of euphausiid fecal pellets. *Limnol. Oceanogr.* 17:293-296.
- Gabrielson, J.O. and R.J. Lukatelich. 1985. Wind-related resuspension in the Peel-Harvey estuarine system. *Estuar., Coast. Shelf Sci.* 20:135-145.
- Glass, L.J. and E.T. Smerdon. 1967. Effect of rainfall on the velocity profile in shallow channel flow. *Trans. Am. Soc. Agr. Eng.* 10:330-332.
- Gordon, C.M. 1974. Intermittent momentum transport in geophysical boundary layer. *Nature* 248:392-394.
- Graf, W.H. 1971. *Hydraulics of Sediment Transport.* McGraw-Hill Book Co., New York. 513p.
- Green, T. and D.F. Houk. 1979. The mixing of rain with near surface water. *J. Fluid Mech.* 90:569-588.
- , 1980. The resuspension of underwater sediment by rain. *Sedimentology.* 27:607-610.
- Gunn, R. and G.D. Kinzer. 1949. Terminal velocity of water droplets in stagnant air. *J. Meteor.* 6:243-248.

- Harlow, F.H. and J.P. Shannon. 1967. The splash of a liquid drop. *J. Appl. Physics*. 38:(10):3855-3866.
- Hawley, N. 1982. Settling velocity distribution of natural aggregates. *J. Geophys. Res.* 87(12):9489-9498.
- Hershfield, D.M. 1961. Rainfall frequency atlas of the United States for durations from 30 minutes to 24 hours and return periods from 1 to 100 years. U.S. Weather Bureau Tech. Rept.40.
- Hobbs, P.V. and A.J.Kezweeny. 1967. Splashing of a water drop. *Science*. 155:1112-1114.
- Honjo, S. 1978. Sedimentation of materials in the Sargasso Sea at a 5,367 m deep station. *J. Mar. Res.* 36(3):469-492.
- and M.R. Romain. 1978. Marine copepod fecal pellets: production, preservation and sedimentation. *J. Mar. Res.* 36(1):45-57.
- Houk, D.F. 1975. The effects of rain on near-surface water. Ph.D. Thesis, University of Wisconsin-Madison. 272p.
- Jamison, A.R. and K.V. Beard . 1982. Raindrop axial ratios. *J. Appl. Meteor* 21:257-259.
- Jones, D.M.A. 1959. The shape of raindrops. Illinois State Water Survey Cir. 77.
- Katsaros, B.C. 1969. Temperature and salinity of the sea surface with particular emphasis on effects of precipitation. Ph.D. Thesis. Univ. Washington.
- Komar, P.D., A.P. Morse and L.F. Small. 1981. An analysis of sinking rates of natural copepod and euphausiid fecal pellets. *Limnol. Oceanogr.* 26(1):172-180.
- Komar, P.D. and G.L. Taghon. 1985. Analyses of the settling velocities of fecal pellets from the subtidal polychaete *Amphicteis caphobranchiata* *J. Mar. Res.* 43:605-614.
- Krutzsch, C.H. 1939. Über eine experimentell beobachtete Erscheinung an Wirbelringen bei ihrer translatorischen Bewegung in wirklichen Flüssigkeiten. *Annalen der Physik*. 35:497-523.

- Laird, B.E. 1976. Effects of tropical storm Agnes on the Chesapeake Bay estuarine system. Chesapeake Res. Consort. Publ. 54.
- Laws, J.O. 1941. Measurements of the fall-velocity of water drops and raindrops. AGU Trans. 22:709-721.
- Laws, J.O. and D.A. Parsons. 1943. The relation of raindrop-size to intensity. AGU Trans. 24:452-459.
- Linden, P.F. 1973. The interaction of a vortex ring with a sharp density interface: A model for turbulent entrainment. J. Fluid Mech. 60:467-480.
- Loder, T.C., J.A. Love, J.P. Kim, and C.G. Wheat. 1983. Nutrient and hydrographic data for the Great Bay Estuarine System, New Hampshire-Maine, Part II. UNH-MP-D/TR-SG-83-4. 149p.
- Luthin, J.N. 1966. Drainage Engineering. John Wiley and Sons. New York. 250p.
- Macklin, W.C. and P.V. Hobbs. 1969. Subsurface phenomena and the splashing of drops on shallow liquids. Science. 166:107-108.
- and G.J. Metaxas. 1976. Splashing of drops on liquid layers. J. Appl. Physics. 47(9):3963-3970.
- Madsen, O.S. 1979. Wave climate of the continental margin: Elements of its mathematical description. In: D.J. Stanley and D.J.P. Swift (eds.) Marine Sediment Transport and Environmental Management. John Wiley and Sons. New York.
- and W.D. Grant. 1976. Sediment transport in the coastal environment. MIT Report No. 209. 105p.
- Magarvey, R.H. and C.S. MacLachy. 1964a. The formation and structure of vortex rings. Can. J. Physics. 42:678-683.
- , 1964b. The disintegration of vortex rings. Can. J. Physics. 42:684-689.
- Maxworthy, T. 1972. The structure and stability of vortex rings. J. Fluid Mech. 51:15-32.

- , 1974. Turbulent vortex rings. *J. Fluid Mech.* 64:227-239.
- , 1977. Some experimental studies of vortex rings. *J. Fluid Mech.* 81:465-495.
- McCall, P.L. 1979. The effects of deposit feeding oligochaetes on particle size and settling velocity of Lake Erie sediments. *J. Sed. Petrol.* 49(3):813-818.
- and M.J.S. Tevesz. 1982. The effects of benthos on physical properties of freshwater sediments. 105-176. In: P.L. McCall and M.J.S. Tevesz (eds). *Animal-Sediment Relations, the Biogenic Alteration of Sediments*. Plenum Press, New York.
- McCool, D.K. 1979. Regional differences in rainfall characteristics and their influence on rainfall simulator design. *Proc. Rainfall Simulator Workshop, Tucson, AZ.* p.17-21.
- McNowen, J.S., J. Malaika, and H. Pramanik. 1951. Particle shape and settling velocity. *Proc. Intern. Assoc. Hydraul. Res., 4th Meeting.* Bombay, India.
- Moss, A.J. and P. Green. 1983. Movements of solids in air and water by raindrop impact and water depth variations. *Austr. J. Soil Res.* 21:257-269.
- Murray, S.P. 1970. Settling velocities and vertical diffusion of particles in turbulent water. *J. Geophys. Res.* 75(9): 1647-1654.
- Mutchler, C.K. 1967. Parameters for describing raindrop splash. *J. Soil and Water Conserv.* 22(3):91-94.
- and K.C. McGregor. 1979. Geographical differences in rainfall. *Proc. Rainfall Simulator Workshop, Tucson, AZ.* p.8-16.
- Nichols, M.M. 1977. Responses and recovery of an estuary following a river flood. *J. Sed. Petrol.* 47:1171-1186.
- Norbury, J. 1973. A family of steady vortex rings. *J. Fluid Mech.* 57(3): 417-431.

- Nowell, A.R.M., P.A. Jumars and J.E. Eckman. 1981. Effects of biological activity on the entrainment of marine sediments. *Mar. Geol.* 42:133-153.
- Oshima, Y. 1972. Motion of vortex rings in water. *J. Physical Soc. Japan.* 34(4): 1125-1131.
- Pruppacher, H.R. and R.L. Pitter. 1971. A semi-empirical determination of the shape of cloud and rain drops. *J. Atmos. Sci.* 28:86-94.
- Pryor, W.A. 1975. Biogenic sedimentation and alteration of argillaceous sediments in shallow marine environments. *Geol. Soc. Am. Bull.* 86:1244-1254.
- Quimpo, R.G. and A. Brohi. 1984. Rainfall energy from drop size data. *Wat. Sci. Tech.* 16:271-283.
- Reynolds, O. 1875. On the action of rain to calm the sea. *Proc. Lit. and Phil. Soc. Manchester.* XIV, Thos. Sowler and Co. London. pp.72-74.
- Rhoads, D.C. 1974. Organism-sediment relations on the muddy sea floor. *Oceanogr. Mar. Biol. Ann. Rev.* 12:263-300.
- and L.F. Boyer. 1982. The effects of marine benthos on physical properties of sediments, a successional perspective. 3-52. In: P.L. McCall and M.J.S. Tevesz (eds.) *Animal-Sediment Relations, The Biogenic Alteration of Sediments.* Plenum Press, New York.
- Richmond, S.B. 1964. *Statistical Analysis.* The Ronald Press Company, New York. 633p.
- Risk, M.J. and J.S. Moffat. 1977. Sedimentological significance of fecal pellets of *Macoma Balithica* in the Minas Basin Bay of Fundy. *J. Sed. Petrol.* 47(4): 1425-1436.
- Robinette, M.J. and D.K. McCool. 1984. Techniques for producing and measuring water drops: A literature review. U.S. Dept. Agr. ARS-11. 18p.
- Robinson, B.H. and T.G. Bailey. 1981. Sinking rates and dissolution of midwater fish fecal matter. *Mar. Biol.* 65: 135-142.

- Rodgers, W.B. 1858. On the formation of rotating rings by air and liquids under certain conditions of discharge. *Am. J. Sci.* 26:246-258.
- Rohatgi, A., M.H.I. Baird, and T. Wairegi. 1979. Mixing effects and hydrodynamics of vortex rings. *Can. J. Chem. Eng.* 57:416-424.
- Rose, C.W. 1960. Soil detachment caused by rainfall. *Soil Sci* 89:28-35
- Rust, L.D. 1980. Temporal and spatial variations in topography and surface texture on a tidal flat in the Great Bay estuary, New Hampshire. M.S. Thesis, University of New Hampshire, 75p.
- Schiller, L. and A. Naumann. 1933. Uber die grundlegenden berechnungen bei der schwerkraftaufbereitung, *Z. VDI.* vol.77.
- Schubel, J.R. 1971. The estuarine environment. AGI Short Course Lecture Notes. Wye Institute, MD.
- Settlemyre, J.L. and L.R. Gardner. 1975. Low-tide storm erosion in a salt marsh. *Southeast. Geol.* 16:205-212.
- Siscoe, G.L. and Z. Levin. 1971. Water drop surface wave interaction. *J. Geophy. Res.* 76(21):5112-5116.
- Small, L.F., S.W. Fowler and M.Y. Unlu. 1979. Sinking rates of natural copepod fecal pellets. *Mar. Biol.* 51:233-241.
- Smayda, T.J. 1969. Some measurements of the sinking rates of fecal pellets. *Limnol. Oceanogr.* (14):621-625.
- Smerdon, E.T. 1964. Effect of rainfall on critical tractive forces in channels with shallow flow. *Trans. Am. Soc. Agr. Eng.* 7:287-290.
- Smith, D.D. and W.H. Wischmeier. 1962. Rainfall erosion. *Adv. Agron.* 14:109-148.
- Spilhaus, A.J. 1948. Drop size, shape and falling speed. *J. Meteor.* 5:108-110.
- Sutherland, A.J. 1966. Entrainment of fine sediments by turbulent flows. Ph.D. Thesis. California Institute of Technology. 199p.

- , 1967. Proposed mechanism for sediment entrainment by turbulent flows. *J. Geophys. Res.* 72(24): 6183-6194.
- Taghon, G.L., A.R.M. Nowell and P.A. Jumars. 1984. Transport and breakdown of fecal pellets: Biological and sedimentological consequences. *Limnol. Oceanogr.* 29(1):64-72.
- Tevesz, M.J.S., F.M. Soster and M.L. McCall. 1980. The effects of size-selective feeding by oligochaetes on the physical properties of river sediments. *J. Sed. Petrol.* 50 (2): 561-568.
- Thompson, J.J. and H.F. Newall. 1885. On the formation of vortex rings by drops falling into liquids and some allied phenomena. *Proc. Roy. Soc. Lond.* 29:417.
- Torobin, L.B. and W.H. Gauvin. 1960. Fundamental aspects of solids-gas flow. Part V: The effects of fluid turbulence on the particle drag coefficient. *Can. Jour. Chem. Eng.* 38:189-200.
- Trask, R.P. 1979. A study of estuarine bottom stress. M.S. Thesis. University of New Hampshire, Durham, N.H. 56p.
- Turner, J.S. 1957. Buoyant vortex rings. *Proc. Roy. Soc. Lond.* A239:61-75.
- U.S. Army Corps of Engineers. 1977. Shore Protection Manual. Coastal Engineering Research Center Publ., Ft. Belvoir, VA.
- Vanoni, V.A. 1977. Sedimentation Engineering. ASCE Manual and Report on Engineering Practice. No. 54. 745p.
- Van Dorn, W.G. 1953. Wind stress on an artificial pond. *J. Mar. Res.* 12(3):249-276.
- Walker, P.H., P.I.A. Kinnell and P. Green. 1978. Transport of a noncohesive sandy mixture in rainfall and runoff experiments. *Soil Sci. Soc. Am. J.* 42:793-801.
- Wanless, H.R., E.A. Burton and J. Dravis. 1981. Hydrodynamics of carbonate fecal pellets. *J. Sed. Petrol.* 51(1): 27-36.
- Ward, L.G. 1981. Suspended-material transport in marsh tidal channels. Kiawah Island, South Carolina. *Mar. Geol.* 40:139-154.

- White, W.R., H. Milli and A.D. Crabbe. 1975. Sediment transport theories: a review. *Proc. Instn. Civ. Engr.* 59:265-292.
- Whitehead, K.D. 1968. The generation and development of a viscous vortex ring. Ph.D. Thesis, Georgia Institute of Technology.
- Widnall, S.E. and J.P. Sullivan. 1973. On the stability of vortex rings. *Proc. Roy. Soc. Lond.* A332:335-353.
- Wischmeier, W.H. and D.D. Smith. 1960. A universal soil loss equation to guide conservation farm planning. 7<sup>th</sup> Intern. Congr. Soil Sci. p418-425.
- , 1978. Predicting rainfall erosion losses. USDA Agricultural Handbook 537.
- Worthington, A.M. 1894. The splash of a drop and allied phenomena. In: *A Study of Splashes*. The MacMillan Co., New York. (A reprint of original articles, published 1964).
- and R.S. Cole. 1897. Impact with a liquid surface. Studied by the aid of instantaneous photography. *Phil. Trans.* A189:137.

## **APPENDIX 1**

**1A. Calculation of Wave Reynolds Numbers**

**1B. Calculation of Energy Dissipation Rates**

## APPENDIX 1A.

Calculation of Wave Reynolds number at the bottom of the water column  
(Madsen and Grant, 1975).

$$Re_w = \frac{u_m(u_m/w)}{\nu} \quad (A1-1)$$

where  $u_m$  = maximum horizontal velocity associated with wave induced to- and fro- motion at the bottom.

$$= \pi d_0 / T_w = \pi H / [T_w \sinh(2\pi z/L)] \quad (A1-2)$$

$u_m/w = a_m = 0.5d_0$  = displacement amplitude of the near bottom water particle motion relative to the bed.

$$d_0 = H / [\sinh(2\pi z/L)] \quad (\text{Komar and Miller, 1973}) \quad (A1-3)$$

$L$  = wave length.

$$= T_w \sqrt{gz} \quad \text{for shallow} \quad (A1-4a)$$

$$= (gT_w^2 / 2\pi) \tanh[(2\pi)^2 z / gT_w^2] \quad \text{for transitional} \quad (A1-4b)$$

$$= gT_w^2 / 2\pi \quad \text{for deep water.} \quad (A1-4c)$$

$H$  = wave height

$z$  = water depth

$T_w$  = wave period

Procedure was to calculate for each depth (2.5 to 40 cm) the wave height and period:

1. Compute  $L$  (using 4a, 4b or 4c).
2. Compute  $d_0$
3. Compute wave Reynolds number.

## APPENDIX 1B

## Calculation of Energy Dissipation Rates

Wave energy dissipation

$$P_d = \tau_b u_b \cos \omega t \quad (A1-5)$$

$$\text{where } u_b = \left[ \frac{\pi H}{T} \right] / \sinh \left( \frac{2\pi z}{L} \right) \\ \tau_b = 0.5 \rho f_w u_b^2 |\cos \omega t| \cos \omega t$$

Example 1:

$$\begin{aligned} Re &= 20000 & P_d &= 2030.9 \text{ ergs/cm}^2/\text{sec.} \\ f_w &= 0.01 \\ H &= 20 \text{ cm} \\ T_w &= 1.5 \text{ sec} \\ L &= 215.7 \text{ cm} \\ z &= 40 \text{ cm} \end{aligned}$$

Example 2:

$$\begin{aligned} Re &= 200 & P_d &= 6.19 \text{ ergs/cm}^2/\text{sec.} \\ f_w &= 0.1 \\ H &= 1 \text{ cm} \\ T_w &= 0.5 \text{ sec} \\ L &= 14.9 \text{ cm} \\ z &= 2.5 \text{ cm} \end{aligned}$$

Rainstorm energy dissipation (Hudson, 1981):

$$E_d = 30 - (125/I), \text{ or} \quad (A1-6)$$

$$E_d = 11.9 + 8.7 \log I \quad (A1-7)$$

Example:

$$\begin{aligned} I &= 4.3 \text{ cm/hr storm (once in 10 years)} \\ E_d &= 27 \text{ joules/m}^2/\text{hr} \\ E_d &= 26 \text{ joules/m}^2/\text{hr} = 7.2 \text{ ergs/cm}^2/\text{sec.} \end{aligned}$$

## **APPENDIX 2**

### **Summary of Analytical Data for the Single Drop Studies**

- 2A. Test Conditions for Drop-Size Variability Experiment
- 2B. Analytical Procedure to Determine Sample Size
- 2C. Summary of Database for Each Single-Drop Experiment
- 2D. Measurement Procedure for Central Jet Dimensions

The original data for the results in Chapter 2 are available in the following data reports archived at the Jackson Estuarine Laboratory

- DR84-1. Effect of Drop Height (1 to 184 cm) on production of vortex rings.
- DR85-1. Relationship between the splash central jet and resultant vortex rings.

APPENDIX 2A. Summary of analytical results for drop-size variability experiment.

TABLE 2A-1. Summary of test conditions for drop-size variability experiment.

Test	No. Sets	Drops per Set	Temp. (C)	Dye (ppm)	Mean Diameter (cm)	Standard Deviation
1	12	10	20-25	----	0.472	0.012
2	12	25	20-25	----	0.471	0.007
3	12	25	20-25	----	0.472	0.006
4	11	25	48-50	2426	0.450	0.011
5	12	25	11-12	2426	0.479	0.005
6	12	25	24-25	608	0.451	0.006
7	12	25	20-25	1823	0.462	0.003
8	12	25	9-10	1823	0.465	0.006
9	10	25	41-42	1823	0.462	0.010
10	12	25	20-25	1215	0.449	0.007
11	12	25	20-25	292	0.474	0.005

TABLE 2A-2. Matrix relating drop variability tests with groups which show no significant variation in drop size at the 95% CI.

DYE	TEMPERATURE		
	Low	Moderate	High
No specs.		III 1 III 2 III 3	
292ppm		III 11	
608		I 6	
1215		I 10	
1823	II 8	II 7	II 9
2426	III 5		I 4

Note: I, II, III are the groups which have significantly different drop sizes at the 95% CI. One to 11 are the individual tests.

TABLE 2A-3. Summary of drop-size measurements for each tip used in the single drop experiments.

Experiment	Tip No.	Mean (cm)	Standard Deviation	Number of Observations
1,2	15	0.464	0.0100	129
3	20V	0.242	0.0032	4
	11V	0.304	0.0005	4
	10V	0.330	0.0013	4
	10	0.399	0.0043	10
	11	0.367	0.0100	4
	15	0.469	0.0014	8
	16	0.545	0.0029	4
4	11	0.351	0.0021	2
	16	0.524	0.0044	4
5	16	0.535	0.0006	3

## APPENDIX 2B. Sample Size Analysis.

The sample size needed to reach a desired level of precision requires a previous knowledge of the population percentage, which one would expect to observe. Knowing this percentage, setting an acceptable level of significance, and defining a range within which the data should fall, one can better estimate the requisite number of observations (Richmond, 1964). A pilot study was conducted using six sample sizes for seven drop heights, because we lacked prior knowledge on the expected percentage of vortex rings produced. This study provided a set of observed frequencies which could be tested against theoretical distribution models, using a single classification technique for Chi Square.

$$\chi^2 = \sum_{i=1}^k \frac{(f_i - F_i)^2}{F_i} \quad (A2-1)$$

where  $k$  = number of categories

$f_i$  = observed  $i^{\text{th}}$  frequency

$F_i$  = theoretical frequency.

Two theoretical models were tested on the data set. The first hypothesis was the chance of observing a vortex ring was 50% at the 95% CI. This hypothesis was rejected for the data set as a whole (Table 2B-1: Model 1). When the data were subdivided by sample size the hypothesis was also rejected. However, when the data were subdivided by height, the hypothesis was accepted at 43 and 160 cm fall heights. The second model divided the data set into three groups based upon the frequency of vortex ring formation. Group A hypothesis was that one drop out of three will form a vortex ring. Group B hypothesis was that one drop out of two will form a ring. Group C hypothesis was that three drops out of four will form a ring. Each hypothesis was tested against drop height. The Group A hypothesis was accepted (95% CI) at drop heights of 5 and 17 cm, Group B at 43 and 160 cm, and Group C at 80, 92 and 125 cm. When the data set was subdivided by sample set size, the hypotheses were rejected at only the 200 drop set (Table 2B-1).

The second model provides a basis for estimating the expected percentages of vortex rings produced by drop impact. The sample size computational technique by Richmond (1964) can be used to determine the range of observations about the expected mean percentage ( $P_m$ ), since the sample sizes were predetermined:

$$P_m \pm Z_{\alpha} S_p \quad (A2-2)$$

TABLE 2B-1. Hypothesis testing for Chi Square analysis on sample size data sets.

No. Drops	Df	Chi Square	Hypothesis
MODEL 1			
Total	41	304.2 (56.93)*	Reject
25	6	25.58 (12.59)**	Reject
50	6	39.44	Reject
75	6	43.74	Reject
100	6	45.70	Reject
150	6	73.84	Reject
200	6	83.88	Reject
MODEL 2			
Total	41	51.85	Accept
25	6	8.45	Accept
50	6	10.08	Accept
75	6	7.09	Accept
100	6	7.13	Accept
150	6	4.98	Accept
200	6	14.02	Reject

where  $z_{\alpha}$  = standard normal deviation at  $\alpha$  significant level  
(at 95% CI,  $z$  is 1.96)

$sp$  = the standard error of a sample percentage or

$$Sp = \sqrt{\frac{P_m(100-P_m)}{n}} \quad (A2-3)$$

where  $n$  = sample size.

The predicted range of observations was computed for each sample size ( $n = 25, 50, 75, 100, 150$  and  $200$  drops) and for each group which would have its characteristic population mean (Group A = 33%; Group B = 50%; and Group C = 75%). The analytical results suggest that a sample size of 25 drops can distinguish Group A population from Group C population (Table 2B-2). A sample size of 150 drops or more was needed to differentiate the three groups at the 95% CI. Based upon this analysis and the experimental limitation that about 50 drops obscured the visibility of the dyed ring in the receiving water, a sample size of 25 drops was used for subsequent experiments.

TABLE 2B-2. Summary of expected ranges for each Group by sample size at the 95% CI.

GROUP		SAMPLE SIZE					
		25	50	75	100	150	200
A	Min	14.9	20.3	22.7	24.1	25.8	26.8
	Mean	33.3	33.3	33.3	33.3	33.3	33.3
	Max	51.7	46.3	43.9	42.5	40.8	39.8
B	Min	30.4	36.1	38.7	40.2	42.0	43.1
	Mean	50.0	50.0	50.0	50.0	50.0	50.0
	Max	69.6	63.9	61.3	59.8	58.0	56.9
C	Min	58.0	63.0	65.2	66.5	68.1	69.0
	Mean	75.0	75.0	75.0	75.0	75.0	75.0
	Max	92.0	87.0	84.8	83.5	81.9	81.0

## APPENDIX 2C. Summary of data base for each experiment.

EXPER.	RUNS					SETS		Total Drops	
	Drop Size	No. Drop Hghts.	Water Depths	Substr. Tex.	Rec. Water Temp.	No. Runs	Drops per Set		No. Sets
1a	1*	1	1	0	3	12	25	4*	300
1b	1	7	1	0	1		"	1	
2	1	184	1	0	1	184	25	2	9200
3	2	12	1	0	1	24	100	1	2400
4	2	4	1	0	3	24	50	1	1200
5	1	1	9	5	1	45	100	3	12900

\* Number of runs or sets.

## APPENDIX 2D. Measurement procedure for central jet dimensions.

Detailed measurements of jet height, cross-sectional area and impulse time were made from the video recording as follows:

1. Identify splash as jet type (jet, jet/bubble, or bubble).
2. Run video frame-by-frame to maximize jet height above the water surface.
3. Align baseline of tracing overlay on monitor screen along water surface, accounting for meniscus.
4. Trace central jet and jet drops, if present.
5. Record the 1-cm length from scale in video field of view (located at same focal length as jet).
6. Check next frame to assure that the recorded jet was at maximum extent.
7. Measure the 1-cm length scale on tracing to nearest fraction of inch, and use as the scaling factor.
8. Measure the height of the jet above the baseline and convert using the scaling factor.
9. Planimeter the cross-sectional area of the jet using a compensated polar planimeter (K&E 62-0005). Average triplicate area measurements and convert using the scaling factor.

The following calculations were made using the reduced data from the video tape:

1. Jet diameter was determined by dividing the cross sectional area by the jet height. The irregular shape of the jet precluded direct measurement of diameter.
2. Drop impact energy was calculated using the measured drop diameter, drop height, and the predicted impact velocity using the results of Laws (1941). Kinetic energy ( $E_i$ ) at impact is then

$$E_i = (\pi\rho/12)D^3U_i^2 \quad (A2-4)$$

where  $U_i$  = velocity of drop at impact.

$D$  = drop diameter

$\rho$  = drop density.

3. Impact energy per unit spherical area was calculated by dividing the energy by the cross-sectional area of the drop.

## **APPENDIX 3**

- 3A. Summary of vortex ring observations in which sediment moved when rings touched bottom.**
- 3B. Shear stress calculation for critical shear of very coarse quartz grains.**

APPENDIX 3A. Summary of observations in which sediment moved when vortex rings touched the bottom. For each depth and sediment size combination there were triplicate runs of 100 drops each.

DEPTH (cm)	SEDIMENT SIZE ( $\phi$ )	RUN			MEAN	STD. DEV.
		1	2	3		
2.5	-0.75	89*	94	97	94.0	5.3
	0.25	100	99	99		
	1.25	--	--	--		
	2.25	96	85	84		
	3.25	95	96	95		
5.0	-0.75	72	67	65	77.6	12.8
	0.25	96	86	89		
	1.25	93	74	84		
	2.25	81	75	73		
	3.25	86	45	78		
7.5	-0.75	20	22	18	46.3	17.3
	0.25	67	43	57		
	1.25	72	30	42		
	2.25	62	53	46		
	3.25	57	44	61		
10.0	-0.75	33	19	20	29.1	10.7
	0.25	41	9	30		
	1.25	42	18	21		
	2.25	40	37	26		
	3.25	46	29	25		
12.5	-0.75	15	7	10	21.2	7.6
	0.25	27	21	27		
	1.25	34	17	16		
	2.25	25	22	21		
	3.25	33	23	20		
15.0	-0.75	12	11	16	20.3	5.7
	0.25	27	21	27		
	1.25	24	27	23		
	2.25	20	22	14		
	3.25	15	27	18		
17.5	-0.75	12	7	6	15.1	6.3
	0.25	7	16	17		
	1.25	23	24	12		
	2.25	11	13	15		
	3.25	25	22	16		
20.0	-0.75	4	3	6	10.9	5.8
	0.25	9	8	9		
	1.25	16	7	5		
	2.25	12	14	16		
	3.25	21	21	12		
22.5	-0.75	--	--	--	11.1	7.1
	0.25	3	2	7		
	1.25	25	12	8		
	2.25	10	21	17		
	3.25	15	21	17		

\* Number of vortex rings which moved sediment out of 100 drops.

APPENDIX 3B. Shear stress calculation  
(Madsen and Grant, 1976)

$$S^* = (d_s/4\nu)\sqrt{(s-1)gd_s}$$

$$\psi = \tau_0/(s-1)\rho gd_s$$

Procedure is to calculate  $S^*$  go into Modified Shields Diagram (Madsen and Grant, 1976) to determine  $\psi$ , then compute  $\tau_0$ .

Example:

- $d_s$  - sediment diameter - 0.168 cm
- $\nu$  = kinematic viscosity = 0.01 cm<sup>2</sup>/sec
- $s$  = specific gravity of sediment - 2.65
- $\rho$  = density of water = 1.0 gm/cm<sup>3</sup>
- $g$  = acceleration due to gravity - 980.66 cm/sec<sup>2</sup>

$$S^* = 69.2$$

at 69.2 then  $\psi=0.04$

$$\tau_0 = 10.87 \text{ dynes/cm}^2$$

## **APPENDIX 4**

**The original data for the results in Chapter 4 are available in the following data reports archived at the Jackson Estuarine Laboratory**

- DR85-13. Multidrop Experiment: Rain induced resuspension of tidalflat sediment.
- DR85-14. Flume Experiment: Rain induced bedload from tidalflat sediments.
- DR85-15. Insitu Multidrop Experiment.
- DR85-16. Natural Storm Event Sampling.

## APPENDIX 5

**5A. Sedimentological Characteristics of Fecal Pellets from  
*M. balthica* and *H. filiformis***

**5B. Critical Shear Stress Calculation for *H. filiformis* pellets**

## APPENDIX 5A

### SEDIMENTOLOGICAL CHARACTERISTICS OF FECAL PELLETS FROM *M. BALTHICA* and *H. FILIFORMIS*

#### Introduction

The muddy intertidal surface is commonly dominated by biogenic reworking (Anderson and Mayer, 1984; Black, 1980; and Rhoads, 1966; 1974). Organisms may influence, not only the microtopography, but also the sedimentological characteristics of the surface material (Anderson *et al.*, 1981; and McCall, 1979). A predominant textural component on the intertidal surface is the fecal pellet produced by benthic organisms (Anderson, 1980; and Anderson and Mayer, 1984). Organisms repackage clay and silt sized particles into sand-sized pellets (Pryor, 1975; Risk and Moffat, 1977; and Tevesz *et al.*, 1980). One would suspect that these pellets are more easily eroded than the original cohesive mud; however, mucus binding may inhibit erosion (Rhoads and Boyer, 1982; Frankel and Meade, 1973). Once suspended however, the pellets will settle faster than the component particles (Hawley, 1982). Thus the pelletization of the muddy intertidal sediment modifies the erosion/deposition characteristics of this sediment (McCall and Tevesz, 1982; Nowell *et al.*, 1981; Rhoads and Boyer, 1982; Tagon *et al.*, 1984; Wanless *et al.*, 1981).

The purpose of the study was to investigate the sedimentological properties of fecal pellets to better understand how the pellet responds to shear stress applied by tidal currents, waves, and rainfall. The approach was to isolate the fecal pellets from the indigenous sediment; analyze in bulk for pellet density, texture and combustibles; and measure individual pellet dimensions and settling velocity. These data provided the comparison between the observed settling velocity and predictive equations presented in the literature. In addition, it was possible to estimate the effects of pellet density variability and pellet shape on the hydrodynamic behavior of the fecal pellets.

The fecal pellets of *Macoma balthica* (Linnaeus, 1758; Bivalvia, Tellinidae), and *Heteromastus filiformis* (Claparede, 1864. Polychaeta, Capitellidae) were selected because of their predominance on the sediment

surface, difference in formation, and resistance to destruction (Black and Anderson, 1978). *M. balthica* feeds on surface organic-rich material through an incurrent siphon. Ingested material is compacted in the gut into cylindrical pellets and voided through the excurrent siphon onto the sediment surface. *H. filiformis* are deep deposit feeders and eject spheroidal shaped fecal pellets onto the sediment surface. The mean breakdown time of *M. balthica* fecal pellets is 10 to 17 days (Black, 1980), thus they are able to survive several tidal cycle events. Although there is no data on the breakdown of *H. filiformis* pellets, it is believed they are at least as rugged as the *M. balthica* pellets.

### Theory

The settling velocities of fecal pellets have been measured or estimated by several researchers (Chase, 1979; Fowler and Small, 1972; Honjo, 1978; Honjo and Romain, 1978; Komar *et al.* 1981; and Komar and Taghon, 1985; McCall, 1979; Robinson and Bailey, 1981; Small *et al.* 1979; Smayda, 1969; Taghon *et al.* 1984; and Wanless *et al.* 1981). Pellet size ranges from relatively small pelagic pellets which settle according to Stokes law, to large benthic pellets which settle according to the impact law. Komar *et al.* (1981) and Komar and Taghon (1985) have presented equations which relate the nominal diameter, shape and density of the pellets to their settling velocity. These studies cover the Stokes range and the coarser portion of the impact range. However, there is an intermediate range between these two extreme cases which has not been investigated to date (Komar and Taghorn, 1985). The fecal pellets investigated in this study fall into this intermediate size range.

It is instructive to review settling theory briefly to put this study into perspective. Settling of spherical particles attain a terminal velocity when the hydrodynamic or resistive forces of the fluid are balanced by gravitational forces of the sphere (Graf, 1971) or

$$C_d D^2 \frac{\pi}{8} (W-v)^2 = D^3 \frac{\pi}{6} (\rho_s - \rho) g \quad (A5-1)$$

where  $C_d$  = drag coefficient

$D$  = diameter of the sphere

$\rho$  = fluid density

$\rho_s$  = density of sphere

$W$  = velocity of sphere

$v$  = velocity of fluid

$g$  = gravitational constant = 980.66 cm/sec

Rearranging and assuming  $V = 0$ , the settling velocity of a spherical particle is

$$W = \left[ \frac{4}{3} \frac{D}{C_d} g \left( \frac{\rho_s - \rho}{\rho} \right) \right]^{1/2} \quad (A5-2)$$

The settling of very small particles is dominated by the viscous effects of the surrounding fluid. The inertial effects of the particle are negligible; therefore Stokes-type settling occurs and the drag on the particle is reduced to an inverse function of the Reynolds number. The Reynolds number, the ratio of inertial to viscous forces, is defined as

$$Re = \frac{\rho D v}{\mu} \quad (A5-3)$$

where  $\mu$  = absolute viscosity.

When  $Re \ll 0.1$ , the Stokes range, the drag coefficient is as follows

$$C_d = \frac{24}{Re} \quad (A5-4)$$

Combining Equations A5-2, -3, and -4 gives the familiar Stokes settling velocity ( $W_s$ ) equation or

$$W_s = \frac{1}{18\mu} (\rho_s - \rho) g D^2 \quad (A5-5)$$

When the  $Re > 2$ , the impact range, the drag coefficient varies in a complex fashion relative to the Reynolds number. Several empirical equations have been developed to relate  $Re$  to  $C_d$  for spheres (Graf, 1971). For example

$$C_d = \frac{24}{Re} \left( 1 + 0.15 Re^{0.687} \right) \quad (A5-6)$$

by Schiller and Naumann (1933).

The effects of shape on a particle settling in the impact law range have been studied empirically (McNown *et al.*, 1951). Their studies extended the work of Corey beyond the Stokes settling range by using a correction factor. This factor was the ratio between the drag coefficient of an equivalent sphere, calculated with Eq. A5-4. In general, shape tends to decrease the settling velocity relative to the settling of a sphere by increasing the drag. Similar results have been reported for non-spherical fecal pellets (Komar and Taghon, 1985).

## Methodology

### Sampling Technique

Fecal pellets were collected by two methods. *H. filiformis* pellets, the most abundant of the two pellets, were obtained directly from the intertidal area. Sampling was conducted toward the end of the tidal flat exposure period to allow build-up of the distinctive *H. filiformis* fecal pellet mounds. Pellets were collected with a spatula from these mounds to minimize contamination by the indigenous sediment. Collection from about twenty mounds was required for each of the six samples analyzed. The fecal pellets were split and a subsample was placed in distilled water to remove sea salts. Removal of sea salts was necessary to obtain an accurate measurement of bulk density. A separate subsample was retained in seawater for the seawater settling measurements. Separation of fecal pellets from broken and non-pellet debris was repeated by gently mixing and decanting.

The *M. balthica* pellets were collected in a different manner, because these pellets are typically intermixed with *H. filiformis* pellets in the field. About 50 bivalves were harvested from the intertidal, cleaned and brought into the laboratory. These bivalves were placed in clean seawater and allowed to egest their fecal pellets. The pellets were then transferred to distilled water (except those used for seawater settling) and cleaned in a manner similar to the *H. filiformis* pellets. Enough pellets for three 50-100 mg samples were collected.

### Individual Pellet Measurements

Individual pellets were analyzed for settling velocity (120 pellets) in both distilled and sea water, and for dimensions (270 pellets). The general procedure was to measure the length and diameter of each pellet under the microscope at 25X using a calibrated ocular, pick-up pellet with an eyedropper, and place into the settling tube. The *H. filiformis* fecal pellet is ellipsoid in shape. It was assumed that the pellet was circular in cross-section. The length was always longer than the width or diameter, thus the pellets are prolate spheroids. The *M. balthica* pellet is cylindrical in shape. Care was taken to reorient the pellet so that both the diameter and length could be measured.

Pellet settling velocity was measured in an Emery Tube (Emery, 1938) with a 2.54 cm diameter. The time for individual pellets to fall 100 cm was recorded. The pellet was allowed to fall about 40 cm before start of timing to assure terminal velocity and stable orientation. Pellets were tested in both distilled water and salt water (ca. 26 ‰). The temperature at the top and bottom of the 100 cm settling distance was measured using a laboratory grade thermometer (+/- 0.2° C). The salinity was measured with an American Optics refractometer (+/- 0.5 ‰).

### Bulk Pellet Measurements

Subsamples were analyzed for bulk properties of density, water content, textural composition and combustibles. Interpellet water was removed by vacuum at 0.18 cm of Hg on Millipore HA type filters. The pellets were carefully removed in bulk from the filter with a razor blade, and immediately weighed to +/- 0.1 mg for net weight on a Cahn TA 450 balance. The pellets were then transferred to a 25 ml pycnometer bottle. The bulk density ( $\rho_s$ ) of the pellets were measured directly by weight difference using

$$S = \frac{X}{A - B + X} = \frac{\rho_s}{\rho} \quad (A5-7)$$

where  $s$  = specific gravity  
 $X$  = wet weight of pellets  
 $\rho$  = Density of distilled water (D.W.)  
 $A$  = Pycnometer weight with D.W. only  
 $B$  = Pycnometer weight with both D.W. and pellets

The contents of the pycnometer bottle were then sonicated and wet sieved to separate the sand and mud fractions (*M. balthica*). The *H. filiformis* samples were separated into silt and clay. Each fraction was dried, weighed, combusted at 500° C for two hours and reweighed. The wet and pre-ignition dry weights were used to determine the water content of the pellets.

### Results

The observed settling velocity of the fecal pellets ranged from 1.8 to 3.0 cm/sec (Figure A5-1). The pellet Reynolds numbers suggest that settling

is according to Newton's impact law (Eq. A5-2). The wide scatter, when settling velocity is compared to the nominal diameter, suggests that variability in pellet shape or density, affecting the drag coefficient, may be important.

Pellet density, based upon bulk samples, was 1.64 g/cc (n=3; standard deviation of 0.2 g/cc) for *M. balthica* pellets, and 1.47 g/cc (n=6; standard deviation of 0.02 g/cc) for *H. filiformis* pellets (Table A5-1). The *H. filiformis* pellet densities are, perhaps, more reliable because of the larger sample sizes, which tended to reduce analytical error. However, the bulk densities of *M. balthica* are consistent with those observed (1.68 g/cc) by Risk and Moffat (1977). For comparison, the bulk density of fecal pellets described in the literature are presented in Table A5-2.

The pellet dimensions vary between *H. filiformis* which are spheroid in shape, and *M. balthica* which are cylindrical in shape. *H. filiformis* pellets average 0.72 mm in length and 0.35 mm in diameter with a mean calculated volume of 0.047 mm<sup>3</sup>. The *M. balthica* pellets averaged 0.50 mm in diameter and 0.32 mm in length with a mean pellet volume of 0.063 mm<sup>3</sup>.

Electron scanning microscope pictures of *H. filiformis* and *M. balthica* at 150X, 500X, 1000X and 5000X to identify the general composition and surface features of the pellet (Figure 5-2). The predominate differences between the pellets was their shape and surface roughness. The *M. balthica* was more cylindrical in shape, while the *H. filiformis* pellets were ellipsoidal. The surface of the *M. balthica* pellets appeared to be much smoother than the *H. filiformis*. This may have been due to differences in how the material in the pellet are bound together. The *M. balthica* pellets appear to have a smooth sheath; in contrast the *H. filiformis* pellets tend to have a network of filaments holding the pellet material together (Figures A5-2G and A5-2L).

The pellet sedimentation texture and combustible composition appear to reflect the sediment upon which the organisms are feeding. This is consistent with observations by Taghon *et al* (1984). In general, *H. filiformis* pellets had a lower water content and less sand, and a higher mud content and combustible fraction than *M. balthica* pellets. *M. balthica* pellets had a composition that was quite similar to the surface sediment. The water content and mud fraction in the *H. filiformis* pellets were similar to the indigenous sediment at 12 cm below the surface (Table A5-1).

FIGURE A5-1. Observed settling velocities of *M. balthica* and *H. filiformis* pellets versus the nominal diameter (diameter of a volumetrically equivalent sphere). The scatter is due to shape effects and bulk density differences.

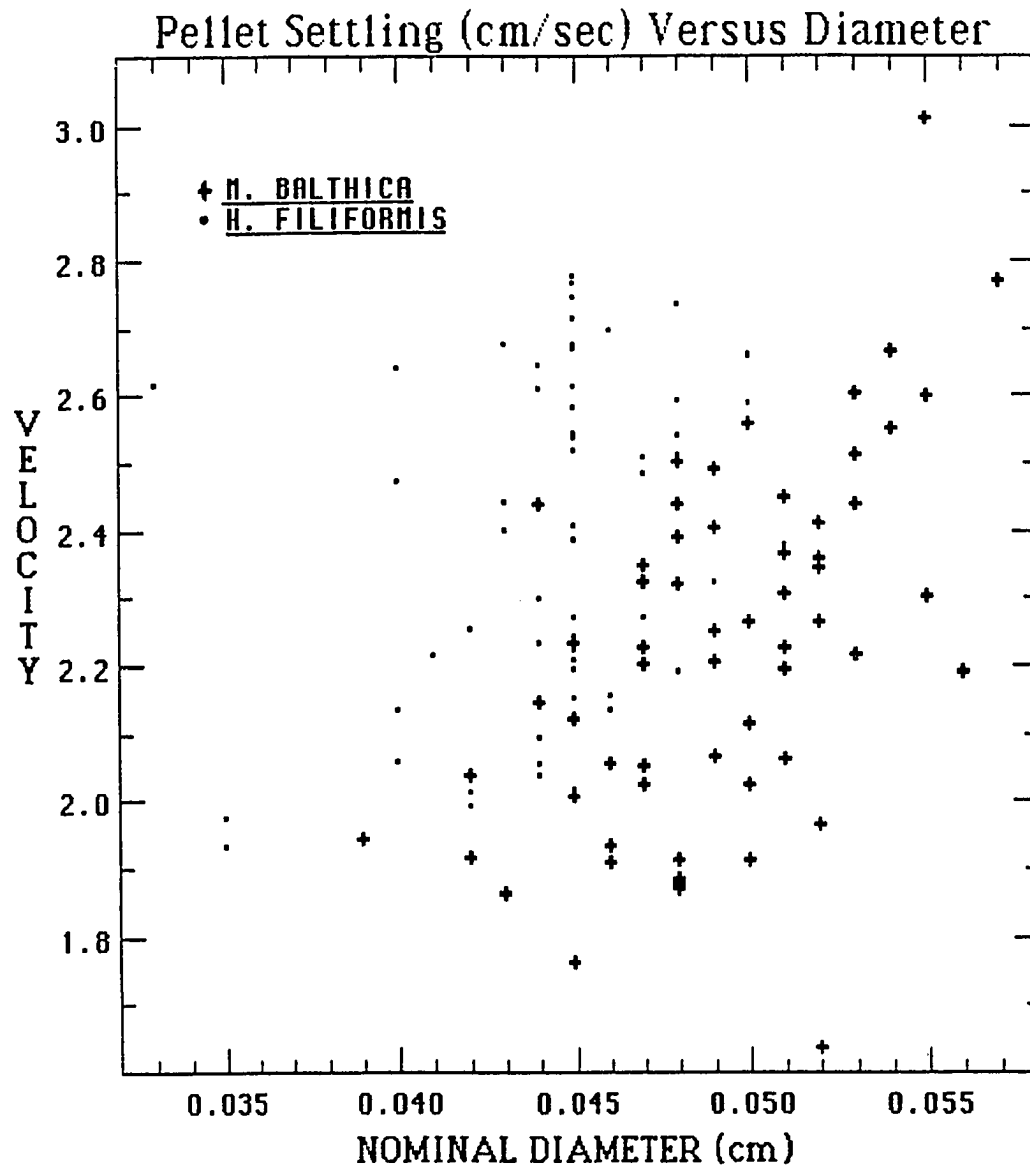


TABLE A5-1. Composition of fecal pellet samples analyzed for bulk density, and indigenous sediment.

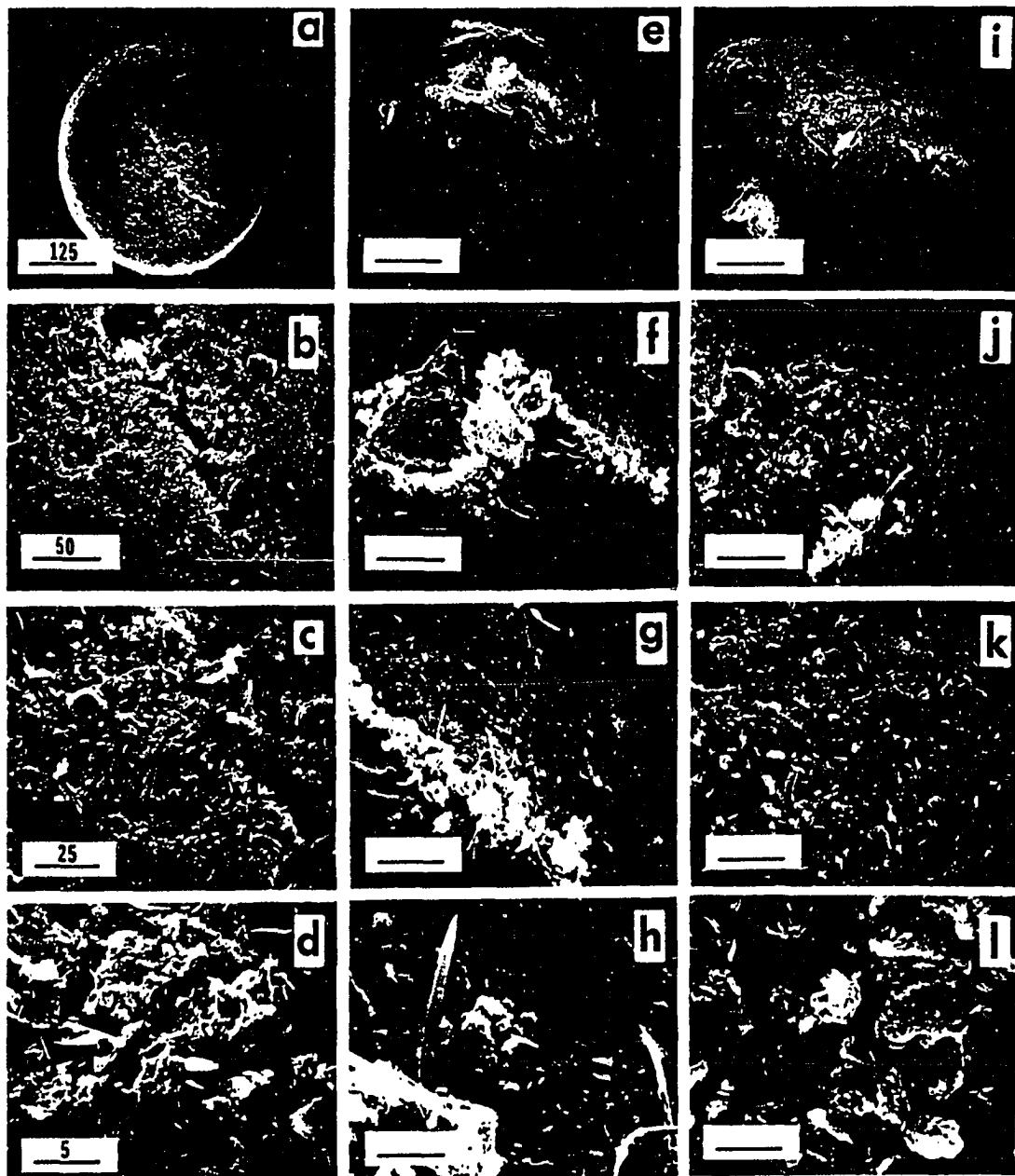
SAMPLE NO.	BULK DENSITY (gm/cc)	WET WGT. (gm)	COMPOSITION (% of Wet Weight)				
			Water Content	Sand	Inorganic Silt	Mud Clay	Total Combustibles
<b><i>H. filiformis</i> Pellets:</b>							
1H	1.471	1.2422	38.4	1.1	32.9	20.1	7.5
2H	1.483	0.2748	31.3	0.9	26.8	35.1	5.9
3H	1.451	1.4710	49.4	0.5	25.6	20.3	4.2
4H	1.489	0.7268	44.6	1.0	27.9	20.2	6.3
5H	1.446	0.4192	36.9	0.5	27.2	24.7	10.7
6H	1.495	0.9913	44.9	1.0	29.5	19.2	5.4
MEAN	1.473	0.8542	40.9	0.8	28.3	23.3	6.7
<b><i>M. balthica</i> Pellets:</b>							
1M	1.837	0.0657	51.9	3.3	40.3		4.4
2M	1.432	0.0990	46.8	6.2	43.3		4.0
3M	1.636	0.0513	46.0	4.7	44.8		4.5
MEAN	1.635	0.0720	48.2	4.7	42.8		4.3
<b>Sediment:</b>							
Surface (0-3 cm)			51.3	3.7	45.2		7.2
Deep (12-15 cm)			42.7	6.1	51.2		—

TABLE 5A-2. Compilation of fecal pellet densities from the literature.

ORGANISM	MEAN BULK DENSITY	REFERENCE
?	1.19 gm/cm <sup>3</sup>	Dillon (1964)
Euphausiids	1.29	Fowler and Small (1972)
Mixed Copepods	1.22*	Small <i>et al.</i> (1979)
<i>A. patersonii</i>	1.15	Small <i>et al.</i> (1979)
?	1.22	Weibe <i>et al.</i> (1976)
Euphausiid		
( <i>Meganctiphanes norvegica</i> )	1.19-1.27	Komar <i>et al.</i> (1981)
Polychaete		
( <i>A. scaphobranchiata</i> )	1.19	Taghon <i>et al.</i> (1984)
<i>Macoma balthica</i>	1.68	Risk and Moffat (1977)
-----		
Polychaete		
( <i>Heteromastus filiformis</i> )	1.47	This study
<i>Macoma balthica</i>	1.67	This study

\* Modal value.

FIGURE 5-2. Electron microscopic pictures of *M. balthica* pellets (A-H) and *H. filiformis* pellets (I-L). The first row of pictures shows the shape of the two types of pellets (note the scale in the lower right hand corner of the picture). The subsequent rows show the pellet surface at increasing magnification. The differences in surface roughness is quite evident in pictures G and L.



## Discussion

Fecal pellets dominate the muddy intertidal sediment surface of Adams Cove in the Great Bay Estuary of New Hampshire. The pellets of *H. filiformis* and *M. balthica* are rugged enough to be transported about the tidal flat without being immediately destroyed. Therefore understanding the hydrodynamic characteristics of these pellets will provide insight into the type of forces acting on the mudflat surface by the flooding and ebbing estuarine water. If the pellets are in dynamic equilibrium with the energy of the environment, then it may be possible in subsequent research to estimate the level of shear forces necessary to cause erosion of the sediment surface.

The settling velocity of fecal pellets is less than the settling of spheres of equivalent volume. The decrease in velocity is most likely due to increased drag associated with the non-spherical shape of the pellets (Figure 5A-3). This is consistent with the observations of Komar and Taghon (1985) for larger fecal pellets. The scatter in the data may be due to differences in the individual pellet density, since the density term used in calculating the drag coefficient was the average bulk density (Figure 5A-4).

Calculation of individual pellet densities is possible by power regression to determine the relationship between drag and Reynolds number, and by assuming the scatter about this relationship is due solely to pellet density variability. Rearranging Equation A5-2 yields

$$\rho_s = \rho + \rho \left[ \frac{3}{4} \frac{\omega^2 C_d}{D_n^2 g} \right] \quad (\text{A5-8})$$

$$\text{where } C_d = 30.2 \text{ Re}^{-0.717}$$

A narrow range of individual pellet densities are required to account for the scatter about the regression relationship (Figure 5A-4). The standard deviations of the individual pellet densities are 0.0411 g/cc for *M. balthica* and 0.0749 g/cc for *H. filiformis*.

Pellet shape effects on settling can be evaluated using the correction factor (K) technique of McNown *et al.* (1951). K is computed by taking the ratio between the drag coefficient determined for the pellet (i.e.  $C_d = 30.2 \text{ Re}$ ), and the Stokes drag coefficient, determined by Equation A5-2 (Figure 5A-5). The different shapes of *H. filiformis* (spheroidal) and *M. balthica* (cylindrical) have a significant effect of settling. *H. filiformis*, which has a L/W ratio >1, has a greater K value than *M. balthica* with a L/W ratio <1 (Figure 5A-6). Both pellets have a K value which is greater than an

FIGURE 5A-3. Comparison of the observed drag coefficient (Eq. 5A-2) and the predicted drag coefficient (Eq. 5A-6) versus Reynolds number.

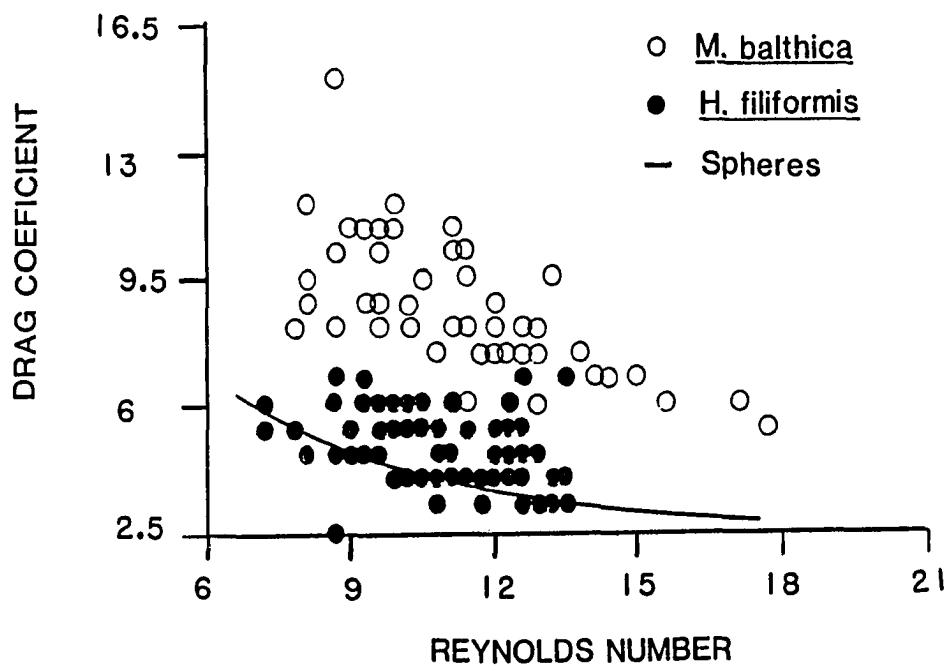


FIGURE 5A-4. Histograms of calculated *H. filiformis*(A) and *M. balthica*(B) pellet densities.

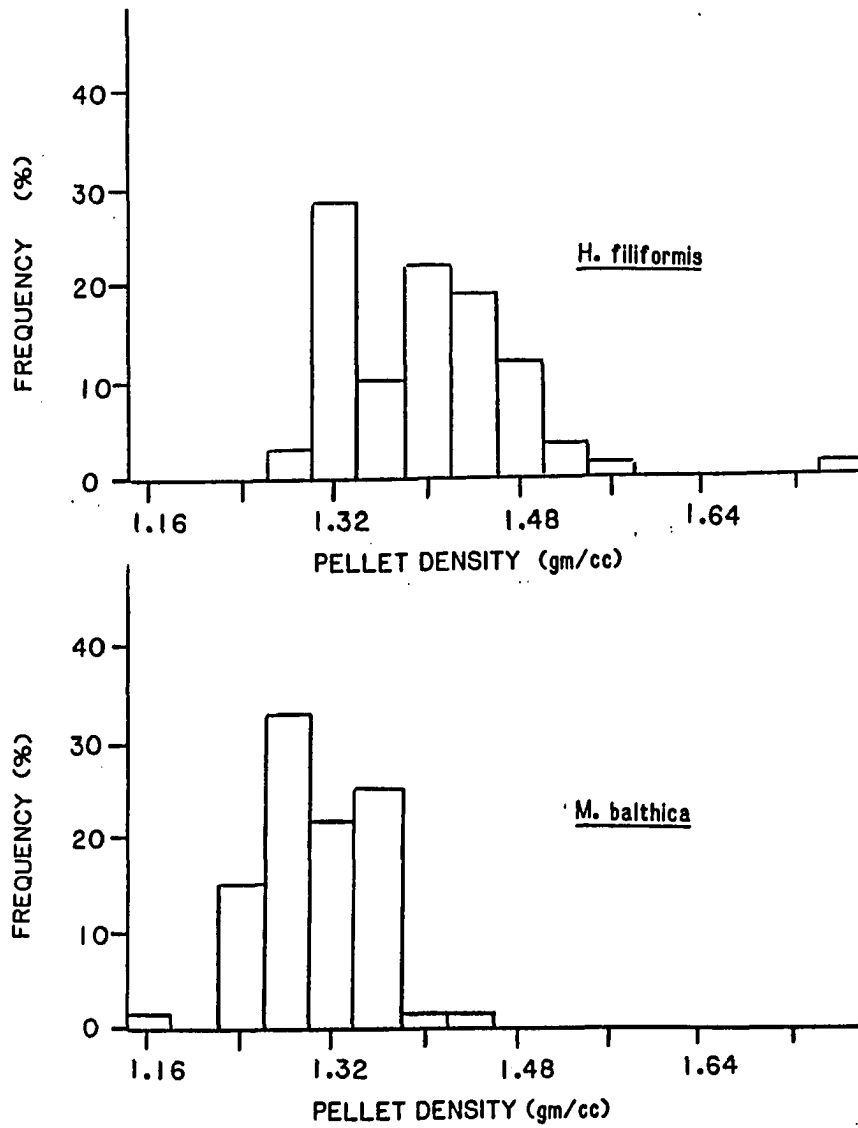


FIGURE 5A-5. Correction factor  $K$  for *H. filiformis* and *M. balthica* pellets, and equivalent spheres versus Reynolds number.

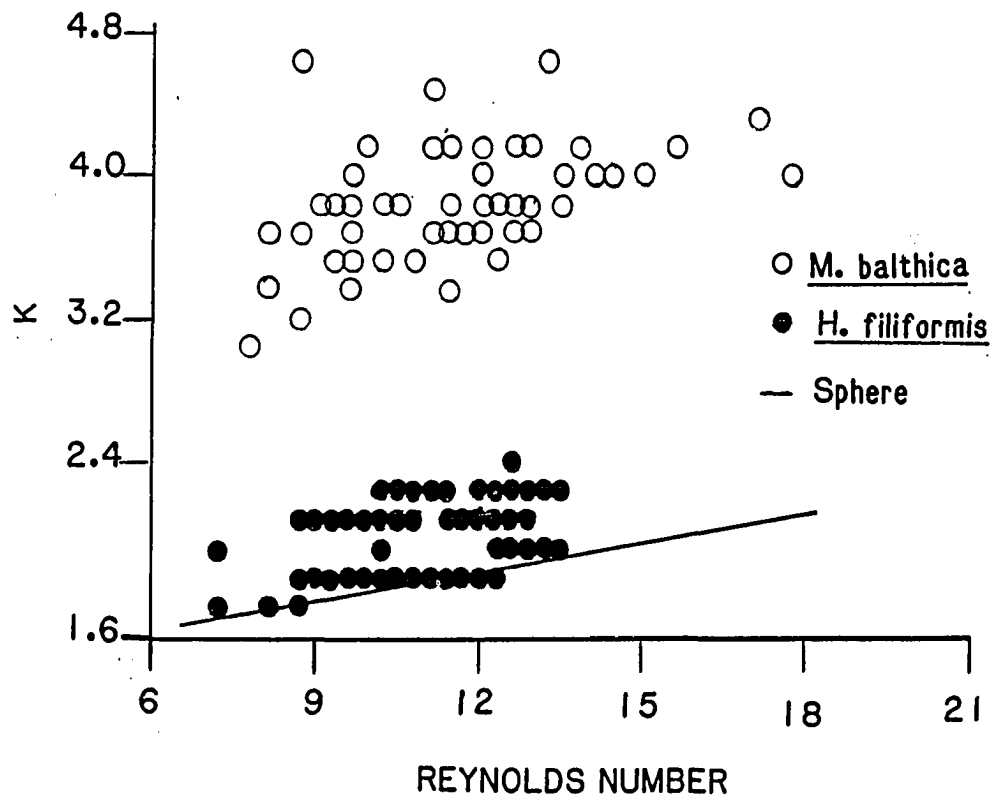
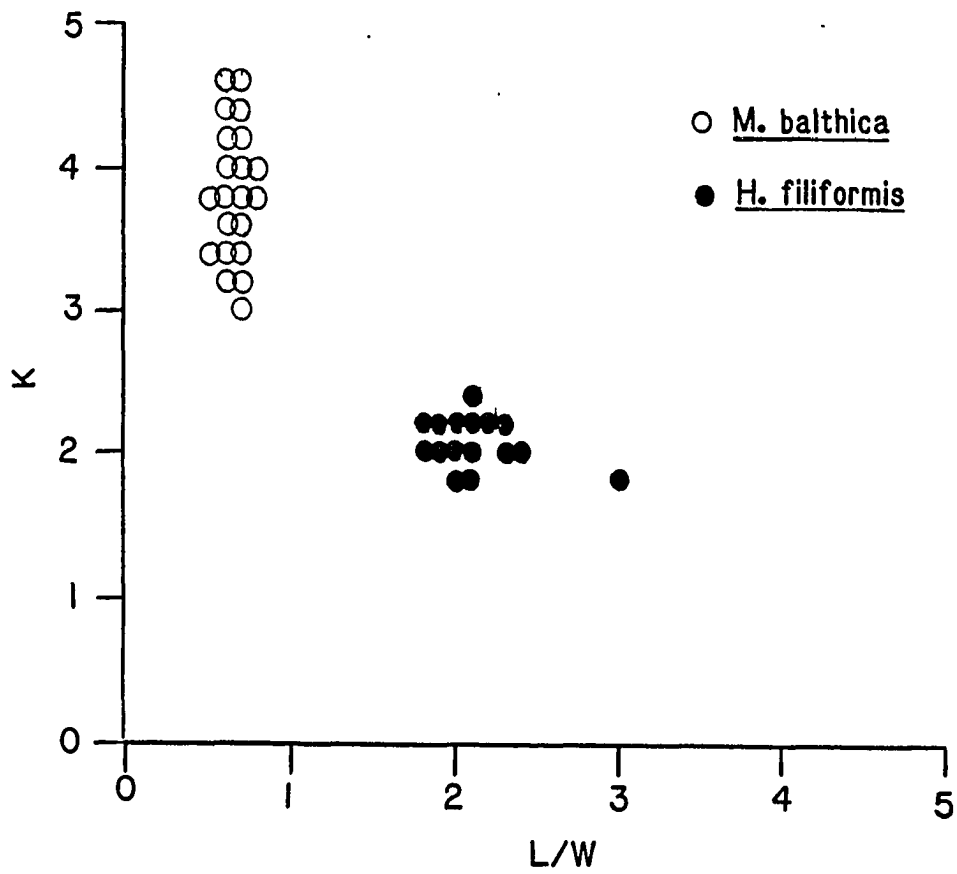


FIGURE 5A-6. Correction factor K versus pellet L/W ratio.



equivalent sphere (Figure 5A-6), but similar values to the non-spherical particle shapes used by McNown *et al* (1951).

Since the correction factor is based upon Stokes settling law, an equation to predict the settling velocity ( $W_p$ ), knowing the correction factor (K), takes the form

$$W_p = \frac{1}{k} \frac{D_n^2}{18\mu} (\rho_s - \rho) g \quad (A5-9)$$

where  $k = 2.15$  for *H. filiformis*  
 $= 3.85$  for *M. balthica*  
 $= 1.79$  for an equivalent sphere.

This predicted settling velocity equation ( $W_p$  on y axis) is a reasonable approximation ( $r = 0.785$ ) for the observed settling velocity ( $W_o$  on x axis) (Figure 5A-7).

Within the range of Reynolds numbers studied in this investigation (7 to 18), an empirical equation solved from the pellet settling velocity ( $W_p^*$ ), can be obtained by rearranging Eq. A5-8 to obtain a form similar to the equation proposed by Komar and Taghon (1985), but with a higher slope (Figure 5A-8):

$$W_p^* = k' \left[ \frac{1}{\nu^2} \left( \frac{\rho_s - \rho}{\rho} g \right)^3 D_n^5 \right]^{1/4} \quad (A5-10)$$

where  $k'$  is function of different pellet shapes  
 $k' = 0.118$  for *H. filiformis*  
 $= 0.079$  for *M. balthica*  
 $\nu$  = kinematic viscosity

These equations indicate that the observed pellet settling is in the impact range, and is slower than equivalent spheres with the same density. The shape of the pellets is very important in controlling the settling velocity.

## Conclusions

Fecal pellets from *H. filiformis* and *M. balthica* are derived from sediment at different levels below the sediment-water interface. The pellet composition is, in general, similar to the sediment ingested by the organism. The bulk density of the *M. balthica* pellets is greater than the *H. filiformis*

FIGURE A5-7. Predicted settling velocity using Eq. 5A-9 versus observed settling velocity.

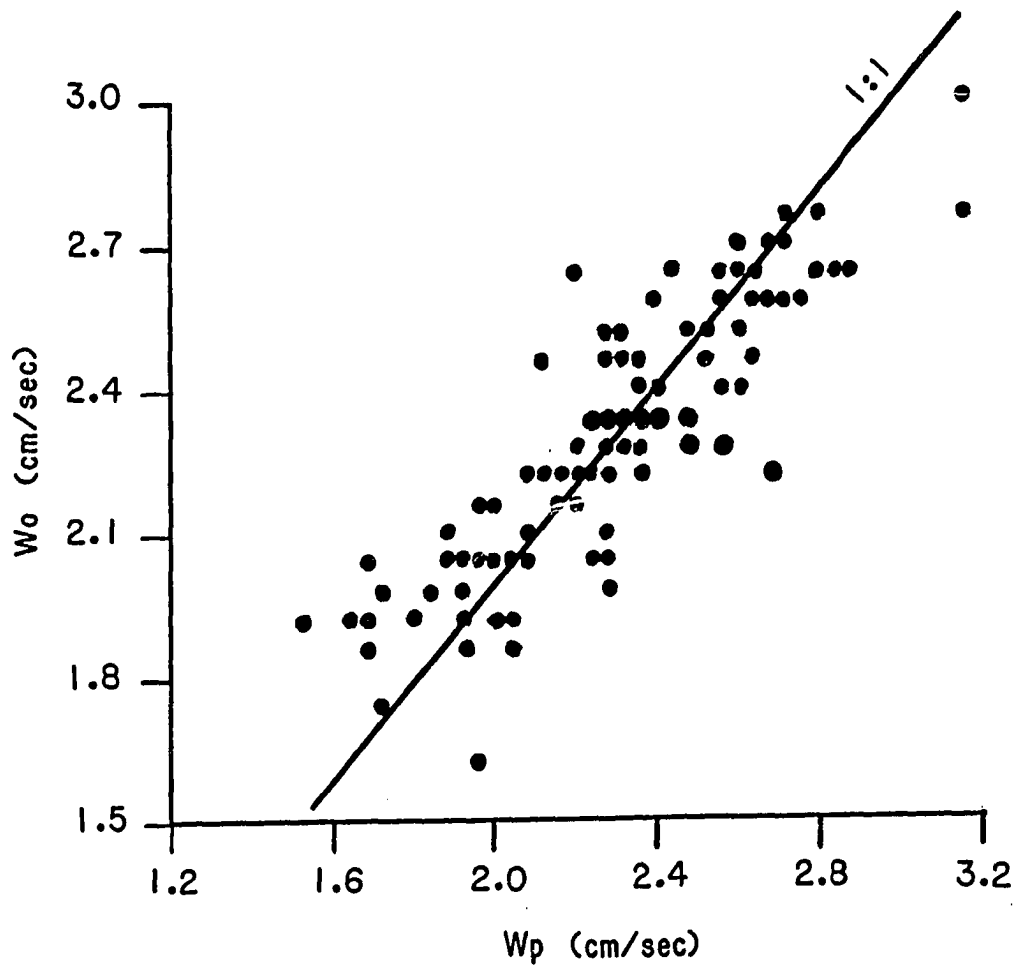
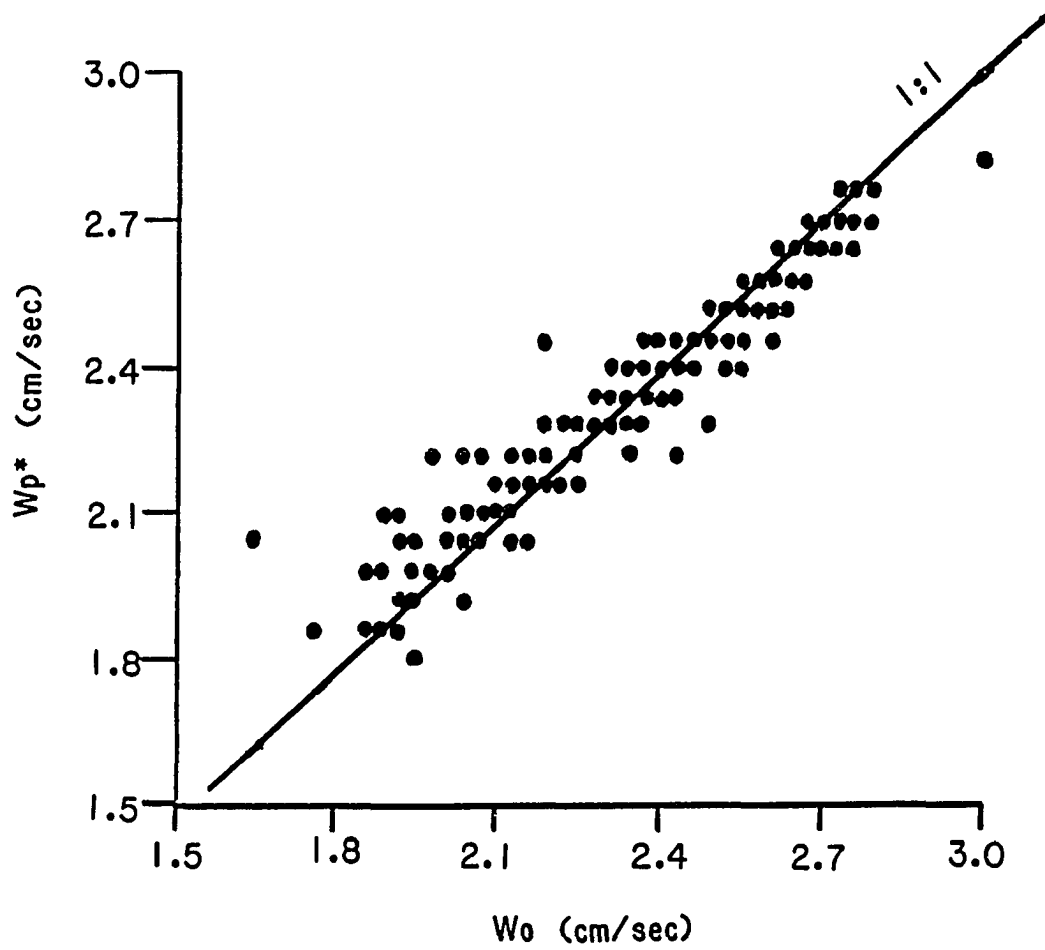


FIGURE A5-8. Predicted settling velocity using Eq. 5A-10 versus observed settling velocity.



pellets (1.64 versus 1.47 g/cc). This difference may be due to the higher amounts of sand in the *M. balthica* pellets (Table A5-1).

Estimating individual pellet density using Eq. A5-7 illustrates the narrow range in densities which create significant variability in the calculation of drag coefficient.

Pellet shape retards the settling velocity relative to an equivalent sphere of equal density. In addition, each pellet type has a different shape effect. Therefore, it is essential that the hydrodynamic behavior of each pellet type be precisely evaluated before using an empirical relationship. Two empirical equations are presented, which predict the settling velocity. These equations describe pellet settling in a region of Reynolds numbers between the work of Komar *et al* (1981) and Komar and Taghon (1985).

## APPENDIX 5B

Shear Stress Calculation for *H. filiformis*

$$S^* = (d_0/4\nu)\sqrt{(s-1)gd_0}$$

$$\psi = \tau_c/[(s-1)\rho gd_0]$$

Example:

$$s = 1.473 \text{ gm/cm}^3$$

$$d_0 = 0.072 \text{ cm}$$

$$\nu = 0.01 \text{ cm}^2/\text{sec}$$

$$\rho = 1.0 \text{ gm/cm}^3$$

$$g = 980.66 \text{ cm/sec}^2$$

$$S^* = 10.4, \text{ then } \psi = 0.034$$

$$\tau_c = 1.14 \text{ dynes/cm}^2$$

## APPENDIX 6

**Summary listing of the data collected  
during the oxygenation experiment**

## AIR PLUS WATER

Level	Time	D.O.	Temp.	Sal.
-------	------	------	-------	------

## Baselevel

3	838	7.20	20.0	16.0
2	843	7.00	20.0	
1	847	1.65	20.0	

## Start @ 8:50 WL=17.7

3	927	5.80	20.0	
2	929	5.60	20.0	
1	931	5.60	20.0	

## Start @ 9:50 WL=19.3

3	951	5.90	19.9	
2	953	5.95	19.8	
1	955	6.00	19.9	

## Start @ 10:16 WL=21.1

4	1017	6.15	19.8	
3	1020	6.20	19.7	
2	1022	6.15	19.5	
1	1024	6.25	19.5	

## Start @ 10:50 WL=22.4

4	1051	6.70	19.2	
3	1053	6.40	19.4	
2	1056	6.60	19.4	
1	1058	6.50	19.2	

## Start @ 11:30 WL=22.4

4	1131	6.80	18.9	18.0
3	1133	6.60	19.0	18.0
2	1136	6.75	19.0	18.0
1	1139	7.00	19.0	18.0

## VORTEX RINGS

Level	Time	D.O.	Temp.	Sal.
-------	------	------	-------	------

## Baselevel

2	853	7.60	19.8	16.6
3	856	7.30	19.8	
1	859	1.55	19.9	

## Start @ 9:05 WL=14.7

3	935	6.65	20.0	
2	937	6.65	20.0	
1	940	5.50	20.0	

## Start @ 9:57 WL=18.5

3	959	6.55	19.9	
2	1000	6.60	20.0	
1	1003	6.30	20.0	

## Start @ 10:26 WL=21.6

4				
3	1027	6.90	19.4	
2	1030	6.90	19.5	
1	1032	6.95	19.3	

## Start @ 11:00 WL=19.0

4	1102	7.40	19.3	16.5
3	1106	7.25	19.3	18.0
2	1109	7.40	19.2	18.0
1	1111	7.35	19.2	17.5

## Start @ 11:44 WL=20.8

4	1145	7.50	19.2	18.0
3	1148	7.40	19.2	18.0
2	1150	7.45	19.1	18.0
1	1153	7.35	19.1	18.0

## AIR PLUS WATER

Level	Time	D.O.	Temp.	Sal.
-------	------	------	-------	------

Start @ 12:18 WL=22.4

4	1219	7.05	18.6	18.0
3	1222	6.75	18.7	18.0
2	1225	6.90	18.5	18.0
1	1228	6.85	18.4	18.0

Start @ 13:05 WL=22.4

4	1306	6.95	18.2	19.0
3	1308	6.95	18.2	19.0
2	1310	7.00	18.1	18.5
1	1313	7.00	18.0	18.5

Start @ 13:44 WL=22.4

4	1345	7.10	18.0	18.5
3	1348	7.10	18.0	19.0
2	1351	7.10	18.0	19.0
1	1353	7.15	18.0	19.0

Start @ 14:24 WL=22.4

4	1424	7.30	17.9	19.0
3	1427	7.20	18.0	19.0
2	1429	7.15	17.9	19.5
1	1432	7.15	17.7	19.5

Start volume rate in 80 ml/min

End volume rate in 97 ml/min

## VORTEX RINGS

Level	Time	D.O.	Temp.	Sal.
-------	------	------	-------	------

Start @ 12:29 WL=21.2

4	1230	7.25	19.0	18.0
3	1233	7.40	19.0	18.0
2	1236	7.40	18.9	18.5
1	1239	7.30	19.0	18.5

Start @ 13:13 WL=21.2

4	1314	7.40	18.9	18.5
3	1318	7.45	18.9	18.5
2	1321	7.50	18.9	18.5
1	1324	7.35	18.8	18.5

Start @ 13:55 WL=21.2

4	1356	7.55	18.8	19.0
3	1359	7.50	18.9	18.5
2	1402	7.50	18.8	19.0
1	1405	7.35	19.0	18.5

Start @ 14:33 WL=21.2

4	1434	7.60	18.8	19.0
3	1437	7.45	18.9	19.0
2	1440	7.65	18.8	19.0
1	1443	7.65	18.8	18.5

End volume rate in 40 ml/min



## WATER ONLY

---

Level	Time	D.O.	Temp.	Sal.
-------	------	------	-------	------

---

Start @ 12:42 WL=21.7

4	1143	6.00	18.3	19.0
3	1145	6.10	18.2	18.0
2	1147	6.05	18.1	18.0
1	1150	6.15	18.1	18.0

Start @ 13:26 WL=21.7

4	1327	6.10	18.0	18.5
3	1329	6.05	17.9	18.5
2	1331	6.10	17.9	18.5
1	1336	6.15	17.9	18.5

Start @ 14:07 WL=21.7

4	1408	6.15	18.0	18.5
3	1410	6.15	17.8	18.5
2	1412	6.15	17.8	19.0
1	1415	6.25	17.8	18.0

Start @ 14:44 WL=21.7

4	1445	6.10	17.8	19.0
3	1447	6.20	17.5	19.0
2	1450	6.15	17.5	19.5
1	1452	6.25	17.5	19.5

NO WATER/NO AIR (Tank D)  
NEW WATER (NW)

---

Level	Time	D.O.	Temp.	Sal.
-------	------	------	-------	------

---

1	1300	2.50	19.5	17.5
NW	1303	6.60	15.6	20.0

1	1339	2.85	19.6	18.0
NW	1342	6.75	15.7	20.0

1	1419	3.10	19.5	18.0
NW	1421	6.70	15.8	20.0

1	1455	3.25	19.3	18.0
NW	1458	6.55	15.6	19.5

---

Start volume rate in 94 ml/min

End volume rate in 88 ml/min